A multi-omics view on the pathogen *Yersinia pseudotuberculosis* - bridging metabolism and virulence

Dissertation

zur Erlangung des Grades

des Doktors der Ingenieurwissenschaften

der Naturwissenschaftlich-Technischen Fakultät III

Chemie, Pharmazie, Bio- und Werkstoffwissenschaften

der Universität des Saarlandes

von

René Bücker

Saarbrücken

2014

Tag des Kolloquiums:	07. November 2014
Dekan:	Prof. Dr.-Ing. Dirk Bähre
Berichterstatter:	Prof. Dr. Christoph Wittmann
	Prof. Dr. Petra Dersch
Vorsitz:	Prof. Dr. Elmar Heinzle
Akad. Mitarbeiter:	Dr. Björn Becker

VORVERÖFFENTLICHUNGEN DER DISSERTATION

Teilergebnisse aus dieser Arbeit wurden mit Genehmigung der Naturwissenschaftlich-Technischen Fakultät III Chemie, Pharmazie, Bio- und Werkstoffwissenschaften der Universität des Saarlandes, vertreten durch den Mentor der Arbeit, in folgenden Beiträgen vorab veröffentlicht.

Publikationen

Bücker R, Heroven AK, Becker J, Dersch P, Wittmann C (2014) The pyruvate-tricarboxylic acid cycle node: a focal point of virulence control in the enteric pathogen *Yersinia pseudotuberculosis*. *J Biol Chem* **289:** 30114-30132

Tagungsbeiträge

Bücker R, Dersch P, Wittmann C: Metabolic flux analysis of enteropathogenic *Yersinia pseudotuberculosis*, VAAM-Jahrestagung, April 2011, Karlsruhe, Germany

Bücker R, Becker J, Heroven AK, Dersch P, Wittmann C: Systems biology of the pathogenic bacterium *Yersinia pseudotuberculosis*, VAAM-Jahrestagung, March 2012, Tübingen, Germany

Bücker R, Becker J, Heroven AK, Dersch P, Wittmann C: Interplay between carbon core metabolism and virulence in the human pathogenic bacterium *Yersinia pseudotuberculosis*, SPP 1316 Host-Adapted Metabolism of Bacterial Pathogens - 2. Statusseminar, October 2012, Obergurgl, Austria

Bücker R, Heroven AK, Becker J, Dersch P, Wittmann C: Combined fluxome and transcriptome profiling of *Yersinia pseudotuberculosis*, SPP 1316 Host-Adapted Metabolism of Bacterial Pathogens - ^{13}C Metabolic Flux Analysis Workshop, February 2013, Braunschweig, Germany

MITWIRKUNG

Kooperationspartner

Dr. Ann Kathrin Heroven (Gruppe von Prof. Dr. Petra Dersch, Abteilung Molekulare Infektionsbiologie, Helmholtz-Zentrum für Infektionsforschung, Braunschweig, Deutschland) hat die gentechnischen Arbeiten, die Transkriptomanalysen und die Mausinfektionsexperimente durchgeführt.

Dr. Aaron Mischa Nuss (Gruppe von Prof. Dr. Petra Dersch, Abteilung Molekulare Infektionsbiologie, Helmholtz-Zentrum für Infektionsforschung, Braunschweig, Deutschland) hat die Western Blot Analysen und fluoreszenzgestützte Durchflusszytometrie der in Kapitel 5.3 gezeigten Experimente durchgeführt.

Studenten

Teile der in dieser Arbeit veröffentlichten Ergebnisse wurden von den nachfolgend aufgeführten Studenten unter Anleitung erarbeitet.

Tabea Rook hat im Rahmen ihrer Bachelorarbeit „Aufklärung metabolischer Stoffflüsse in *Yersinia pseudotuberculosis* unter Einfluss therapeutisch relevanter Antibiotika“ (2012) am Institut für Bioverfahrenstechnik in Braunschweig die Kultivierungen und die anschließende Analytik der in Kapitel 5.2 bearbeiteten Fragestellung durchgeführt.

Sandra Zimmermann hat im Rahmen ihrer Bachelorarbeit „Analyse der Bistabilität des temperaturabhängigen Virulenzfaktors RovA in *Yersinia pseudotuberculosis*“ (2012) am Institut für Bioverfahrenstechnik in Braunschweig Kultivierungen und Probenaufarbeitungen für die in Kapitel 5.3 bearbeitete Fragestellung durchgeführt.

DANKSAGUNG

An erster Stelle möchte ich mich ganz herzlich bei meinem Doktorvater Prof. Dr. Christoph Wittmann für die Betreuung und für die Übernahme des Referats bedanken. Ich habe es sehr geschätzt, dass es neben der sehr guten und intensiven Betreuung immer ausreichend Raum für eigene Ideen gab. Die daraus resultierende Mischung aus konstruktiver Anleitung und wissenschaftlicher Freiheit ist jedem Doktoranden zu wünschen.

Bei Prof. Dr. Petra Dersch bedanke ich mich für die Übernahme des Korreferats, die hervorragende Kooperation und die vielen konstruktiven Gespräche.

Bei Dr. Judith Becker bedanke ich mich für das stets offene Ohr, die vielen Ratschläge und den Anstoß zur Promotion in dieser Arbeitsgruppe.

Dr. Ann Kathrin Heroven und Dr. Aaron Mischa Nuss danke ich für die sehr gute Kooperation.

Yvonne Göcke, Elena Kempf, Sandra Hübner und Cord Hullmann möchte ich für die immer perfekt organisierten und einsatzbereiten Labore danken. Darüber hinaus war bei Problemen und Fragen immer einer von euch zur Stelle, besser geht es nicht.

Mein besonderer Dank gilt Detlev Rasch. Ohne deine handwerklichen Fähigkeiten und Verbesserungsvorschläge hätte ich viele Ideen nicht umsetzen können.

Meinen Studenten Sören Starck, Tabea Rook, Sandra Zimmermann, Lea Tchaptchet und Sabine Will danke ich für die gute Zusammenarbeit.

Weiterhin möchte ich allen Mitgliedern des „SPP 1316: Wirtsadaptierter Metabolismus von bakteriellen Infektionserregern“ für die wissenschaftlichen Vorträge, Diskussionen sowie für die netten Runden im Anschluss danken.

Der Deutschen Forschungsgemeinschaft und dem Future Fund der TU Braunschweig danke ich für die finanzielle Unterstützung.

Rudolf Schäfer danke ich für das geduldige Zuhören und Beratschlagen über das merkwürdige Verhalten pathogener Mikroorganismen sowie für die vielen technisch versierten Diskussionen, die auch mal über laborrelevante Themen hinausgingen.

Dem ganzen Team aus Braunschweig und Saarbrücken danke ich für die gute Zusammenarbeit, das hervorragende Arbeitsklima und für die vielen netten Abende. Ein ganz besonderes Highlight in fast jeder Woche war das gemeinsame Fußballspiel und der schön zelebrierte Videoabend. Suit up!

Meinen Eltern möchte ich von ganzem Herzen dafür danken, dass sie mir den Weg bis zur Promotion so leicht wie möglich gemacht haben. Ich konnte immer auf eure volle Unterstützung bauen. Das werde ich euch nie vergessen.

Meinen Großeltern und meiner Schwester danke ich für das Interesse an meiner Arbeit und für die motivierenden Worte. Ohne euch wäre das Leben nur halb so schön.

Am Ende möchte ich dir, der wichtigsten Person in meinem Leben, danken. Wir haben so ziemlich alles bis hierhin gemeinsam erlebt und dazu gehört nun auch die Promotion. Luise, ich danke dir für die vielen Aufmunterungen, für deine Geduld und für deine Hilfe in allen Lebenslagen.

TABLE OF CONTENTS

SUMMARY

Yersinia pseudotuberculosis is a human pathogen that causes acute intestinal and systemic diseases. This study investigated the link between pathogenic traits and the metabolic core machinery of *Y. pseudotuberculosis* using a systems biology approach: the integration of gene expression profiles with metabolic pathway fluxes in the wild type and virulence regulator mutants. The absence of specific virulence regulators particularly perturbed fluxes and gene expression of pyruvate metabolism and tricarboxylic acid cycle, suggesting an involvement of this metabolic node in the virulence management system. Mutants, genetically perturbed in regulators of this metabolic branch point and one of its central enzymes, showed a significant reduction of virulence in an oral mouse infection model. This revealed the pyruvate-TCA cycle node as a focal point for controlling host colonization. Flux rerouting was also identified as response to applied antibiotic therapies. The examination of *Yersinia's* fine-tuned adaptation was expanded to temperature, an important infection parameter, using a continuous culture with advanced temperature control to mimic the infection process. The virulence regulator RovA, known to respond to temperature and to control metabolic, stress, and virulence genes, was quantified by Western blot analysis and fluorescence-activated cell sorting. RovA showed a bistable behavior that generally maximizes survival by heterogeneity.

ZUSAMMENFASSUNG

Das humanpathogene Bakterium *Yersinia pseudotuberculosis* verursacht ernsthafte intestinale und systemische Erkrankungen. In dieser Arbeit wurde die Verknüpfung von Pathogenität und Metabolismus in *Yersinia pseudotuberculosis* unter Verwendung von Transkriptom- und metabolischen ^{13}C-Stoffflussanalysen untersucht. Virulenz-Regulator-Mutanten wiesen im Vergleich zum Wildtyp starke Veränderungen im Pyruvatmetabolismus und im Zitratzyklus auf. Die gezielte genetische Deregulation dieses Stoffwechselknotenpunktes führte zu Mutanten mit stark reduzierter Virulenz im Mausmodell. Der Pyruvat-Zitronensäure-Knoten konnte demnach als ein zentraler Punkt der Virulenzregulation identifiziert werden. Der Einfluss verschiedener Antibiotika auf die Stoffflussverteilung wies darüber hinaus auf einen komplexen Zusammenhang von Metabolismus und inhärenter Resistenz hin. Die feinregulierte Anpassung des Organismus während der Infektion wurde weiterführend anhand des temperaturabhängigen Transkriptionsregulators RovA untersucht, der Gene des Metabolismus, der Stressantwort und des Virulenzprogramms der Zelle kontrolliert. Der Infektionsprozess wurde dazu in einer kontinuierlichen Kultur mit präziser Temperaturführung simuliert. Western Blot Analysen und fluoreszenzgestützte Durchflusszytometrie zeigten bistabiles Verhalten des Proteins RovA. Die daraus hervorgehende Heterogenität der Population kann die Überlebenswahrscheinlichkeit der Gesamtpopulation erhöhen.

1 INTRODUCTION

In 2010, approximately 10 million people died worldwide through infectious diseases, accounting for about 20% of all death cases. More than half of such fatal infections are related to common diseases like diarrhea, lower respiratory infections, or meningitis (Lozano *et al,* 2012). Favorably, intensive research has decreased the danger and death cases of infections. However, in terms of the number of victims, infectious diseases are still a significant burden for public health and further deserve intensive investigation. This is complicated by the emergence of new threats. New pathogens are constantly released from animal reservoirs and from human-adapted agents, respectively, by virulence gene transfer and mutation (Morens & Fauci, 2013). As an example, the emergence of *Yersinia pestis* from the zoonotic bacterium *Yersinia pseudotuberculosis* is responsible for one of the most fatal pandemics in human history resulting in 50 million deaths (Morens *et al,* 2008). Although genetically almost identical, *Y. pseudotuberculosis* and *Y. pestis* differ significantly in terms of host entry and process of infection. *Y. pseudotuberculosis* enters the host via oral uptake and subsequent adhesion to and translocation through intestinal cells (Grützkau *et al,* 1990; Isberg & Leong, 1990) leading finally to diarrhea, enteritis, and colitis (Figure 1). In contrast, *Y. pestis* is transmitted via flea bites (Achtman *et al,* 1999) and causes severe septicemia that mostly leads to death, if it remains untreated (Bosio *et al,* 2012). *Yersinia enterocolitica*, the third pathogenic yersiniae member, is phylogenetically more distant to *Y. pseudotuberculosis,* but causes a rather similar infection process (Wren, 2003). At the intersection of two different pathogenic life styles, the analysis of *Y. pseudotuberculosis* provides the opportunity to gain an in-depth understanding of virulence. The infection process of yersiniae is accompanied by constantly changing environmental conditions and the immune

defense mechanisms of the host. *Y. pseudotuberculosis*, e.g., passes the acidic stomach and then enters the different parts of the intestine. Here, *Yersinia* competes with the indigenous microbiota. Every member of this microbial community is perfectly coordinated with one another and inhabits a specific niche (Njoroge *et al,* 2012).

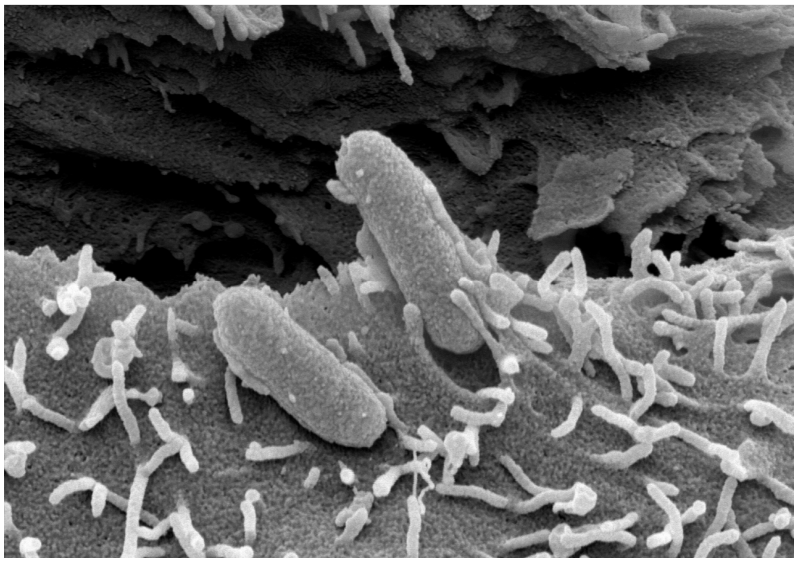

Figure 1. Raster electron micrograph of *Yersinia pseudotuberculosis* on Caco-2 cells (Picture by Manfred Rohde, Department of Molecular mechanisms of streptococci, Helmholtz Centre for Infection Research, Braunschweig, Germany).

Hence, *Y. pseudotuberculosis* faces strong competition for carbon and energy sources and has to defense against the immune system of the host. Thus, a successful colonization relies on accurate adjustment of virulence gene expression to use scarce resources effectively (Njoroge *et al,* 2012). In this context, the question arises, whether virulence factors are controlled by available trigger substances (Lawhon *et al,* 2002) or even by specific metabolic phenotypes as consequence of an integrated output of impact factors. Since systems-wide approaches have been proven useful to find relations between so far unassociated microbial behaviors, their application to pathogenic bacteria promises enhanced understanding of such complex systems.

2 OBJECTIVES

The main object of the present work aims at understanding the role of metabolism in virulence control of the pathogenic model bacterium *Y. pseudotuberculosis*. In anticipation of the complexity of the involved metabolic and regulatory networks, a systems biology approach using state-of-the-art ^{13}C-based fluxome and array-based transcriptome analysis should be developed and applied. As such analyses require high reproducibility and accuracy, a convenient cultivation strategy for *Y. pseudotuberculosis* should be developed first. The established cultivation set-up should subsequently be used to analyze defined gene deletion mutants lacking major virulence regulators with different hierarchical positions within the virulence control cascade. The determined metabolic phenotype, i.e., the fluxome, should then be integrated with transcriptome data to correlate metabolic states with virulence control. The integration should provide new insights into the life style of *Y. pseudotuberculosis.* In addition, the contribution of the core metabolism of *Y. pseudotuberculosis* should be investigated in context of its defense role against external threats like antimicrobial agents. At best, promising novel targets, identified from the systems biology analysis and related to virulence control, should be characterized through profiling of second generation mutants, including mouse infection studies to investigate their relevance *in vivo*. Finally, selective studies should also explore the dynamic of metabolic and regulatory networks of *Yersinia pseudotuberculosis.*

3 THEORETICAL BACKGROUND

3.1 Clinical relevance of *Yersinia pseudotuberculosis*

In mammals, including humans, *Yersinia pseudotuberculosis* causes gut-associated diseases, such as diarrhea, enteritis, and colitis. The threat of *Yersinia pseudotuberculosis* is underdetermined by the fact that it causes severe bloodstream infections with a death probability up to 75% (Mandell *et al,* 2009; Kaasch *et al,* 2012). Several recent foodborne outbreaks in industrial countries like Finland or Japan further indicate an on-going impact of this Gram-negative pathogen on society (Nakano *et al,* 1989; Hannu *et al,* 2003; Jalava *et al,* 2006; Rimhanen-Finne *et al,* 2009). Obviously, *Yersinia* remains a serious threat for foodborne infections. Due to its wide-spread distribution among sheep, deer, pig, hare, and even birds, contamination of vegetable fields by an animal reservoir seems likely (Tauxe, 2004). In addition to its clinical relevance, *Y. pseudotuberculosis* is important as an evolutionary ancestor of *Y. pestis*, the agent of plague (Achtman *et al,* 1999). *Y. pestis* evolved just 1,500 – 20,000 years ago and shows an almost identical genetic background. There seems to be only one exclusive determinant that significantly enhances infection by *Y. pestis* as compared to *Y. pseudotuberculosis*: a plasmid encoded phospholipase D homolog (Achtman *et al,* 1999). Acquisition of plasmid pFra, coding for the phospholipase D homolog, appears sufficient for *Y. pseudotuberculosis* to evolve to one of the world's worst pathogen. Due to this, the investigation of the life style and the infection process of *Y. pseudotuberculosis*, as aimed in this work, is important towards understanding of two human pathogenic bacteria.

3.2 *Yersinia pseudotuberculosis* - Life style and infection process

The typical infection route of *Y. pseudotuberculosis* occurs via oral uptake and binding to the intestinal epithelium (Isberg & Leong, 1990). Contact and invasion of the epithelia is mediated by invasin. It recognizes β_1 chain integrins that are exclusively provided by microfold cells (M cells). After translocation, *Yersinia* attaches to phagocytic cells located within the encountered region between epithelium and Peyer's patches, the subepithelial dome. The immune response is then paralyzed by several Yersinia outer proteins (Yop) that are channeled through a type III secretion apparatus into immune cells (Isberg & Barnes, 2001). Subsequently, the pathogen spreads into the lymphatic system, where it rapidly multiplies and colonizes deeper tissues, such as mesenteric lymph nodes, liver, and spleen (Figure 2) (Dube, 2009).

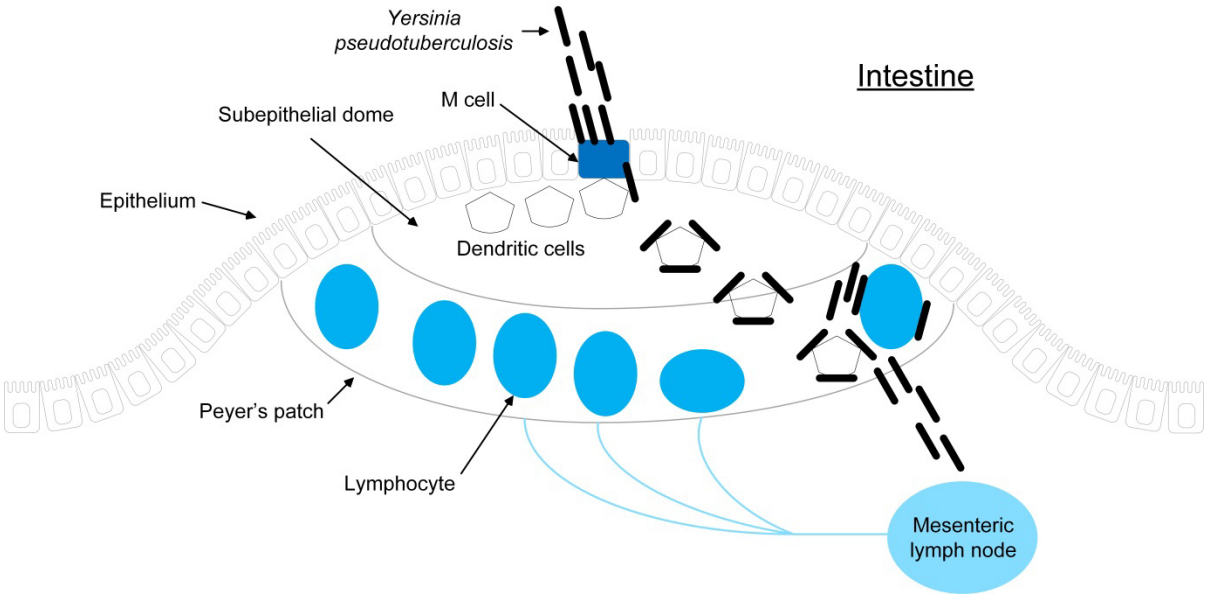

Figure 2. Process of infection. After attachment, internalization, and translocation of microfold cells (M cells), *Yersinia* reaches the subepithelial dome. Here, attachment to dendritic cells and inactivation of the immune defense occurs. Paralyzed dendritic cells then carry the pathogen into the Peyer's patches, where it rapidly multiplies and disseminates into deeper tissues. The figure is adapted from (Mowat, 2003) and (Isberg & Barnes, 2001).

In order to promote its pathogenic life style, *Y. pseudotuberculosis* has developed global regulatory cascades that coordinate physiological processes and virulence

factors and initiate infection by expression of the major invasive factor: invasin. Several regulators of these cascades suggest a link between virulence and core metabolism of the pathogen. Over the last few years, it has become evident that the catabolite repressor protein (Crp) and the carbon storage regulator A (CsrA) are involved in virulence management in addition to their well-known function as metabolic regulators (Figure 3) (Heroven *et al,* 2012a; Heroven *et al,* 2012b). CsrA is a RNA-binding regulator protein, which itself is controlled by the small non-coding RNAs CsrB and CsrC. CsrA is also involved in controlling the major transcriptional regulator of virulence (RovA) and its transcriptional repressor (RovM). In the absence of CsrA, expression of RovM is reduced, and lower levels of the repressor then lead to higher amounts of RovA (Heroven *et al,* 2008) and subsequent expression of invasin, thus mediating attachment to and entry into the intestinal epithelium (Figure 2) (Nagel *et al,* 2001). The Crp protein influences the expression of *rovA* through counter-regulation of the Csr RNAs either directly or through the UvrY response regulator (Figure 3). Crp and CsrA are pivotal for a successful *Yersinia* infection (Heroven *et al,* 2012b). Crp also affects the virulence and metabolism of *Y. pestis* (Zhan *et al,* 2008). In addition to the coordinated expression of virulence factors, the ability to efficiently compete for nutrients is crucial for a successful infection, i.e., the bacteria must outcompete the gut microbiota and persist long-term within the intestinal tract (Chang *et al,* 2004; Hofreuter *et al,* 2008). As described above, the expression of RovA is crucial for the scheduled provision of invasin. In addition to concerted regulation of RovA by Crp, CsrA, and RovM (Figure 3), RovA abundance varies with temperature, osmolarity, pH, growth phase, and nutrient status. Maximum levels are found at ambient temperature (20 - 28°C) and in stationary growth phase.

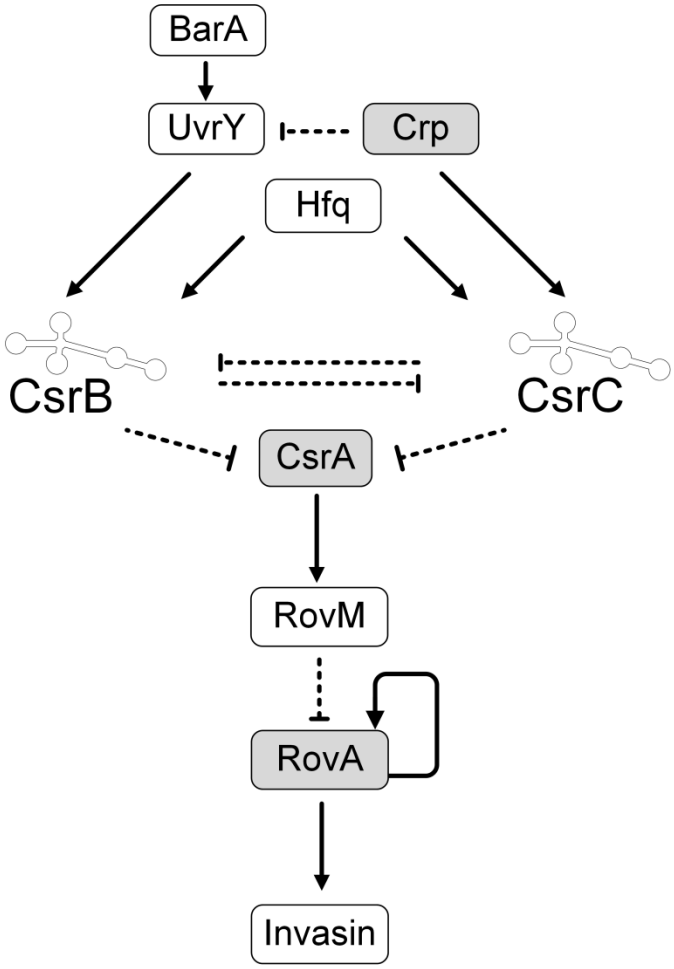

Figure 3. Regulatory network of the virulence genes of *Y. pseudotuberculosis*. The interactions involve activation (arrows) and repression (dashed lines). The impact of the catabolite repressor protein (Crp), the carbon storage regulator protein A (CsrA), and the regulator of virulence A (RovA) on central metabolism was investigated in this work. The corresponding regulators are displayed in grey boxes. This figure is adapted from (Heroven *et al,* 2012b).

During batch culture, *rovA* expression emerges within the mid-log phase and then increases continuously (Nagel *et al,* 2001). An osmolarity level equal to the physiological value of the gut (Sleisenger, 1981) is favorable for *rovA* expression. In contrast, pH lower than seven results in drastic decrease of RovA. Host temperature significantly reduces RovA abundance, independent of further parameters (Herbst *et al,* 2009). Nutrient rich media favor *rovA* expression, whereas minimal media stimulate *rovA* expression only weakly. Additionally, *rovA* expression is auto-regulated (Figure 4) (Nagel *et al,* 2001).

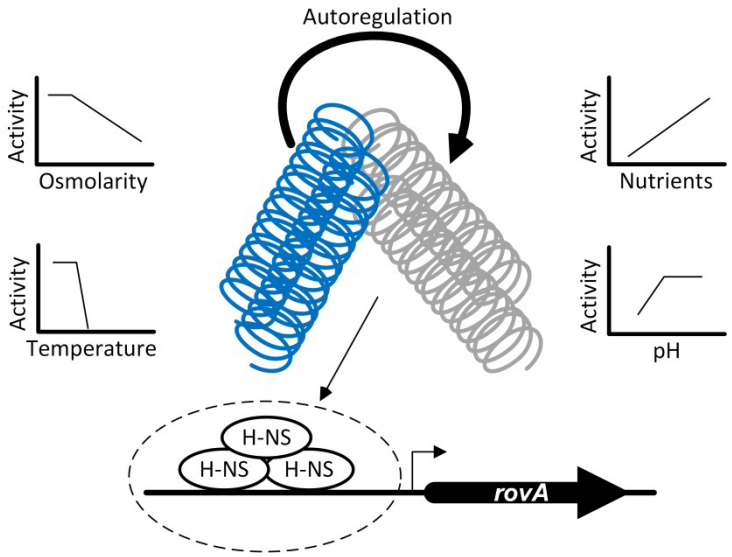

Figure 4. Factors that influence the expression of RovA (regulator of virulence A) in *Yersinia pseudotuberculosis*. Expression is reduced at high osmolarity, low pH values, low nutrient availability (Nagel *et al,* 2001), and at 37°C (Herbst *et al,* 2009). The nucleoid-associated protein (H-NS) binds with high affinity to the promoter region of *rovA* and, thus, inhibits positive autoregulation (Heroven *et al,* 2004). At ambient temperature, RovA shows higher affinity and is able to suppress H-NS. Given plots schematically illustrate the tendency of RovA activity as function of the individual parameters.

Taken together, temperature has a prominent impact on virulence control of *Yersinia pseudotuberculosis*. Therefore, further studies have investigated temperature dependence of RovA in more detail. At host temperature, a reversible conformational change occurs, which leads to reduced promoter affinity to target genes and increased susceptibility to degradation (Herbst *et al,* 2009). Furthermore, the nucleoid-associated protein H-NS binds with high affinity to the promoter of *rovA*, and hence, prevents transcription. At 25°C, a drastically increased promoter affinity of RovA suppresses H-NS binding and leads to readmission of *rovA* expression (Figure 4) (Heroven *et al,* 2004). To date, the temperature dependence of RovA was mainly described qualitatively. A more precise quantitative correlation of RovA levels with temperature would allow the construction of kinetic models towards better understanding of the underlying interaction.

3.3 Virulence promoting metabolism of *Yersinia pseudotuberculosis*

One of the key questions that arise from our current knowledge of *Yersinia's* virulence revolves around the metabolic core machinery of the cell. A first cross-view on *Yersinia's* metabolic repertoire can be obtained from its genome annotation (Kyoto Encyclopedia of Genes and Genomes) (Figure 5). *Y. pseudotuberculosis* harbors phosphotransferase systems (PTS) for uptake of carbohydrates, such as glucose. Glycolytic conversion of glucose 6-phosphate occurs via the Embden-Meyerhof-Parnas (EMP) pathway and the Entner-Doudoroff (ED) pathway, respectively. However, the major role of the ED pathway seems to be related to catabolism of specific carbohydrates, like gluconate (Conway, 1992). In accordance with its close relative *Escherichia coli,* a complete pentose phosphate (PP) pathway for NADPH supply by glucose 6-phosphate dehydrogenase and by 6-phosphogluconate dehydrogenase, respectively, is present in *Y. pseudotuberculosis*. The pyruvate metabolism encompasses anaplerotic PEP (phosphoenolpyruvate) carboxylase, gluconeogenetic PEP carboxykinase, and NADP-dependent malic enzyme. For maintaining appropriate NAD/NADH ratios at substrate overflow, *Yersinia* possesses lactate and acetaldehyde/alcohol dehydrogenases. A quinone-reducing pyruvate dehydrogenase delivers quinol as alternative reducing equivalent. Acetyl-CoA can either be metabolized via the tricarboxylic acid (TCA) cycle or via the glyoxylate shunt (Figure 5). Although metabolic regulators are directly involved in the control of crucial infection determinants, metabolic requirements of *Yersinia* for adapting to and surviving in different host niches are largely unknown.

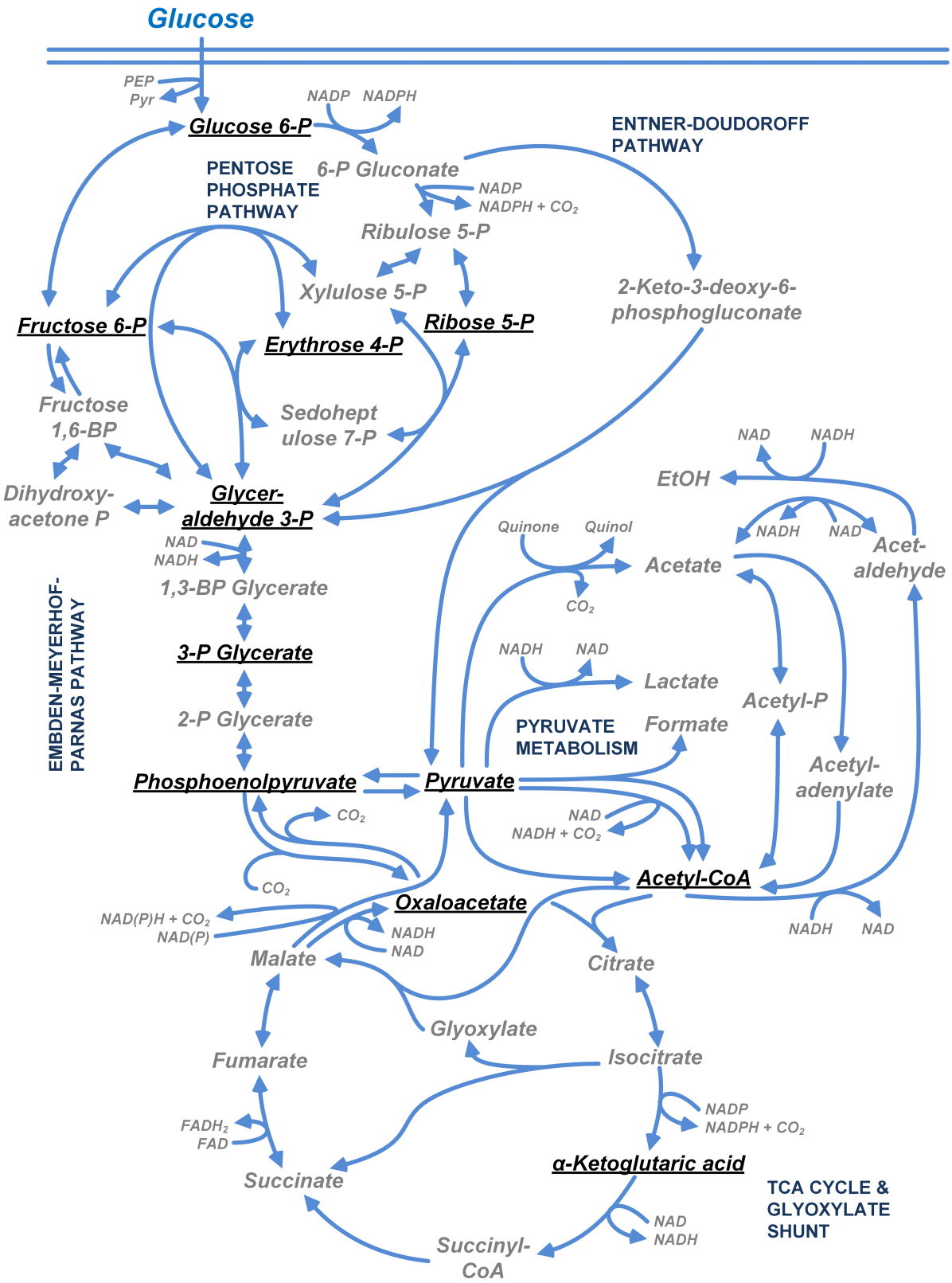
Glucose
PEP
Pyr
NADP NADPH
Glucose 6-P
ENTNER-DOUDOROFF PATHWAY
PENTOSE PHOSPHATE PATHWAY
6-P Gluconate
NADP
NADPH + CO2
Ribulose 5-P
Xylulose 5-P
2-Keto-3-deoxy-6-phosphogluconate
Fructose 6-P
Ribose 5-P
Erythrose 4-P
Fructose 1,6-BP
Sedohept ulose 7-P
NAD NADH
EtOH
Dihydroxy-acetone P
Glycer-aldehyde 3-P
Quinone Quinol
NADH NAD
Acet-aldehyde
NAD
NADH
Acetate
1,3-BP Glycerate
CO2
EMBDEN-MEYERHOF-PARNAS PATHWAY
3-P Glycerate
NADH NAD
Lactate
Acetyl-P
2-P Glycerate
PYRUVATE METABOLISM
Formate
Acetyl-adenylate
Phosphoenolpyruvate
Pyruvate
CO2
NAD
NADH + CO2
CO2
Acetyl-CoA
Oxaloacetate
NAD(P)H + CO2
NAD(P)
NADH
NAD
NADH NAD
Malate
Citrate
Glyoxylate
Fumarate
Isocitrate
NADP
NADPH + CO2
FADH2
FAD
α-Ketoglutaric acid
Succinate
TCA CYCLE & GLYOXYLATE SHUNT
NAD
NADH
Succinyl-CoA

◄**Figure 5.** Central carbon metabolism of *Yersinia pseudotuberculosis* (YPIII). The reaction arrows point towards the physiological direction (glucose as sole carbon source, fully aerobic growth). In *Yersinia*, a wide set of pathways is available: Embden-Meyerhof-Parnas (EMP) pathway, Entner-Doudoroff (ED) pathway, pentose phosphate (PP) pathway, tricarboxylic acid (TCA) cycle and glyoxylate shunt. Pyruvate metabolism encompasses conversion by anaplerotic phosphoenolpyruvate (PEP) carboxylase (*ppc*) and by gluconeogenetic PEP carboxykinase (*pckA*). For maintaining appropriate NAD/NADH ratios at substrate overflow, *Yersinia* possesses lactate and acetaldehyde/alcohol dehydrogenase (*ldh*, *adhE*). NADPH is provided by glucose 6-phosphate dehydrogenase (*zwf*), 6-phosphogluconate dehydrogenase (*gnd*), malic enzyme (*maeB*) and isocitrate dehydrogenase (*icdA*). Furthermore, reducing equivalents are supplied by glyceraldehyde 3-phosphate dehydrogenase (*gapA*), pyruvate dehydrogenase (*aceEF*, *lpdA*), α-ketoglutarate dehydrogenase (*sucAB*), succinate dehydrogenase (*sdhABCD*), malate dehydrogenase (*mdh*, *sfcA*) and quinone-reducing pyruvate dehydrogenase (*poxB*). Substrate-level phosphorylation is catalyzed by phosphoglyceratekinase (*pgk*), by pyruvate kinase (*pykAF*), by succinyl-CoA synthetase (*sucCD*) and by acetate kinase (*ackA*). Intermediary metabolites serving as biomass precursors are given in black letters. Data are taken from genome annotation (Kyoto Encyclopedia of Genes and Genomes).

First studies indicate a highly complex network of interactions, e.g., insufficient supply of PTS-sugars activate adenylate cyclase (Escalante *et al,* 2012), which then activates Crp and subsequent virulence regulatory cascades (Heroven *et al,* 2012b). It remains to be elucidated, how metabolism and pathogenic habits are intertwined in *Y. pseudotuberculosis*. Further evidence on close connections between metabolism and pathogenicity comes from studies that investigated resistance in pathogenic bacteria. Recent exometabolome profiling of *Staphylococcus aureus*, treated with antibiotics, revealed an accumulation of pyruvate and fermentation products (Birkenstock *et al,* 2012). Genomic studies further identified selected enzymes of central carbon metabolism to support persistence under antibiotic treatment (Spoering *et al,* 2006; Ma *et al,* 2010; Girgis *et al,* 2012; Leung & Lévesque, 2012). Obviously, detailed analysis of metabolism may even help to identify new drug targets.

3.4 Metabolism as part of the resistome – the intrinsic bacterial resistance

The intrinsic resistome comprises natively encoded elements of the chromosome, which directly or indirectly provide an increased resistance to administered antimicrobial agents (Figure 6) (Olivares *et al,* 2013).

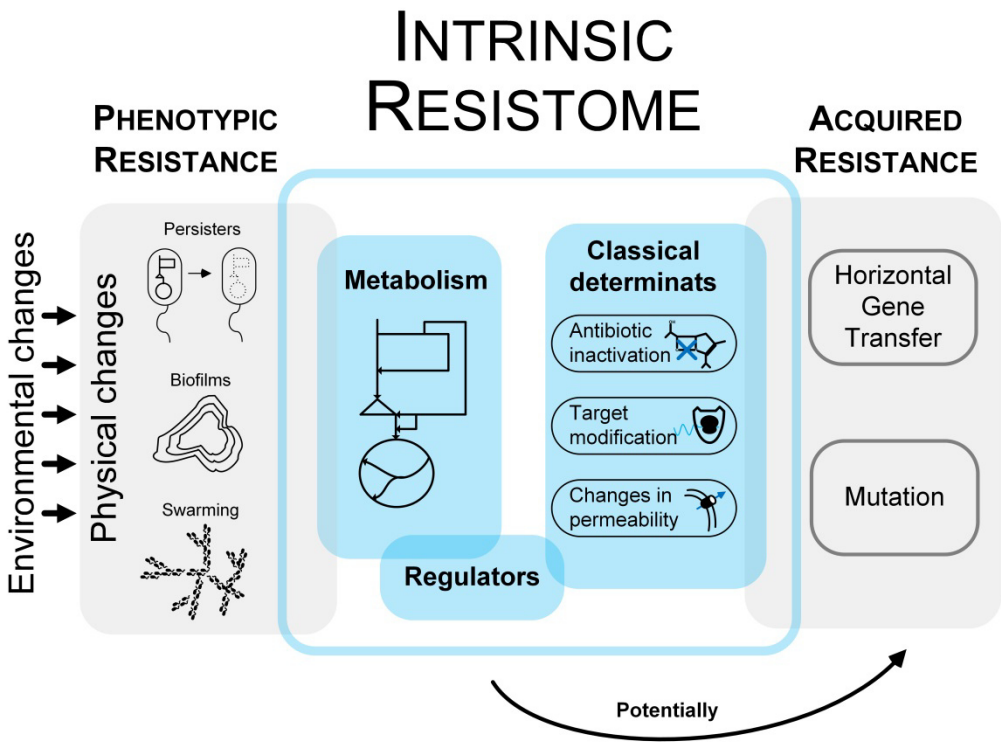

Figure 6. The intrinsic resistome comprises elements of metabolism, regulation, and classical determinants that contribute to resistance against antimicrobial agents. Classical determinants, e.g., antibiotic inactivating enzymes can further be acquired by means of horizontal gene transfer or mutation. These elements do not belong to the intrinsic resistome. Phenotypic resistance like biofilm formation can be classified as a consequence of the bacterial intrinsic capabilities to counteract antibiotic agents. This figure is adapted from (Olivares *et al,* 2013).

In addition to classical resistant determinants like multi drug efflux pumps, antibiotic-inactivating or target-modifying enzymes, respectively, the resistome encompasses all kinds of regulators and metabolic factors that contribute to bacterial resistance and have not been acquired as a consequence of antibiotic use in society (Olivares *et al,* 2013). A regulator of the intrinsic resistome is not necessarily involved

in control of classical resistance determinants or the general stress response. However, expression of the DNA repair machinery, as consequence of quinolone treatment, is a famous example of intrinsic resistance (Howard *et al,* 1993; Olivares *et al,* 2013). Further beneficial regulatory events may concern rather general aspects of bacterial metabolism (Olivares *et al,* 2013). In this context, activation of proton-motif force in persister cells by administration of specific metabolites was shown to increase susceptibility to aminoglycosides (Allison *et al,* 2011). Thus, the metabolic state of an organism plays a crucial role for intrinsic resistance. Analysis of the complex conjunction of metabolism, regulation and resistance bear the chance to uncover new targets for antimicrobial agents that have not been considered so far. A detailed understanding of the underlying processes of the intrinsic resistome may further help to avoid actions that favor evolution of resistance (Olivares *et al,* 2013).

3.5 Systems-level analysis of biological systems

Although there is lot of available information about virulence and first insights into metabolic responses to administration of antimicrobial agents, it was not possible so far to elucidate the underlying processes to great detail. Based on recent advances in systems biology, powerful tools are now available that allow experimental and computational analyses of complex biological systems. Shortly, such systems biology approach investigates the cells' state through global monitoring of component concentrations (Sauer, 2006). Although analysis of the transcriptome successfully unraveled *Yersinia's* virulence regulation cascade (Heroven *et al,* 2012b), this technology fails to describe the cells actual status on its own. The relative abundance of mRNA does not *per se* correlate with protein activity and despite all efforts made to ensure significance, a serious chance for misinterpretation is left.

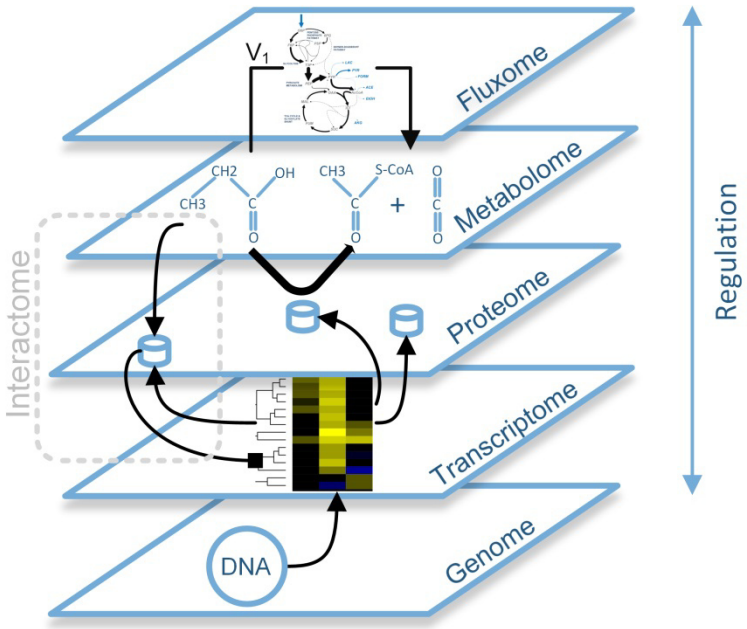

Figure 7. Interplay of transcriptome, proteome and metabolome as complex functions of each other with the fluxome as integrated output and, hence, metabolic phenotype of the cell. The genome functions as the source of information. This figure is adapted from (Kohlstedt *et al,* 2010) and (Nielsen & Oliver, 2005).

Protein and metabolite concentrations are also subject to a non-consistent correlation between quantity and activity. To sum up some essential points, translation is dependent on transcript availability and the overall activity of the translational apparatus. The overall activity of derived protein is then controlled by, e.g., abundance, phosphorylation status, presence of degrading enzymes, and metabolites acting either as reactants, activators, or inhibitors. The concentration of each metabolite is in turn subject to the integration of all enzymatic reactions that consume or build this component (Nielsen & Oliver, 2005). The integrated output of all these interactions is the metabolic phenotype, represented by the metabolic flux distribution of the cell: the fluxome (Figure 7). Therefore, the fluxome is at the heart of analyzing complex systems. A combined approach of fluxomics and transcriptomics appears useful to integrate metabolic and regulatory networks (Krömer *et al,* 2004; Buschke *et al,* 2013). The latter will help to evaluate the underlying regulation principle and may link the metabolic response of central carbon metabolism to further

unknown properties of the cell. This appears particularly useful to unravel the obviously complex links between virulence and metabolism. Admittedly, there is only one study that analyzes *Yersinia* virulence mechanisms with a systems biology approach (Ansong *et al,* 2013). Metabolic flux analysis evolved mainly in biotechnology research as flux data proved useful to guide rational strain design (Kohlstedt *et al,* 2010). A large number of successful applications confirmed ^{13}C metabolic flux analysis as a powerful tool to unveil specific pathways as crucial control elements towards formation of the target product. In lysine-producing *Corynebacterium glutamicum*, the NADPH delivering pentose phosphate (PP) pathway was identified as such a control element. This insight was deciphered by comparing different mutants on the metabolic flux level (Wittmann & Heinzle, 2002). Through subsequent genomic modifications, lysine production was increased by about 50% (Becker *et al,* 2007). In more recent years, ^{13}C metabolic flux analysis has been extended to a broader field of applications. The investigation of the network-wide balancing of reducing equivalents (Fuhrer & Sauer, 2009), the disclosure of flux distributions in the rarely analyzed clade of *Roseobacter* (Fürch *et al,* 2009), identification of unusual metabolic routes in *Mycobacterium tuberculosis* (Beste *et al,* 2011), and niche specific metabolic adaption of different clinical isolates of *Pseudomonas aeruginosa* (Berger *et al,* 2014) are excellent examples for the advanced appropriability of this technology.

3.6 Concept of ^{13}C metabolic flux analysis

The typical work-flow to assess the intracellular flux distribution of an intact and living cell under a certain condition can be divided into an experimental (A) and a computer-assisted (B) part (Figure 8). The calculation of intracellular fluxes typically requires measurement of substrate uptake, by-product formation, biomass formation, biosynthetic requirements, and ^{13}C labeling data from ^{13}C tracer experiments. Input and output fluxes can be directly inferred from measurements in culture broth using, e.g., HPLC or enzymatic assays. The complex and intertwined pathways of central carbon metabolism, some of which include complex fine structures as parallel or cyclic reactions, can only be calculated with direct information from reaction participants (Kohlstedt *et al,* 2010). This information is accessible by use of ^{13}C-labeled substrates. Depending on the underlying metabolism, a characteristic mass isotopomer distribution is derived from different positional isotopomers (molecules with a specific number and position of ^{13}C carbon atoms) (Wittmann, 2002). Labeling patterns can be obtained from intracellular metabolites and from amino acids that reflect the carbon backbone of these metabolites by mass spectrometry. Amino acids are much more abundant, stable and easier accessible through cell extracts and hydrolyzed biomass. They can be separated by gas chromatography within less than 30 minutes and provide data with measurement errors below 0.5% (Wittmann, 2007).

Second, the calculation of intracellular fluxes is performed by isotopomer and metabolite balancing (Wittmann & Heinzle, 2002; Krömer *et al,* 2004). The open source software OpenFlux, e.g., compiles the required isotopomer and metabolite balance models from user input (Quek *et al,* 2009). The user input comprises a linear system of equations that represents the stoichiometry of the reaction network and information about the carbon transition of each reaction.

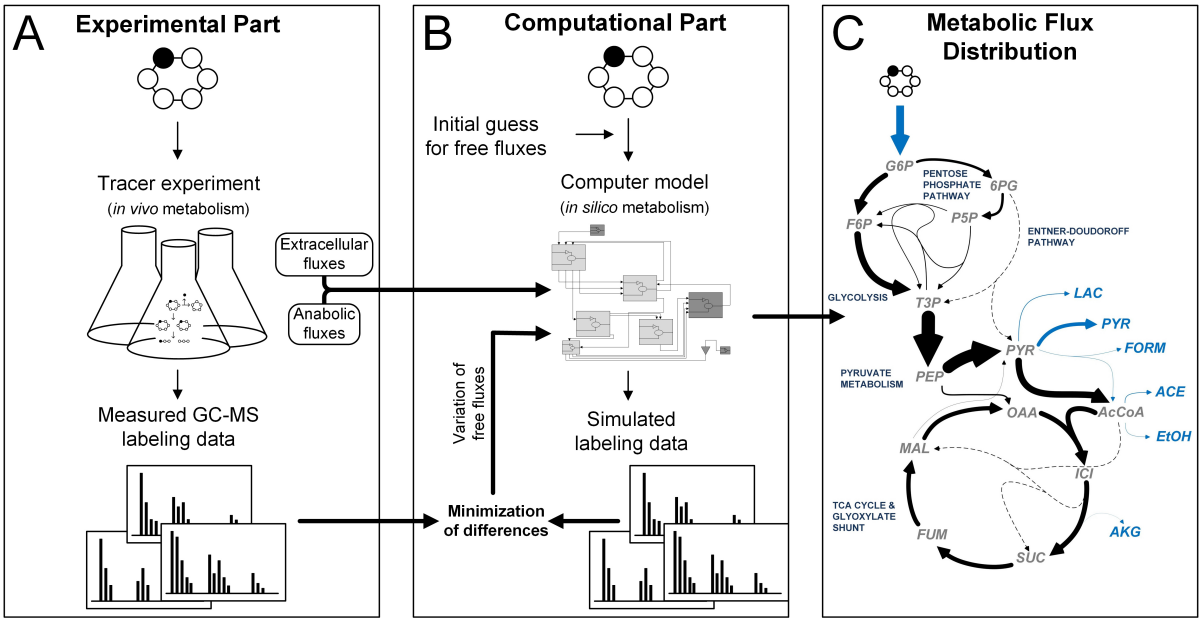

Figure 8. Schematic overview of ^{13}C metabolic flux analysis. Plane **A** illustrates the experimental part. Here, all information is generated by tracer experiments with subsequent analysis of substrate uptake, by-product formation, biomass formation, and labeling patterns. ^{12}C-atoms of intermediary metabolites are illustrated as empty circles, ^{13}C-atoms as filled circles. The computational part **(B)** comprises the construction of the metabolic reaction network, the integration of experimental data, least-square parameter estimation and parameter sensitivity analysis with the modeling software OpenFlux (Quek *et al,* 2009). Plane **C** shows the visualized result of metabolic flux analysis. The relative carbon flux is indicated by the thickness of the arrows. Black arrows are intracellular carbon fluxes, blue arrows represent in- and output fluxes. Abbreviations: G6P, glucose 6-phosphate; F6P, fructose 6-phosphate; 6PG, 6-phosphogluconate; P5P, pentose 5-phosphates; T3P, triose 3-phosphates; PEP, phosphoenolpyruvate; PYR, pyruvate; OAA, oxaloacetate; ICI, isocitrate; SUC, succinate; FUM, fumarate; MAL, malate; LAC, lactate; FORM, formate; ACE, acetate; EtOH, ethanol; AKG, α-ketoglutaric acid; AcCoA, acetyl-CoA. This figure is adapted from (Wittmann, 2007).

At branch points free and independent fluxes need to be assigned. The calculation starts with an initial guess for free fluxes and the subsequent computation of dependent fluxes via stoichiometric mass balances. Gradient solvers can then be used to perform an iterative optimization of free fluxes towards minimal residual errors between computed and measured labeling data. The weighted sum of least-squares is best used as error criterion, thus accuracy of label measurement can be

taken into account. The identification of a global minimum can be verified by variation of initial start values for the free fluxes and repetitive flux estimation (Wittmann & Heinzle, 2002). The best solution of the parameter estimation delivers almost identical ^{13}C labeling data compared to experimental values and, therefore, represents the metabolic fluxes in the living cell (Quek *et al,* 2009).

4 MATERIALS AND METHODS

4.1 Bacterial strains and mutant construction

The strains, plasmids, and primers for genetic construction, used in this work, are listed in Table 1 and 2. The wild type strain *Y. pseudotuberculosis* (YPIII) and the mutants YP3 (Δ*rovA*), YP53 (Δ*csrA*), and YP89 (Δ*crp*) were obtained from (Bölin *et al,* 1982), (Nagel *et al,* 2001), (Heroven *et al,* 2008), and (Heroven *et al,* 2012b), respectively.

Additionally, a set of defined mutant strains was constructed for this work in the group of Petra Dersch (Department of Molecular Infection Biology, Helmholtz Centre for Infection Research, Braunschweig, Germany). Particularly, these were single gene deletion strains: YP49 (Δ*arcA*), YP252 (Δ*ptsN*), YP253 (Δ*pykF*), and YP274 (Δ*pdhR*). DNA manipulation and transformation were performed using standard genetic and molecular techniques, as previously described (Miller, 1992; Sambrook & Green, 2001). For construction of the mutagenesis plasmids pAKH175, pAKH177, and pAKH187, respectively, a PCR fragment harboring a kanamycin resistance gene (*kan*) was generated for insertion into the *ptsN*, *pykF*, or *pdhR* gene (*ptsN*::Kan^R, *pykF*::Kan^R, or *pdhR*::Kan^R). The kanamycin gene was amplified using primer pair I661/I662 and plasmid pKD4 as template. Next, *Yersinia* YPIII genomic DNA was used as template to amplify 300-500 bp regions flanking the target genes. The upstream fragment was amplified with a primer pair of which the reverse primer contained additional 20 nt at the 5′-end which were homologous to the start of the kanamycin cassette (*ptsN*$_{up}$: primer IV971/IV972; *pykF*$_{up}$: primer IV977/IV978; *pdhR*$_{up}$: primer V567/V548). The downstream fragment was amplified with a primer pair of which the forward primer contained additional 20 nt at the 3′-end which were

homologous to the end of the kanamycin cassette (*ptsN*$_{down}$: primer IV973/IV974; *pykF*$_{down}$: primer IV979/IV980; *pdhR*$_{down}$: primer V549/V550). In the next step, a PCR reaction was performed with the forward and the reverse primer using the upstream and downstream PCR products of the respective target gene and the *kan* gene fragment as templates. The resulting fragment was digested with *Sac*I and ligated into the *Sac*I site of pAKH3. Construction of the *Y. pseudotuberculosis* YPIII *arcA*::Kan^R mutant YP49 was performed by allelic exchange as described previously (Derbise *et al,* 2003; Heroven *et al,* 2008). The kanamycin gene was amplified from pACYC177 with the primer pair 360/361. The upstream and downstream fragment, flanking the *arcA* gene, was amplified with primer pair 655/656 and 657/658, respectively. Each fragment contained 20 nucleotides, homologous to the *kan* gene. In the next step, a PCR reaction was performed with the forward primer of the upstream fragment and the reverse primer of the downstream fragment, using the upstream and downstream PCR products of the target gene and the *kan* PCR fragment as template. The PCR fragment was transformed into *Y. pseudotuberculosis* YPIII pKOBEG-*sacB*. Chromosomal integration of the fragment was selected by plating on solid LB medium, supplemented with kanamycin. Mutants were subsequently grown on LB agar plates without NaCl plus 10% sucrose, and faster growing colonies without pKOBEG-*sacB* were selected and proven by PCR and DNA sequencing. The *Yersinia* mutants YP252 (YPIII *ptsN*::Kan^R), YP253 (YPIII *pykF*::Kan^R) and YP274 (YPIII *pdhR*::Kan^R) were constructed as described in (Heroven *et al,* 2012b), using the suicide plasmids pAKH175, pAKH177, and pAKH187.

Table 1. Bacterial strains and plasmids.

Strains, plasmids	Description	Source and reference
E. coli		
S17-λpir	*recA1 thi pro hsdR*$^-$ RP4-2Tc::Mu Km::Tn7 λpir	(Herrero *et al,* 1990)
Y. pseudotuberculosis		
YPIII	pIB1, wild type	(Bölin *et al,* 1982)
YP3	pIB1, *rovA*::Tn*10*(60)[a], Cml^R	(Nagel *et al,* 2001)
YP49	pIB1, Δ*arcA*, Kan^R	This study
YP53	pIB1, Δ*csrA*, Kan^R	(Heroven *et al,* 2008)
YP89	pIB1, Δ*crp*	(Heroven *et al,* 2012b)
YP252	pIB1, Δ*ptsN*, Kan^R	This study
YP253	pIB1, Δ*pykF*, Kan^R	This study
YP274	pIB1, Δ*pdhR*, Kan^R	This study
Plasmids		
pACYC177	Cloning vector, p15A, Ap^R, Kan^R	(Chang & Cohen, 1978)
pAKH3	pGP704, *sacB*$^+$, Ap^R	(Heroven *et al,* 2012b)
pAKH175	pAKH3, *ptsN*::Kan^R	This study
pAKH177	pAKH3, *pykF*::Kan^R	This study
pAKH187	pAKH3, *pdhR*::Kan^R	This study
pKD4	kanamycin cassette template, Kn^R, Ap^R	(Datsenko & Wanner, 2000)
pKOBEG-*sacB*	recombination vector, *sacB*$^+$, Cm^R	(Derbise *et al,* 2003)
pkH70	pFU76, P*rovA*::*rovA-gfp*LVA, Amp^R, ΔR6Kmob, ori29807; containing *rovA* promoter fragment from -622 to +170	(Herbst, 2011)

Table 2. Oligonucleotides used as primers for genetic engineering of *Y. pseudotuberculosis*. Restriction sites for *Sac*I are underlined. Nucleotides homologous to the kanamycin resistance cassette are given in bold.

Number	Sequence	site
I661	GTGTAGGCTGGAGCTGCTTC	
I662	CATATGAATATCCTCCTTAGTTCC	
IV971	GCGGCGGAGCTC CGAGAGTCGTTATCCATCCC	*Sac*I
IV972	**GAAGCAGCTCCAGCCTACAC**CTCATCTTTCACTTAAGCGC	
IV973	**ACTAAGGAGGATATTCATATG**CCTAGTTTGGGGCCAATACG	
IV974	GCGGCGGAGCTCCTATCGGCAAGTGTACTTGC	*Sac*I
IV977	GCGGCGGAGCTCCGTCACTTACCGCTTATAATAC	*Sac*I
IV978	**GAAGCAGCTCCAGCCTACAC**GACGGATTTTTTCTACAAGTTG	
IV979	**ACTAAGGAGGATATTCATATG**CTTCAGTACACGTGTTATAATTCC	
IV980	GCGGCGGAGCTCCGTCAGAAGACAGTTGATCG	*Sac*I
V567	GCGGCGGAGCTCGAGTCATGTGTGCTTTCTAGG	*Sac*I
V548	**GAAGCAGCTCCAGCCTACAC**GGTGTAAGCCGTATTGAGTG	
V549	**ACTAAGGAGGATATTCATATG**CGAAATGTTGGCCACTGTGAG	
V550	GCGGCGGAGCTCCCCAAGACCTGATCAATCAG	*Sac*I
360	GGTGATTTTGAACTTTTGCTTTG	
361	CCAGTGTTACAACCAATTAACC	
655	CATCGCCATAATGCCAAGAG	
656	**GCAAAGCAAAAGTTCAAAATCACC**GCTACCTAAAATTGCCAACAAAATA GAAATAGGAAGTACAGAAGTCTTTG	
657	**GGTTAATTGGTTGTAACACTGG**CTTTCGCGAATAGAGACGGAAAGAGC CAGCACACAGATGCTGGCTTTTTTG	
658	GGTATTAAAGGCGGATTGGG	

4.2 Cultivation

4.2.1 Strain conservation

Cells were stored in 1 mL of 10% glycerol solution with 50 mg L^{-1} lactose at -80°C in stock culture tubes.

4.2.2 Batch cultivation for metabolic flux analysis

Cells were cultivated at 25°C and 200 rpm under aeration on a rotary shaker (Lab Shaker, B. Braun Melsungen, Melsungen, DE) with a shaking diameter of 5.0 cm. First pre-cultures were inoculated with single colonies from 2 days old LB agar plates (per liter: 10 g tryptone, 5 g yeast extract, 5 g NaCl, 15 g agar) and grown in a 1:1 mixture of HAM's F-12 Nutrient Mixture (Invitrogen, Carlsbad, US) and liquid DMEM (Biochrom, Berlin, DE). Second pre-cultures and main cultures were grown in a *Yersinia* minimal medium (YMM) that was developed in the present work. YMM at pH 6.8 contained the following per liter: 8 g glucose, 6.62 g KH_2PO_4, 13.26 g K_2HPO_4, 0.31 g NaCl, 5 g $(NH_4)_2SO_4$, 0.20 g $MgSO_4 \cdot 7H_2O$, 30 mg 3,4-dihydroxybenzoic acid, 0.5 mg $FeSO_4 \cdot 7H_2O$, 1.3 mg $ZnSO_4 \cdot 7H_2O$, 2 mg $FeCl_3 \cdot 6H_2O$, 2 mg $MnSO_4 \cdot H_2O$, 0.2 mg $CuCl_2 \cdot 2H_2O$, 0.2 mg $Na_2B_4O_7 \cdot 10H_2O$ and 0.1 mg $(NH_4)_6Mo_7O_{24} \cdot 4H_2O$. In tracer experiments for metabolic flux analysis, the natural glucose was replaced by 99% [1-^{13}C] glucose (Euriso-top, Saint-Aubin Cedex, FR), and the inoculum level was below 1% of the sampled cell concentration (Wittmann, 2007). The dissolved oxygen concentration was quantified on-line by immobilised sensor spots (Wittmann *et al,* 2003).

4.2.3 Continuous cultivation for temperature shift experiments

First, single colonies were taken from selective carbenicillin LB agar plates (per liter: 10 g tryptone, 5 g yeast extract, 5 g NaCl, 0.1 g carbenicillin, 15 g agar) and were used to inoculate pre-cultures performed in baffled shake-flasks. The complex

ingredients were obtained from Becton, Dickinson and Company (Franklin Lakes, US). After 16 h, cells were harvested by centrifugation for 5 min at 9,016 x *g* and 25°C (Heraeus Multifuge X1R, Thermo Fisher Scientific, Waltham, US), washed with sterile 0.9% NaCl and used for inoculation. Main cultures were carried out in a lab scale bioreactor (Vario 500, Medorex, Nörten-Hardenberg, DE), which was specifically modified for precise temperature programming and control. The reactor contained 220 mL of selective LB broth. After inoculation, an initial batch phase was performed at 25°C. When cells reached a specific growth rate of $\mu = 0.32\ h^{-1}$, as monitored via the optical density (OD_{600}), the system was switched to continuous cultivation mode ($D = 0.32\ h^{-1}$). OD_{600}, pH and oxygen saturation were used to check for steady-state. Once steady-state was confirmed, i.e., after at least five residence times, individual temperature programs were initiated.

The reactor was equipped with a pH-probe (Mettler-Toledo, Gießen, DE) and an amperiometric electrode for measurement of dissolved oxygen (InPro, Mettler-Toledo, Greifensee, CH). Process parameters were assembled by the system's control unit (FCU 05, Medorex, Nörten-Hardenberg, DE). Dissolved oxygen was kept above 30% by mixing oxygen and air as aeration gasses (5850 TR, Brooks Instrument, Hatfield, US connected to a WMR-C4 control unit, Westphal Mess- und Regeltechnik, Ottobrunn, DE). The aeration rate was set to 0.77 vvm. The temperature was precisely controlled by a combination of the integrated heating rod of the reactor and of a self-constructed water jacket. The latter was manually controlled by an Ecoline RE 107 thermostat (Lauda, Lauda-Königshofen, DE). The liquid condenser in the exhaust gas duct was supplied with periodic air pulses, to transfer excess liquid from the condenser back into the reactor, which improved process stability. The pulse was automatically conducted every 30 seconds by a clock generator (KPT 31 KD, Schleicher, Berlin, DE) through a magnetic valve

(244DVF, M&M International, Mailand, IT). The imposed pressure was 0.4 bar in closed and 0.2 bar in open valve position, respectively. Mixing (400 rpm) was performed with a self-constructed two-blade-stirrer, each blade with 0.8 cm height and width, respectively, assembled at a stirrer shaft attachment with same dimensions. The stirrer was placed 1.5 cm above the reactor bottom for efficient mixing. Pumping of fresh medium into the reactor, of exhaust medium out of the reactor, and circulation of condenser cooling water, respectively, was maintained by a peristaltic pump (101 U/R, Watson Marlow, Cornwall, UK).

4.3 Analytical Methods

4.3.1 Glucose, organic acids, and amino acids

Glucose concentration was measured by enzymatic analysis (YSI 2700 Select, YSI Incorporated, Yellow Springs, US). Organic acids and alcohols were quantified by HPLC (Becker *et al,* 2013). Amino acid quantification was conducted as previously described (Krömer *et al,* 2005).

4.3.2 Cell concentration

The cell concentration was measured as optical density at 600 nm (OD_{600}) with a photometer (Libra S11, Biochrom, Cambridge, GB). In addition, the cell dry weight (CDW) was determined by gravimetric analysis. For this purpose, 15 mL samples of culture broth were taken at different time points during the exponential growth phase. Cells were harvested by centrifugation for 15 min at 6,800 x *g* and 4°C in pre-weighed tubes (Sigma 2K15C, Sigma GmbH, Osterode, DE) and washed with ice chilled 0.9% NaCl and water. The cells were then dried to constant weight at 80°C. From both measurements, conducted for the wild type, a correlation factor of 0.325 (g_{CDW} L^{-1}) = 1 OD_{600} unit was obtained (Figure 9). This correlation was used to infer

cell dry weight from measurement of optical density, whereby the value for the wild type was also used for mutant strains.

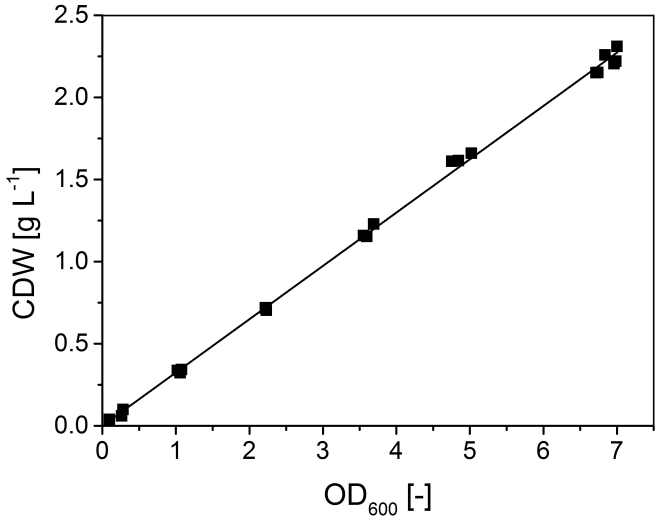

Figure 9. Correlation of gravimetrically determined cell dry weight (CDW) with optical density at 600 nm (OD_{600}). From both measurements a correlation factor of 0.325 (g_{CDW} L^{-1}) = 1 OD_{600} was obtained.

4.3.3 GC-MS labeling analysis

Mass isotopomer distributions of proteinogenic amino acids were quantified by gas chromatography-mass spectrometry (GC-MS) after derivatization with *N*-methyl-*N*-*tert*-butyldimethylsilyl-trifluoroacetamide (Wittmann *et al,* 2002). GC-MS analysis was performed as previously described (Kiefer *et al,* 2004; Wittmann *et al,* 2004). To check for potential isobaric interference, all samples were first measured in scan mode. The labeling analysis was then conducted in duplicate by selective ion-monitoring of representative ion clusters for each analyte. The chosen settings allowed complete separation of all analytes of interest (Figure 10).

For metabolic flux estimation the following ion clusters were measured: alanine (*m/z* 260, 261, 262, 263), glycine (*m/z* 246, 247, 248), valine (*m/z* 288, 289, 290, 291, 292, 293), serine (*m/z* 390, 391, 392, 393), threonine (*m/z* 404, 405, 406, 407, 408), phenylalanine (*m/z* 336, 337, 338, 339, 340, 341, 342, 343, 344, 345), aspartate (*m/z*

418, 419, 420, 421, 422), glutamate (*m/z* 432, 433, 434, 435, 436, 437), tyrosine (*m/z* 466, 467, 468, 469, 470, 471, 472, 473, 474, 475).

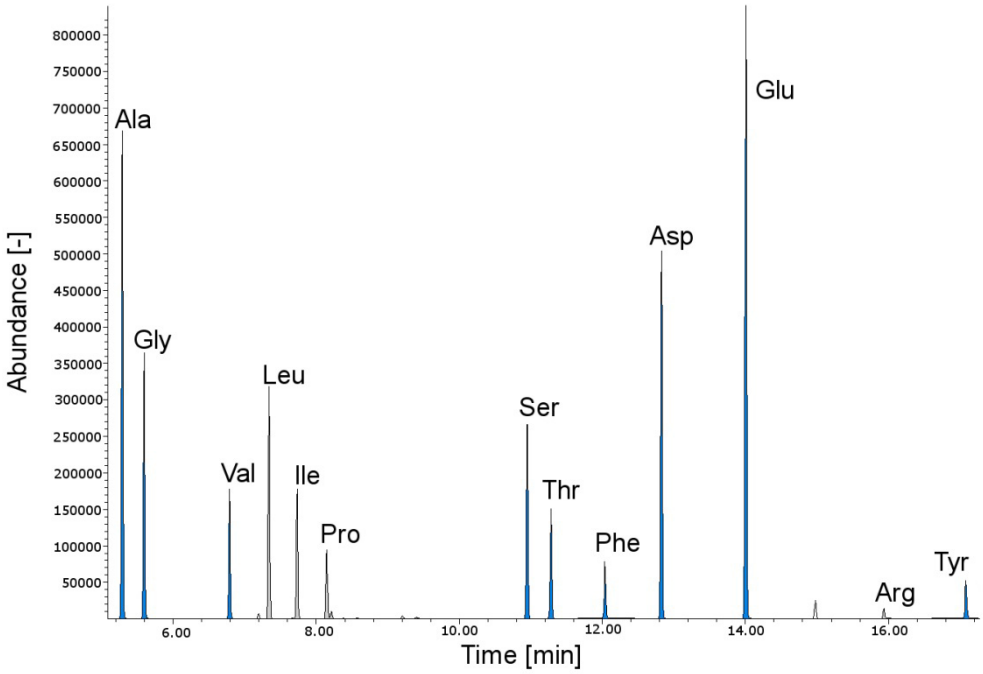

Figure 10. GC-MS spectrum of *t*-butyl-dimethylsilyl-derivatized proteinogenic amino acids of *Yersinia pseudotuberculosis* in selective ion-monitoring mode. Blue signals represent amino acids used for calculation of metabolic flux distribution. Amino acids were identified by their retention time and compound-specific ions as described by (Wittmann *et al,* 2002).

4.3.4 Quantification of RovA by Western blot analysis

From cells, sampled by centrifugation from culture broth for 2 min at 16,060 x *g* and 4°C (Biofuge fresco, Heraeus, Hanau, DE), whole cell extracts were prepared by addition of 100 µL SDS (sodium dodecyl sulfate) sample buffer per 0.65 mg_{CDW} and repeated pipetting at 25°C for 10 seconds. Aqueous SDS sample buffer contained per 50 mL: 5 mL Tris-HCl solution (121.14 g L^{-1} Tris, pH 6.8), 20 mL glycerol, 5 mL β-mercaptoethanol, 8 mL SDS solution (200 g L^{-1}) and 0.1 g bromophenol blue (Sambrook & Green, 2001). For DNA digestion, one percent by volume of benzonase (Merck, Darmstadt, DE) was added to whole cell extracts, and the mixture was incubated for 1 h at 37°C. Separation of cell extracts and Western blotting were performed as previously described (Heroven *et al,* 2004) and conducted by the group

of Petra Dersch (Department of Molecular Infection Biology, Helmholtz Centre for Infection Research, Braunschweig, Germany).

4.3.5 Quantification of RovA by fluorescence-activated cell sorting

A volume of 200 µL culture broth was centrifuged for 1 min at 16,100 x *g* and 25°C (Centrifuge 5415R, Eppendorf, Hamburg, DE). Harvested cells were fixed for 20 min with 1 mL paraformaldehyde (4%, pH 7.5) at 25°C. Fixed cells were washed twice with phosphate buffered saline (PBS, contained per liter: 8 g NaCl, 0.2 g KCl, 0.61 g Na_2HPO_4, 0.2 g KH_2PO_4, pH 7.3), re-suspended in 1 mL PBS and subsequently stored at 4°C. Following appropriate dilation, fixed cell samples were used for measurement of fluorescence in a BD LSR II flow cytometer (BD Biosciences, Franklin Lakes, US). The evaluation of 100.000 counted cells per run was performed with the software FlowJo (Version 9.3.1., Tree Star Inc., Ashland, US). The measurement was conducted by the group of Petra Dersch (Department of Molecular Infection Biology, Helmholtz Centre for Infection Research, Braunschweig, Germany).

4.4 Analysis of cellular composition of *Y. pseudotuberculosis*

In this work, thorough analysis of cellular composition was conducted to provide precise and most representative data for anabolic fluxes in metabolic flux studies with *Y. pseudotuberculosis*.

4.4.1 Protein content and amino acid composition

Protein content was determined after enzymatic treatment of frozen cell pellets. For this purpose, the cell pellet was re-suspended in lysis buffer with 25 U mL^{-1} benzonase and 10 KU mL^{-1} lysozyme (Bug Buster, Merck, Darmstadt, DE) and incubated for 1 h at 170 rpm and 25°C on a rotary shaker. To ensure efficient digestion, the cell concentration was adjusted to between 3 and 15 mg_{CDW} L^{-1}. Subsequently, the sample was clarified from cell debris by

centrifugation for 20 min at 6,800 x *g* and 4°C (Sigma 2K15C, 137 Sigma GmbH, Osterode, DE). The protein amount was then quantified by UV absorption measurement at 280 and 260 nm (Nanodrop ND-1000, Thermo Fisher Scientific, Waltham, US) in the supernatant. The protein concentration was calculated as described previously (Walker, 2002). The amino acid composition of cell protein was quantified after acidic hydrolysis of cells in 50 µL 6 M HCl per mg of cell dry weight at 105°C for 24 h. Amino acids in the hydrolyzates were then quantified by HPLC as described above. Values for cysteine, methionine, and tryptophan, respectively, were not accessible, because these were degraded during the hydrolysis procedure. Accordingly, these data were inferred from the closely related gut bacterium *Escherichia coli* (Neidhardt *et al,* 1990).

4.4.2 RNA content and nucleotide composition

For quantification of the RNA content cells were washed twice with ice cold killing buffer (20 mM Tris/HCl pH 7.5; 5 mM $MgCl_2$; 20 mM NaN_3) to prevent RNA degradation. RNA preparation was performed as described previously (Dauner & Sauer, 2001), followed by quantification using a Nanodrop ND-1000 at 260 nm. The nucleotide composition of RNA was calculated from the sequences of the 5S, 16S and 23S rRNA genes of *Y. pseudotuberculosis* (NCBI reference sequence of the genome: NC_010465), based on the assumption that the total RNA pool is mainly composed of rRNA (Brown, 2002).

4.4.3 DNA content and nucleotide composition

The DNA content was determined after phenol-chloroform-extraction. For this purpose, cells were harvested by centrifugation at 16,100 x *g* and 4°C for 5 min. An appropriate amount of cells (0.2 - 0.5 mg cell dry weight) was re-suspended in 560 µL lysis buffer (pH 8.0) containing per liter 2.88 g Tris, 6.96 g EDTA

(ethylenediaminetetraacetic acid), 97.80 g sucrose, and 0.48 mg lysozyme and then disrupted by incubation at 800 rpm and 30°C for 30 min (Thermomixer comfort, Eppendorf, Hamburg, DE). A second disruption was performed with FastPrep-24 (MP Biomedicals, Santa Ana, US) involving two cycles of 40 s each at 6.0 m s^{-1} and 4°C. Subsequently, 140 µL RES buffer with RNaseA (NucleoBond Xtra, Macherey-Nagel, Düren, DE) was added to degrade RNA residues, otherwise interfering with the subsequent analysis. The aqueous DNA solution was extracted twice with 700 µL Roti-P/C/I (Carl-Roth, Karlsruhe, DE) and 700 µL chloroform. Precipitation of DNA was performed after addition of 65 µL sodium acetate (3 M) and 1.3 mL ethanol (100%). The DNA pellet was washed with 70% ethanol, dried and re-suspended in deionized water. All centrifugation steps were performed at 16,100 x *g* and 4°C for 10 min. Quantification was carried out by measuring the absorbance at 260 nm using a Nanodrop ND-1000 (Thermo Fisher Scientific, Waltham, US). The nucleotide composition of DNA was calculated from the genomic GC content of 47.5% (NCBI reference sequence of the genome: NC_010465).

4.4.4 Glycogen and Lipids

Data for glycogen, lipids and minor shares of further biomass constituents were taken from *E. coli* (Neidhardt *et al,* 1990).

4.5 Gene expression profiling

Global gene expression was analyzed with DNA microarrays (Agilent, Waldbronn, DE, 8 × 15 K format). The analysis comprised three biological replicates for each strain and samples from three different time points during exponential growth phase to validate constant expression during cultivation. Array design, RNA extraction, and hybridization were performed as previously described (Heroven *et al,* 2012b). Microarray data processing was conducted using the Limma package (Smyth, 2005)

from the R/Bioconductor framework (Gentleman *et al,* 2004). Unprocessed array intensity values were read-in using the function read.maimages, and the background was corrected with the improved saddle-point approximation to the maximum likelihood method (Silver *et al,* 2009) using an intensity offset of 50. The array intensities were normalized within each array using loess normalization (Yang *et al,* 2002) and between arrays using quantile normalization (Bolstad *et al,* 2003; Yang & Thorne, 2003) to obtain similar distributions of expression intensities. To obtain reliable gene expression values, normalized intensities of at least three probes targeting the same gene were averaged. Differentially expressed genes were determined using the lmFit function for linear modeling and by computing moderated t-statistics and log-odds with the function eBayes (Smyth, 2004). P-values from the moderated t-tests were corrected for multiple testing using the Benjamini-Hochberg procedure for controlling the false discovery rate. Finally, the set of differentially expressed genes was filtered by the fold change (|log2FC| >=0.8). All array data generated in this study were deposited in the Gene Expression Omnibus (GEO) database and are available under accession number GSE54547. Hybridization and data processing was conducted by the group of Petra Dersch (Department of Molecular Infection Biology, Helmholtz Centre for Infection Research, Braunschweig, Germany).

4.5.1 Hierarchical clustering analysis

Hierarchical clustering of transcriptome data was conducted with the heatmap.2 function of the R package gplots (Warnes *et al,* 2012).

4.6 Metabolic flux analysis

4.6.1 Metabolic network and biomass requirements

The metabolic network of *Y. pseudotuberculosis* was constructed from its genome-encoded pathway repertoire (NCBI Reference Sequence: NC_010465.1). The network comprised all relevant central metabolic pathways, i.e., the Embden-Meyerhof-Parnas (EMP) pathway, the pentose phosphate (PP) pathway, the Entner-Doudoroff (ED) pathway, and the tricarboxylic acid (TCA) cycle, as well as the anaplerotic glyoxylate shunt, phosphoenolpyruvate (PEP) carboxylase, PEP carboxykinase, and malic enzyme. Furthermore, biosynthetic pathways for by-product formation and anabolism were implemented. The requirement of *Y. pseudo-tuberculosis* for anabolic precursors was estimated on the basis of its cellular composition, which was experimentally determined. The full set of reactions is given in the appendix (Table 11).

4.6.2 Metabolic flux calculation and statistical evaluation

For calculation of metabolic fluxes the reconstructed metabolic network, extracellular and anabolic fluxes, and labeling data were implemented into the open source software OpenFlux 2.1 (Quek *et al,* 2009). Extracellular fluxes were obtained by thorough analysis of all organic acids, amino acids, sugars, alcohols, and glucose as the sole carbon source. All anabolic fluxes were calculated from the determined cellular composition and the biomass yield on glucose. Mass isotopomer distribution data was obtained from GC-MS analysis of *t*-butyl-dimethylsilyl-derivatized proteinogenic amino acids. Matlab 7.11 (MathWorks Inc., Natick, US) was used as a numerical computing environment. The gradient solver FMINCON (Optimization Toolbox of Matlab) was used to perform an iterative optimization of free fluxes towards minimal residual errors between computed and measured labeling data. The

weighted sum of least-squares was used as error criterion, thus, accuracy of label measurement was taken into account. The identification of a global minimum was verified by variation of initial start values for the free fluxes and repetitive flux estimation (Wittmann & Heinzle, 2002). The best solution of the parameter estimation delivered almost identical ^{13}C labeling data compared to experimental values and, therefore, represents the metabolic fluxes in the living cell (Quek *et al,* 2009). Subsequent statistical analysis by a Monte-Carlo approach was performed to calculate 95% confidence intervals (Wittmann & Heinzle, 2002).

4.7 *In vivo* mouse studies

4.7.1 Mouse infections

The bacteria used for oral infection were grown overnight at 25°C in LB medium and re-suspended in PBS (contained per liter: 8 g NaCl, 0.2 g KCl, 0.61 g Na_2HPO_4, 0.2 g KH_2PO_4, pH 7.3). To assess the effect of single gene deletions on *Y. pseudotuberculosis* virulence, groups (n=20) of 7-week-old female BALB/c mice (Janvier, Saint Berthevin, FR) were orally infected with an equal mixture of 10^7 bacteria of the wild type strain (YPIII) and an isogenic mutant strain, i.e., YP49 (Δ*arcA*), YP252 (Δ*ptsN*), YP253 (Δ*pykF*), or YP274 (Δ*pdhR*). At 5 days post-infection, the mice were euthanized by CO_2 asphyxiation. Peyer's patches (PPs), mesenteric lymph nodes (MLNs), and the liver and spleen were isolated. The ileum was rinsed with sterile PBS and incubated with 100 µg mL^{-1} gentamicin to kill the bacteria on the luminal surface. After 30 min, gentamicin was removed by extensive washing with PBS. Subsequently, all organs were weighed and homogenized in sterile PBS at 30,000 rpm for 20 s using a Polytron PT 2100 homogenizer (Kinematica, Lucerne, CH). The bacterial organ burden was determined by plating three independent serial dilutions of the homogenates on LB plates with and without kanamycin. The colony-

forming units (CFU) were counted and are given as CFU per gram of organ/tissue. The levels of statistical significance for differences in the organ burden between test groups were determined by the Mann-Whitney test. The competitive index relative to the wild type strain YPIII was calculated as previously described (Monk *et al,* 2008). Mouse *in vivo* studies were conducted in the group of Petra Dersch (Department of Molecular Infection Biology, Helmholtz Centre for Infection Research, Braunschweig, Germany).

4.7.2 Ethics statement

All animal work was performed in strict accordance with the German Recommendations of the Society for Laboratory Animal Science (GV-SOLAS) and the European Health Recommendations of the Federation of Laboratory Animal Science Associations (FELASA). The animal protocol was approved by the Niedersächsisches Landesamt für Verbraucherschutz und Lebensmittelsicherheit (animal licensing committee permission no. 33.9-42502-04-12/1010). Animals were handled with appropriate care and welfare, and all efforts were made to minimize suffering.

5 RESULTS AND DISCUSSION

5.1 Integration of virulence and metabolism - A systems biology approach

5.1.1 Glucose-grown *Y. pseudotuberculosis* secretes high amounts of pyruvate under fully aerobic conditions

When grown on minimal medium, *Y. pseudotuberculosis* completely consumed the carbon source glucose within 8.8 h, indicating high activity of the cultured bacteria (Figure 11).

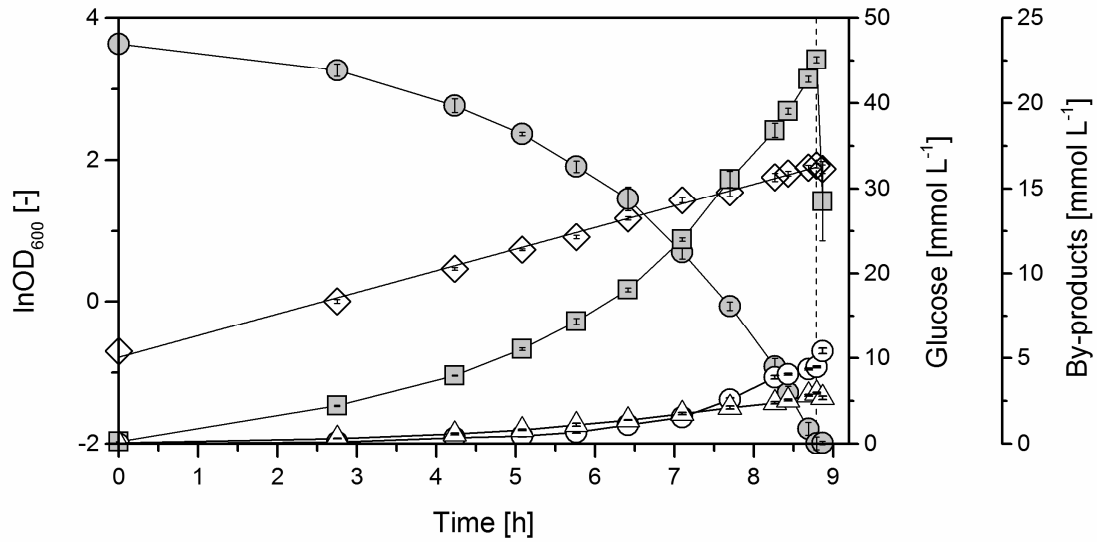

Figure 11. Cultivation profile of wild type *Y. pseudotuberculosis* in YMM with glucose as the sole source of carbon and energy. The data comprise the concentrations of glucose (*gray circle*), pyruvate (*gray square*), lactate (*open circle*), acetate (*open triangle*), and the optical density (*open diamond*) and represent the mean of three biological replicates with the corresponding deviations given as error bars.

Indeed, the specific rates of growth (0.32 h^{-1}) and substrate uptake (7.1 mmol g^{-1} h^{-1}) were consistently maintained at high levels throughout the cultivation (Table 4). Glucose, however, was only partially converted into biomass, as indicated by a low biomass yield (45.2 g mol^{-1}). A range of metabolites was secreted into the medium. Surprisingly, high amounts of pyruvate accumulated (22.6 mmol L^{-1}). Lactate

(5.4 mmol L^{-1}) and acetate (3.0 mmol L^{-1}) were also observed (Figure 11). Additional by-products (formate, ethanol, α-ketoglutarate, succinate, and fumarate) were found at lower levels (Table 4). The level of dissolved oxygen, which was monitored on-line, remained above 30% of saturation throughout the entire cultivation period (Figure 12). This finding indicates that the observed overflow metabolism was active in fully aerobic cells. The developed set-up enabled highly reproducible growth for the wild type (Figure 11, Figure 12) and for all investigated deletion mutants (Figure 13).

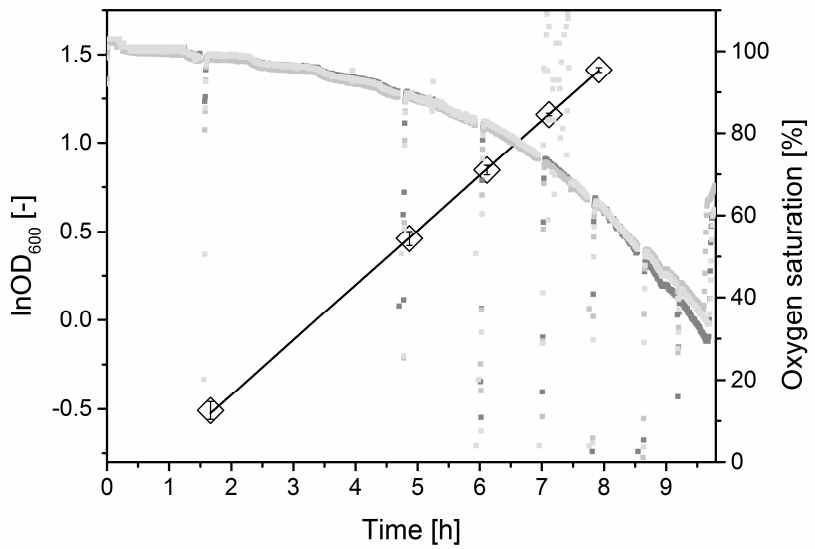

Figure 12. Dissolved oxygen remained above 30% of saturation throughout the entire cultivation. Oxygen measurement was carried out on-line by non-invasive oxygen sensor spots in triplicate. Samples were taken at different time points to monitor the cell concentration by optical densities OD_{600} (*open diamond*). Data of dissolved oxygen are given in gray shades.

Efficient expression of RovA is an indicator for virulence promoting conditions and was hence an important pre-requisite for the subsequent fluxome analysis. Thus far, efficient expression of RovA has only been achieved in complex media (Nagel *et al,* 2001). However, fluxome profiling, as performed here, requires defined conditions (Wittmann, 2002), which excludes the use of a complex medium due to the unresolvable effects expected from the utilization of undefined nutrient mixtures. A thorough analysis of the expression of RovA revealed a significant influence of

monovalent and bivalent ions. Increased levels of bivalent iron and of the iron chelator 3,4-dihydroxybenzoic acid stimulated RovA expression, whereas calcium and sodium ions reduced the level of the virulence regulator (Table 3).

Table 3. Impact of monovalent and bivalent ions on the expression of the early stage virulence regulator RovA in *Y. pseudotuberculosis*. The tested conditions comprise growth in complex medium (DMEM/F12) as a positive control and in *Yersinia* minimal medium (YMM) with variations in the added amounts of Ca^{2+}, Na^{+}, Fe^{2+}, and the chelating agent 3,4-dihydroxybenzoic acid. The level of RovA was visualized by Western blotting using a polyclonal antibody as previously described (Heroven *et al,* 2004).

Type of medium	Ca^{2+} [mmol L^{-1}]	Na^{+} [mmol L^{-1}]	Fe^{2+} [µmol L^{-1}]	3,4-DHB [mmol L^{-1}]	RovA
DMEM/F12	2.1	304	3	-	
YMM	2.0	5	2	-	
YMM	1.0	5	2	-	
YMM	-	93	2	-	
YMM	-	5	2	-	
YMM	-	5	2	0.2	
YMM	-	5	20	0.2	

5.1.2 Influence of the global regulators RovA, CsrA, and Crp on the growth behavior and overflow metabolism of *Y. pseudotuberculosis*

Next, the manner in which RovA, CsrA, and Crp affect the overall growth behavior of *Y. pseudotuberculosis* was investigated. Deletion of each of the regulators affected the fitness and product formation. *Y. pseudotuberculosis* YP3 (Δ*rovA*) showed a 21% enhanced secretion of pyruvate. The growth, substrate uptake, and spectrum of other by-products were approximately maintained at the values of the wild type (Table 4). The loss of CsrA resulted in a 56% reduction in the growth and substrate uptake. The pyruvate excretion increased by 13%, whereas the formation of all other by-products was much weaker or even diminished.

Table 4. Growth characteristics of the *Y. pseudotuberculosis* wild type strain YPIII and the mutants YP3 (Δ*rovA*), YP53 (Δ*csrA*), YP89 (Δ*crp*). The data comprise the specific growth rate (μ), the specific rate of glucose uptake (q_{Glc}), and yields on glucose for biomass ($Y_{X/S}$), pyruvate ($Y_{Pyr/S}$), lactate ($Y_{Lac/S}$), acetate ($Y_{Ace/S}$), formate ($Y_{Form/S}$), succinate ($Y_{Suc/S}$), fumarate ($Y_{Fum/S}$), ethanol ($Y_{EtOH/S}$), and α-ketoglutarate ($Y_{Akg/S}$). The values represent the mean of three biological replicates and the corresponding standard deviations.

Strain	μ	q_{Glc}	$Y_{X/S}$	$Y_{Pyr/S}$	$Y_{Lac/S}$	$Y_{Ace/S}$	$Y_{Form/S}$	$Y_{Suc/S}$	$Y_{Fum/S}$	$Y_{EtOH/S}$	$Y_{Akg/S}$
	[h^{-1}]	[mmol g^{-1} h^{-1}]	[g mol^{-1}]	[molar percentage of the specific glucose uptake rate]							
YPIII (Wt)	0.32 ± 0	7.1 ± 0.3	45.2 ± 2.0	46.4 ± 1.4	7.1 ± 0.6	6.7 ± 0.3	3.0 ± 0.4	0.2 ± 0	0.1 ± 0	3.3 ± 0.7	1.1 ± 0.1
YP3 (Δ*rovA*)	0.31 ± 0.01	7.1 ± 0.2	44.9 ± 2.8	56.1 ± 4.6	8.2 ± 0.8	6.9 ± 0.5	2.6 ± 0.1	0.2 ± 0	0.1 ± 0	4.0 ± 0.7	1.5 ± 0.1
YP53 (Δ*csrA*)	0.14 ± 0	3.1 ± 0.3	45.0 ± 0.9	52.5 ± 2.4	3.5 ± 0.2	3.0 ± 1.0	0.3 ± 0.4	< 0.1	<0.1	0.2 ± 0.4	0.9 ± 0.1
YP89 (Δ*crp*)	0.11 ± 0	1.5 ± 0	69.3 ± 3.3	<0.1	1.0 ± 0.1	0.2 ± 0.1	0.8 ± 0.1	< 0.1	<0.1	-2.0 ± 2.5	0.9 ± 0

Values below 0.1% for the by-product yields were below the detection limit.

The *crp* mutant (YP89) exhibited a further reduction of fitness. This mutant secreted almost no by-products and showed enhanced anabolism (Table 4). In summary, various fluxes, ranging from glucose to biomass and to extracellular products, were affected in all three regulator mutants. The extent of the cellular response clearly matched the hierarchy of the control of proteins within the virulence cascade (Figure 3).

5.1.3 Metabolic and isotopic steady state – two important prerequisites for metabolic flux analysis

The applied flux analysis requires a metabolic and isotopic steady state to ensure flux calculation that is valid for the whole exponential growth phase. As previously shown, the set-up provides constant specific growth with sufficient supply of oxygen (Figure 11, Figure 12). Metabolic steady state was further proven by constant by-product yields on glucose (Figure 13).

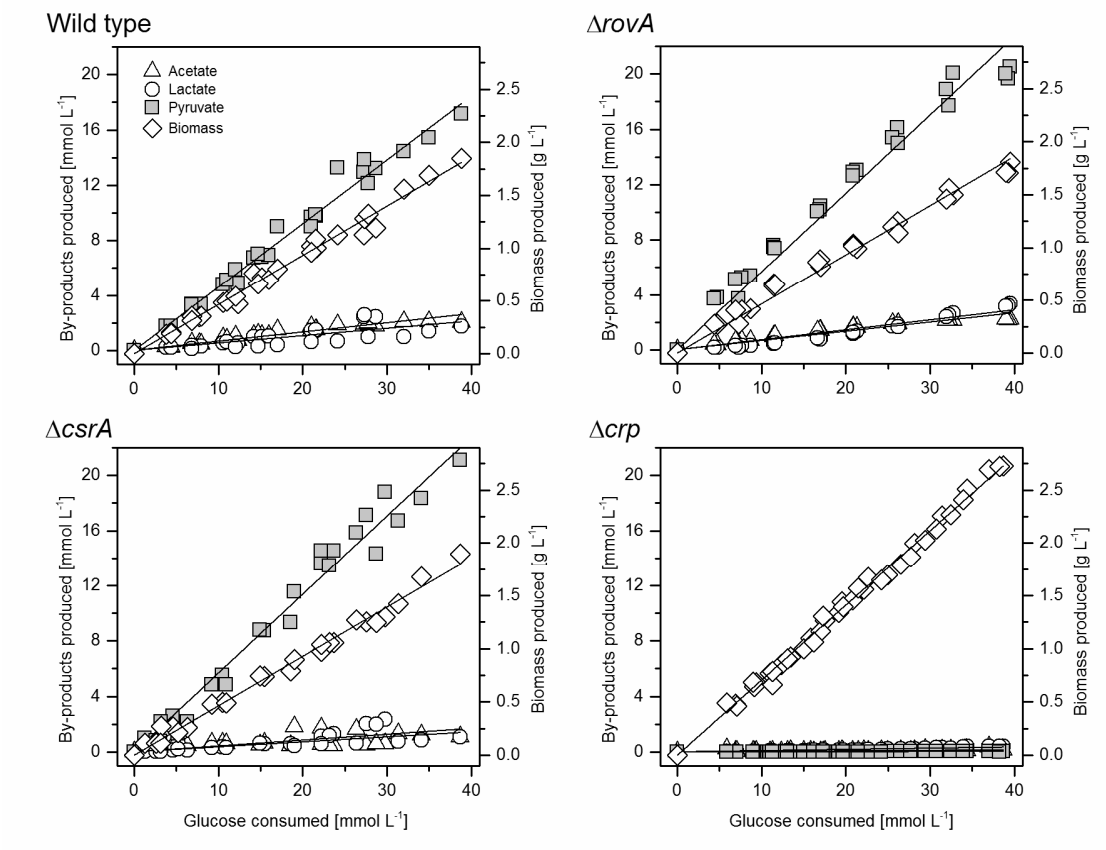

Figure 13. Stoichiometry of by-product formation during cultivation of the *Y. pseudotuberculosis* wild type strain (YPIII) and of single gene deletion mutants: YP3 (Δ*rovA*), YP53 (Δ*csrA*), and YP89 (Δ*crp*). The linear correlation between formed pyruvate (*gray square*), acetate (*open triangle*), lactate (*open circle*) and consumed glucose indicates metabolic steady state. All cultivations were performed in triplicate.

To ensure isotopic steady state, samples were taken from parallel tracer experiments with [1-^{13}C] glucose at different cell dry mass concentrations, reflecting different cultivation time points. Subsequently, proteinogenic amino acids were analyzed in respect to their labeling patterns (Figure 14). The constant mass isotopomer distributions of nonlabeled (M_0), single labeled (M_1), and double labeled (M_2) *t*-butyl-dimethylsilyl derivates of proteinogenic alanine, serine, phenylalanine, glutamate, and aspartate, reflecting different parts of central carbon metabolism, verified isotopic steady state (Figure 14).

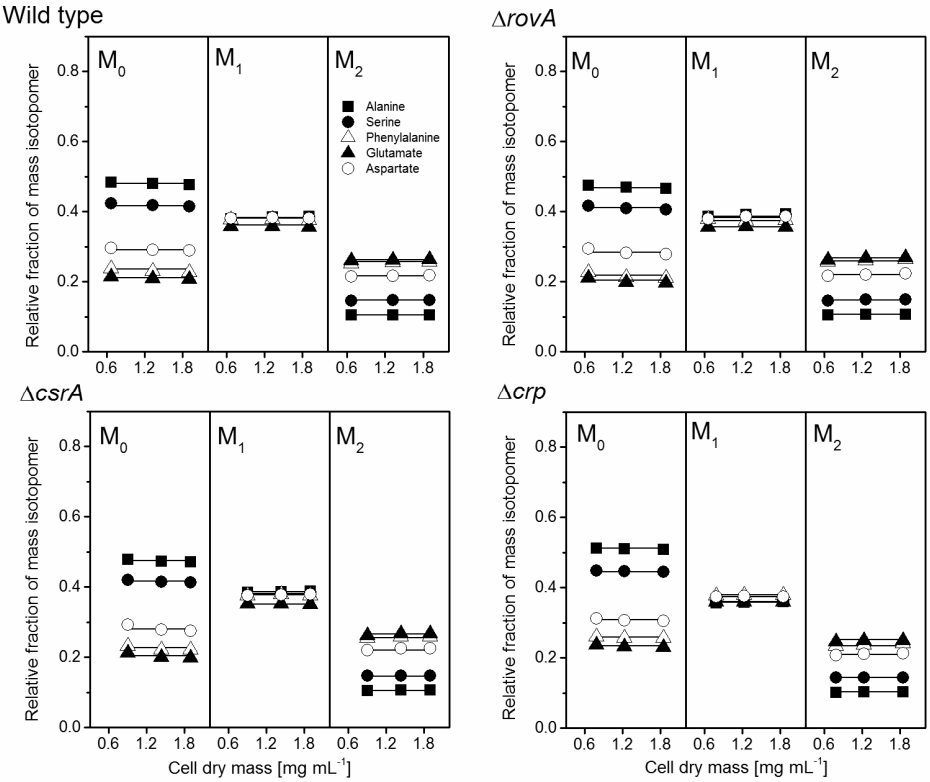

Figure 14. Verification of isotopic steady state during ^{13}C tracer studies of *Y. pseudotuberculosis* wild type (WT) and of single gene deletion mutants YP3 (Δ*rovA*), YP53 (Δ*csrA*), and YP89 (Δ*crp*) grown on 99% [1-^{13}C] glucose by constant labeling patterns of *t*-butyl-dimethylsilyl derivates of proteinogenic amino acids at different cell dry mass (CDM) concentrations, reflecting different cultivation time points. The data comprise the relative fractions of nonlabeled (M_0), single labeled (M_1), and double labeled (M_2) M-57 fragments of alanine, serine, phenylalanine, glutamate, and aspartate.

5.1.4 Cellular composition of *Yersinia pseudotuberculosis*

The determination of the biomass composition is a crucial prerequisite for an accurate analysis of carbon flux distribution. All macromolecules for biomass formation derive from 12 precursor molecules that are part of central carbon metabolism. Hence, the demand for a certain precursor influences the flux distribution. Thereby, a thorough investigation of the cellular composition was performed (Table 5). The NADPH demand that arises from the underlying precursor demand was determined to 17,428 µmol g_{CDW}^{-1}. This amount of co-factor has to be supplied by NADPH forming reactions of PP pathway and TCA cycle and thus bears significant influence on the flux distribution.

Table 5. Anabolic precursor demand of *Y. pseudotuberculosis* for biomass synthesis derived from analysis of the cellular composition and the underlying pathway stoichiometry. The latter was deduced from the genomic inventory of biosynthetic pathways of *Y. pseudotuberculosis* (Kyoto Encyclopedia of Genes and Genomes). Abbreviations: G6P, glucose 6-phosphate; F6P, fructose 6-phosphate; R5P, ribose 5-phosphate; E4P, erythrose 4-phosphate; GAP, glyceraldehyde 3-phosphate; PGA, glycerate 3-phosphate; PEP, phosphoenolpyruvate; PYR, pyruvate; AcCoA, acetyl-CoA; OAA, oxaloacetate; AKG, alpha-ketoglutaric acid.

Precursor	Demand [µmol g^{-1}]	G6P	F6P	R5P	E4P	GAP	PGA	PEP	PYR	AcCoA	OAA	AKG	NADPH
Alanine	604								1				1
Arginine	277											1	4
Aspartate/Asparagine	572										1		1
Cysteine	92						1						5
Glutamate/Glutamine	557											1	1
Gycine	483						1						1
Histidine	98			1									1
Isoleucine	236								1		1		5
Leucine	463								2	1			2
Lysine	340								1		1		4
Methionine	155										1		8
Phenylalanine	180				1			2					2
Proline	297											1	3
Serine	275						1						1
Threonine	270										1		3
Tryptophan	57			1	1			1					3
Tyrosine	91				1			2					2
Valine	333								2				2
Protein				**155**	**328**		**850**	**598**	**2,772**	**463**	**1,573**	**1,131**	**11,940**
ATP	117			1			1						1
UTP	92			1							1		1
GTP	140			1			1						
CTP	99			1							1		1
RNA				**448**			**257**				**191**		**307**
dATP	55			1			1						2
dTTP	55			1							1		3
dGTP	49			1			1						1
dCTP	49			1							1		2
DNA				**208**			**104**				**104**		**421**
Lipid						**129**	**129**			**2,116**			**3,870**
LPS components		**51**	**16**	**24**			**24**	**24**		**329**			**470**
Peptidoglycan			**55**					**28**	**83**	**55**	**28**	**28**	**193**
Glycogen		**154**											
C1-units							**49**						**49**
Polyamines												**59**	**178**
Total		**205**	**71**	**834**	**328**	**129**	**1,412**	**649**	**2,855**	**2,963**	**1,895**	**1,218**	**17,428**

5.1.5 Intracellular fluxes of glucose-grown *Yersinia pseudotuberculosis* strongly differ from those of its relative *Escherichia coli*

The fluxes could be precisely determined throughout the entire central metabolism, as indicated by the narrow confidence intervals (Figure 15, Table 11). Moreover, the excellent agreement between the measured and simulated mass isotopomer distributions demonstrated high confidence in the obtained flux distributions (Table 6). The *in vivo* carbon flux distribution revealed that *Y. pseudotuberculosis* channelled 33% of the consumed glucose into the pentose phosphate (PP) pathway (Figure 15A). This flux exceeded the requirement for PP pathway-derived anabolic precursors. Carbon was channelled back from the PP pathway into the Embden-Meyerhof-Parnas (EMP) pathway at the level of fructose 6-phosphate and glyceraldehyde 3-phosphate. The Entner-Doudoroff (ED) pathway was found to be inactive, and approximately 67% of the glucose uptake was catabolized by the EMP pathway. Although this part of the metabolism upstream of the phosphoenolpyruvate (PEP) node is similar to that of the related gut bacterium *E. coli* (Sauer *et al,* 2004; Haverkorn van Rijsewijk *et al,* 2011), the fluxes through the downstream pathways differ significantly between the two microorganisms for growth under aerobic conditions on glucose. *Y. pseudotuberculosis* showed a high flux through the TCA cycle. The flux through the entry step, which is catalyzed by citrate synthase, was 63% in *Y. pseudotuberculosis*, whereas only 27% has been reported for *E. coli* (Haverkorn van Rijsewijk *et al,* 2011). In addition, the anaplerotic fluxes in *Y. pseudotuberculosis* were generally very low. The pathogen did not exhibit any activity in the glyoxylate shunt, whereas *E. coli* has shown a carbon flux of approximately 10% (Haverkorn van Rijsewijk *et al,* 2011). Similarly, the flux through PEP carboxylase was also substantially lower in *Y. pseudotuberculosis* (17%) compared with the value of 32% for *E. coli* (Haverkorn van Rijsewijk *et al,* 2011).

Table 6. Relative mass isotopomer fractions of *t*-butyl-dimethylsilyl derivates of proteinogenic amino acids used for ^{13}C metabolic flux analysis of *Y. pseudotuberculosis* YPIII and of the single gene deletion mutants YP3 (Δ*rovA*), YP53 (Δ*csrA*), and YP89 (Δ*crp*) cultivated on 99% [1-^{13}C] glucose. The data set comprises experimental values with deviations from replicate GC/MS measurement (Exp) and calculated values (Calc), predicted by the solution of the mathematical model that corresponded to the optimized set of fluxes.

		Wild type			**YP3 (Δ*rovA*)**			**YP53 (Δ*csrA*)**			**YP89 (Δ*crp*)**		
		M_0	**M_1**	**M_2**	**M_0**	**M_1**	**M_2**	**M_0**	**M_1**	**M_2**	**M_0**	**M_1**	**M_2**
Ala	Exp	0.480 (±0.06%)	0.384 (±0.02%)	0.105 (±0.30%)	0.469 (±0.03%)	0.392 (±0.06%)	0.106 (±0.04%)	0.474 (±0.13%)	0.387 (±0.11%)	0.106 (±0.32%)	0.510 (±0.04%)	0.358 (±0.03%)	0.102 (±0.13%)
(*m/z*) 260	Calc	0.474	0.381	0.111	0.465	0.390	0.111	0.470	0.384	0.112	0.508	0.354	0.107
Val	Exp	0.301 (±0.12%)	0.411 (±0.13%)	0.208 (±0.63%)	0.286 (±0.13%)	0.415 (±0.11%)	0.217 (±0.03%)	0.292 (±0.09%)	0.409 (±0.02%)	0.212 (±0.10%)	0.340 (±0.25%)	0.399 (±0.18%)	0.187 (±0.30%)
(*m/z*) 288	Calc	0.299	0.409	0.209	0.286	0.413	0.216	0.296	0.410	0.211	0.346	0.398	0.185
Thr	Exp	0.287 (±0.35%)	0.385 (±0.34%)	0.217 (±0.07%)	0.282 (±0.02%)	0.385 (±0.07%)	0.222 (±0.07%)	0.274 (±0.14%)	0.379 (±0.23%)	0.225 (±0.00%)	0.303 (±0.03%)	0.377 (±0.02%)	0.211 (±0.29%)
(*m/z*) 404	Calc	0.288	0.380	0.219	0.282	0.382	0.221	0.274	0.378	0.227	0.303	0.374	0.213
Asp	Exp	0.291 (±0.35%)	0.383 (±0.24%)	0.217 (±0.54%)	0.281 (±0.11%)	0.386 (±0.09%)	0.220 (±0.18%)	0.278 (±0.07%)	0.378 (±0.12%)	0.224 (±0.07%)	0.307 (±0.29%)	0.375 (±0.12%)	0.210 (±0.10%)
(*m/z*) 418	Calc	0.287	0.379	0.219	0.281	0.381	0.221	0.274	0.377	0.227	0.303	0.374	0.213
Glu	Exp	0.210 (±0.38%)	0.357 (±0.01%)	0.263 (±0.03%)	0.199 (±0.08%)	0.358 (±0.05%)	0.268 (±0.01%)	0.201 (±1.19%)	0.353 (±0.16%)	0.267 (±0.73%)	0.233 (±0.38%)	0.359 (±0.01%)	0.249 (±0.17%)
(*m/z*) 432	Calc	0.207	0.357	0.263	0.198	0.356	0.268	0.199	0.353	0.266	0.235	0.359	0.247
Ser	Exp	0.417 (±0.04%)	0.383 (±0.19%)	0.147 (±0.18%)	0.409 (±0.12%)	0.389 (±0.09%)	0.149 (±0.10%)	0.415 (±0.07%)	0.383 (±0.22%)	0.148 (±0.70%)	0.446 (±0.19%)	0.360 (±0.20%)	0.143 (±0.27%)
(*m/z*) 390	Calc	0.420	0.379	0.148	0.410	0.386	0.150	0.415	0.381	0.150	0.447	0.359	0.144
Phe	Exp	0.231 (±0.41%)	0.379 (±0.57%)	0.256 (±0.17%)	0.213 (±0.62%)	0.374 (±0.19%)	0.261 (±0.29%)	0.221 (±0.29%)	0.378 (±0.30%)	0.259 (±1.88%)	0.257 (±0.15%)	0.378 (±0.78%)	0.237 (±0.77%)
(*m/z*) 336	Calc	0.229	0.381	0.255	0.213	0.377	0.265	0.223	0.378	0.259	0.259	0.379	0.237
Gly	Exp	0.754 (±0.01%)	0.175 (±0.02%)		0.754 (±0.02%)	0.175 (±0.03%)		0.747 (±0.09%)	0.181 (±0.26%)		0.743 (±0.08%)	0.184 (±0.01%)	
(*m/z*) 246	Calc	0.755	0.174		0.755	0.174		0.749	0.179		0.745	0.182	
Tyr	Exp	0.203 (±0.21%)	0.351 (±0.77%)	0.266 (±0.37%)	0.191 (±0.29%)	0.346 (±0.04%)	0.267 (±0.24%)	0.196 (±2.39%)	0.344 (±0.04%)	0.267 (±1.62%)	0.225 (±0.12%)	0.351 (±0.35%)	0.249 (±0.30%)
(*m/z*) 466	Calc	0.197	0.352	0.266	0.184	0.347	0.274	0.192	0.348	0.269	0.223	0.353	0.252

Moreover, *Y. pseudotuberculosis* exhibited a high flux of almost 50% towards extracellular pyruvate, whereas *E. coli* typically does not secrete this metabolite under similar respiratory conditions. The formation and secretion of large amounts of pyruvate is surprising because this metabolic route does not provide additional ATP, in contrast to the acetate pathway preferred by *E. coli* (Valgepea *et al,* 2010).

5.1.6 The lack of RovA, CsrA, and Crp perturbs the intracellular carbon fluxes in *Y. pseudotuberculosis*

Deletion of the virulence-promoting metabolic regulator genes *rovA*, *csrA,* and *crp* resulted in a significant perturbation of the *Y. pseudotuberculosis* carbon flux (Figure 15B-D, Figure 16). The lack of the most specific virulence regulator RovA decreased the flux through the PP pathway and the TCA cycle. Both pathways deliver NADPH, and the TCA cycle also provides NADH and FADH. Overall, this change resulted in a decreased amount of reducing power. The reduced TCA cycle flux originated from the increased pyruvate secretion, which withdrew carbon from the core metabolism. In addition, *Y. pseudotuberculosis* YP53 (Δ*csrA*) and YP89 (Δ*crp*) showed a substantial difference in the metabolic flux distribution compared with that of the wild type. In YP53 (Δ*csrA*) and YP89 (Δ*crp*), the TCA cycle flux was significantly upregulated by approximately 10% and 45%, respectively, coinciding with a reduced formation of pyruvate-derived by-products (Figure 15C-D, Figure 16). Overall, the deletion of the global regulator Crp led to the most extensive change in flux. This deletion also affected additional pathways, including the PP and EMP pathways, and several anabolic reactions, and most strikingly, it resulted in the disappearance of all overflow fluxes (Figure 15D, Figure 16).

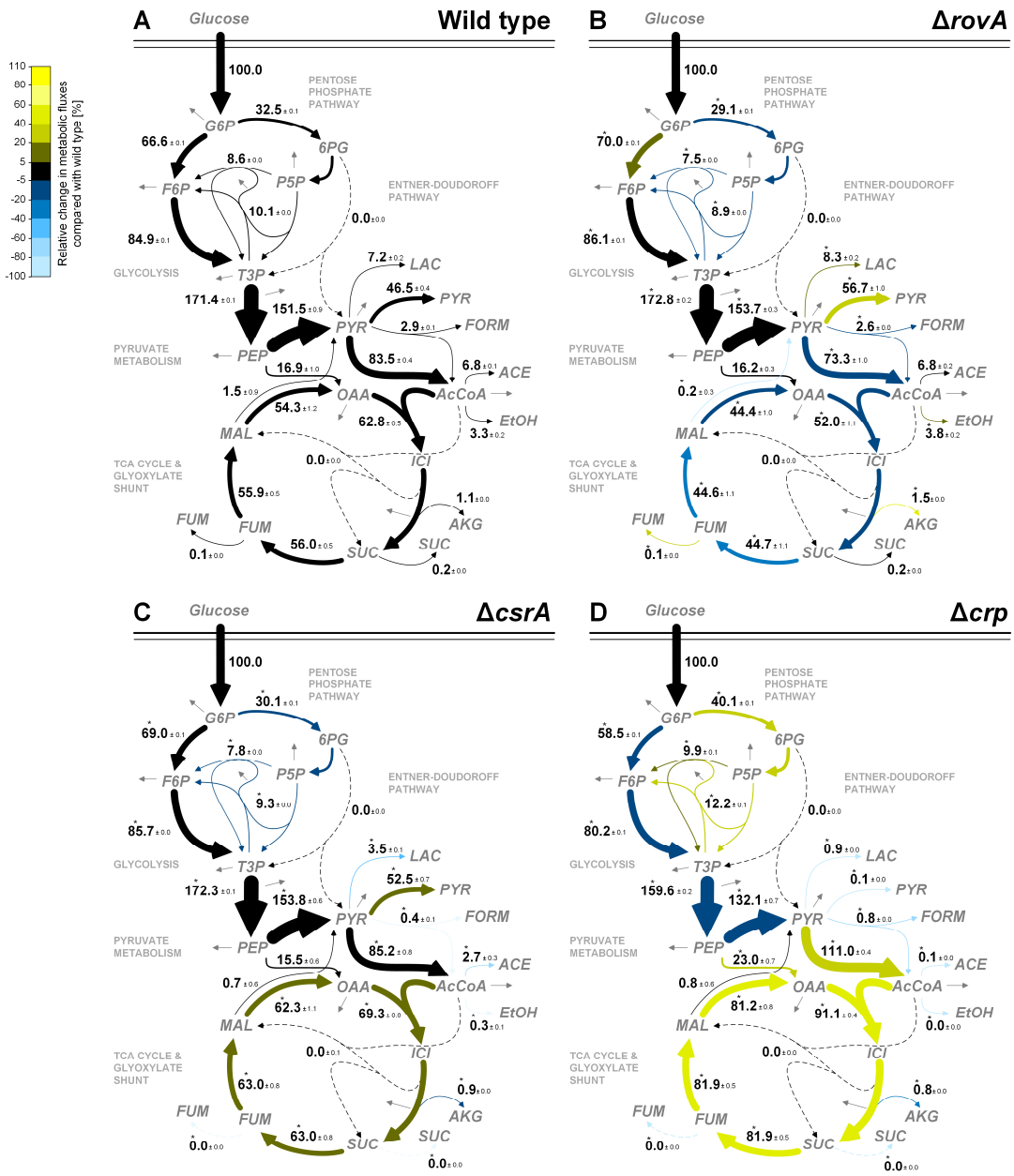

Figure 15. *In vivo* carbon flux distribution of glucose-grown *Y. pseudotuberculosis* (YPIII) (**A**) and the single gene deletion mutants *Y. pseudotuberculosis* YP3 (Δ*rovA*) (**B**), YP53 (Δ*csrA*) (**C**), and YP89 (Δ*crp*) (**D**) estimated from the best fit to the experimental results using a comprehensive approach of combined metabolite balancing and ^{13}C tracer experiments with labeling measurements of proteinogenic amino acids. For flux analysis, cells were grown on [1-^{13}C] glucose as a tracer substrate, which has been shown to resolve the major catabolic routes in *Y. pseudotuberculosis*, i.e., the PP, EMP, ED pathways, and TCA cycle (Wittmann, 2007). All fluxes are expressed as a molar percentage of the corresponding specific glucose uptake rate (7.1 mmol g^{-1} h^{-1}, 7.1 mmol g^{-1} h^{-1}, 3.1 mmol g^{-1} h^{-1} and 1.5 mmol g^{-1} h^{-1}), which was set as 100%. Significantly altered fluxes ($p<0.01$) are marked (*) and color indicates the relative change in metabolic fluxes compared with wild type. The errors represent 95% confidence intervals and were calculated by Monte-Carlo analysis.

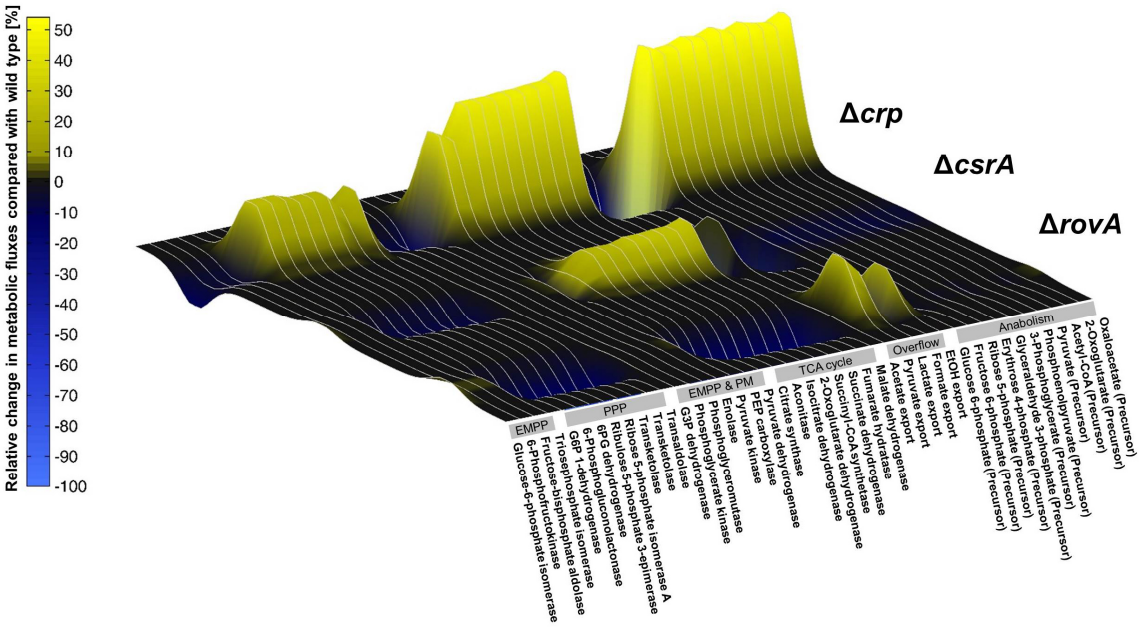

Figure 16. Control of the metabolic fluxes of *Y. pseudotuberculosis* YPIII by the catabolite repressor protein (Crp), the carbon storage regulator (CsrA), and the regulator of virulence (RovA). The data indicate the relative flux changes in the defined virulence mutants YP3 (Δ*rovA*), YP53 (Δ*csrA*), and YP89 (Δ*crp*), normalized to the wild type flux. The data refer to the intracellular flux distributions (Figure 15).

5.1.7 Mutants deficient in RovA, CsrA, and Crp reveal an altered expression pattern of virulence-associated, stress adaptation, and metabolic genes

To gain a more comprehensive understanding of how the virulence regulators interact with metabolism and mediate flux adaptations, changes in the fluxome were correlated with alterations in the gene expression pattern. For this purpose, microarray analyses were performed using total RNA isolated from the *Y. pseudotuberculosis* YPIII (wild type), YP3 (Δ*rovA*), YP53 (Δ*csrA*), and YP89 (Δ*crp*) cultures, which were also used for the fluxome analyses. The most representative changes in virulence and metabolic genes are given in Figure 17 and Figure 18, respectively. Additional transcriptional changes are provided in the appendix (Table 13). Of all of the protein-encoding chromosomal (4172) and virulence plasmid genes (92), the following changes (>1.7-fold, $p<0.01$) were observed compared with the wild type: 316 genes were affected in the *rovA* mutant (128 upregulated/188 down-

regulated), 913 genes were affected in the *csrA* mutant (475 upregulated/438 downregulated), and 729 genes were affected in the *crp* mutant (336 upregulated/393 downregulated) (Table 13). Classification according to the genome annotation of *Y. pseudotuberculosis* YPIII showed that the altered genes belonged to the following categories: virulence, motility and chemotaxis, stress adaptation, information storage and processing, and metabolism. The lack of each regulator caused a rather specific change in expression, i.e., only a subset of genes responded similarly in the different mutants (Figure 17, Figure 18, Table 13).

In all of the regulator deletion strains, multiple virulence-associated genes were affected (Figure 17, Table 13). *Y. pseudotuberculosis* YP3 (Δ*rovA*) exhibited specific changes in the expression of genes linked to host-pathogen interactions and serum resistance, including the previously identified RovA-dependent virulence genes of *Y. pestis* and *Y. enterocolitica* (Cathelyn *et al,* 2006; Cathelyn *et al,* 2007). *Y. pseudotuberculosis* YP53 (Δ*csrA*) and YP89 (Δ*crp*) showed a broader set of affected genes, e.g., regulators involved in initial colonization of the intestine and other host tissues (e.g., *rovA, invA, psaAB,* multiple adhesins and fimbrial factors), pathogenicity genes responsible for dissemination and immune defense during an ongoing infection (*yadA, ailA*, *ysc* and *yop* genes*)*, and type VI secretion systems that support survival in the host (Figure 17, Table 13) (Heesemann *et al,* 2006; Cascales, 2008).

In addition to the classical pathogenicity factors, several virulence-associated physiological processes showed changes in expression. The *flhDC* operon and several FlhDC-induced genes (*motAB, cheAWD, fli, flg* and *flh* genes) controlling the synthesis of flagella and motility were downregulated in the *crp* and *csrA* mutants.

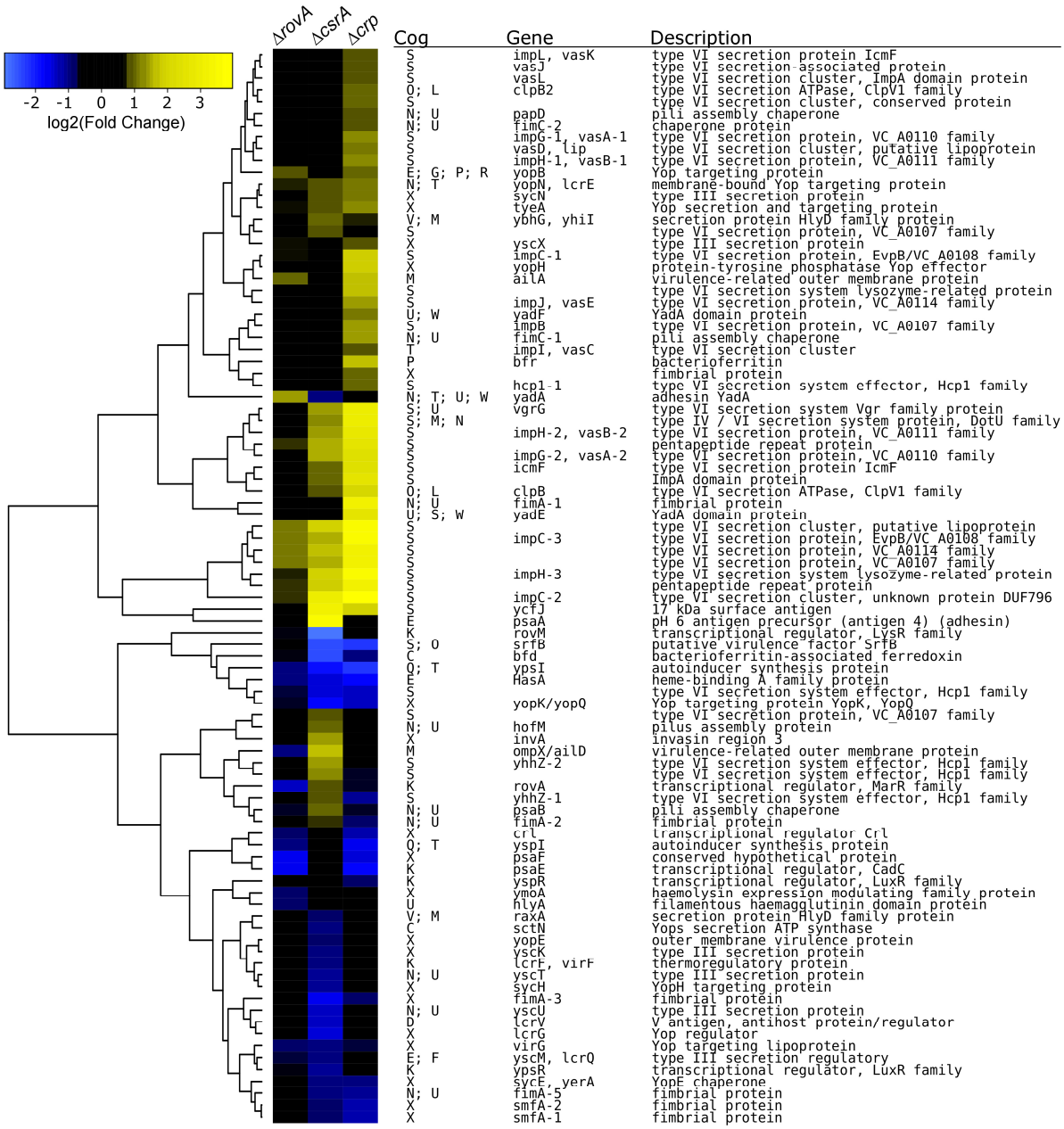

Figure 17. Impact of the virulence regulators RovA, CsrA, and Crp on expression of virulence genes of *Y. pseudotuberculosis*. The data are given as the fold change in expression in the single gene deletion mutants YP3 (Δ*rovA*), YP53 (Δ*csrA*), and YP89 (Δ*crp*) compared with the wild type YPIII expression and are arranged according to the hierarchical clustering analysis by the complete linkage clustering algorithm. The clusters of orthologous groups (cog) of proteins were used to classify the genes. “X” denotes non-existing classification. The data were obtained from three biological replicates, each with three samples.

Motility was previously shown to be activated by CsrA and was found to promote the host cell invasion and virulence of *Yersinia* (Young *et al,* 2000; Heroven *et al,* 2008; Heroven *et al,* 2012a). Several autoinducer systems were differently expressed in the *crp* mutant (*yspIR, ypsI*, and *luxS*) known to affect the biofilm formation, autoinducer AI-2 production, and pathogenicity of *Yersinia* species (Atkinson *et al,* 2008; Atkinson *et al,* 2011; Yu *et al,* 2013). In addition, many of the identified Crp- and CsrA-dependent genes are involved in the adaptation to environmental changes, such as heat shock (e.g., *ibpAB*, *groEL*, and *groES*), cold shock (*cspA-D* genes), carbon starvation (*cstA*), and other stress resistance genes (*katA, katY, sodA, sodC, clpA*, and *htrA*), which altogether seem to adapt and maximize biological fitness during the infection process (Table 13).

Inspection of the metabolic genes controlled by the different virulence-promoting regulators revealed the pyruvate-TCA cycle node as the focal point of transcriptional control (Figure 18). The TCA cycle was affected in all three mutant strains. The transcriptional response was most pronounced in *Y. pseudotuberculosis* Δ*csrA*. This mutant exhibited upregulation of multiple TCA cycle genes, i.e., *gltA, acnA, acnB, icdA*, and *fumA,* as well as the *sdhBADC* and *sucABCD* operons, whereas the *rovA* and *crp* mutants exhibited a partly downregulated and upregulated TCA cycle. In addition, a large set of genes encoding metabolic enzymes that are active at the junction between pyruvate and the TCA cycle node were induced in the absence of Crp and/or CsrA. This induction included a mild upregulation of the glyoxylate shunt (*aceA* and *aceB*) and of gluconeogenesis (*pckA, sfcA, maeB*, and *ppsA*). This change was complemented by upregulation of *poxB*, which encodes pyruvate oxidase as a ubiquinone-reducing alternative pathway for acetate formation.

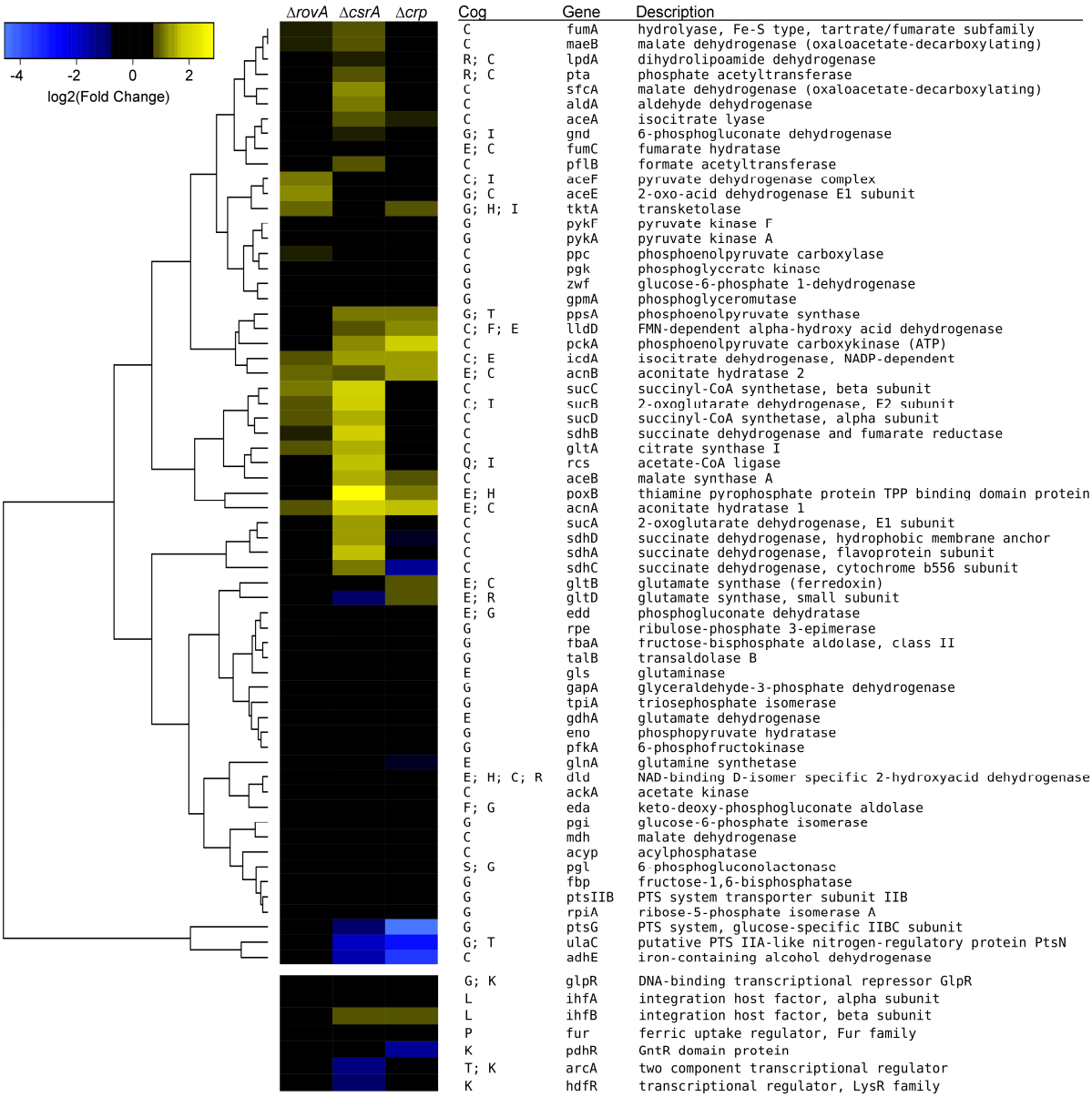

Figure 18. Impact of the virulence regulators RovA, CsrA, and Crp on the expression of genes related to the core metabolism of *Y. pseudotuberculosis* and of known transcriptional regulators (GlpR, IhfA/B, Fur, PdhR, ArcA, and HdfR) (Haverkorn van Rijsewijk *et al,* 2011). The data are given as the fold change in expression in the single gene deletion mutants YP3 (Δ*rovA*), YP53 (Δ*csrA*), and YP89 (Δ*crp*) compared with the wild type YPIII expression and are arranged according to the hierarchical clustering analysis by the complete linkage clustering algorithm. The clusters of orthologous groups (cog) of proteins were used to classify the genes. The data were obtained from three biological replicates, each with three samples.

In contrast, NADH-consuming alcohol dehydrogenase (*adhE*) was significantly downregulated in the Δ*csrA* and Δ*crp* mutants. Furthermore, the expression levels of catabolic enzymes, which are responsible for the uptake and utilization of carbohydrates and amino acids, and glycogen synthesis (*glgXAP*) were affected in the different mutant strains. Multiple phosphotransferase systems, permeases, and ABC transporters were differentially expressed in the *crp* and the *csrA* mutant. In particular the *ptsG* gene encoding the EIIBC subunit of the glucose phosphotransferase system (PTS), the *ulaABC*/*sgaTBA* operon encoding a putative ascorbate PTS system, and *glnQPH* for polar amino acid transport were strongly altered in the *crp* mutant and to a smaller extent in the *csrA* deficient strain. In agreement with previous results (Heroven *et al,* 2012b), also expression of *ptsIH, fruKB, manXZ, glpFK, mglBAC* for the uptake of glucose, fructose, mannose/sorbose, glycerol, and galactose were affected in the absence of the virulence-promoting metabolic regulator Crp, and several amino acid peptide transporter-encoding operons (*opp, ddp, tau*) were affected by the loss of Crp and/or CsrA. In addition, several genes involved in the nucleotide and fatty acid uptake and metabolism were regulated by Crp, CsrA, and/or RovA (e.g., *nupC1, ndk, pyrD, cdd, gpt, udp, xanP, uhpC, accA, fadBA, fadLIJ*) (Table 13).

5.1.8 The pyruvate-TCA cycle node as metabolic switch point of virulence

Taken together, the data strongly support a central role of the virulence-promoting regulator cascade in host-adapted re-adjustment of the carbon core metabolism in *Y. pseudotuberculosis*. In particular, Crp and CsrA seem to tightly coordinate the expression of virulence-associated traits with the operation of the central metabolic switch point: the pyruvate-TCA cycle node. To test this hypothesis and investigate the effect of this metabolic control point for virulence, targeted perturbations were focused. Different master regulators and enzymes are known to control the flux

through this central metabolic switch point in related bacteria (Haverkorn van Rijsewijk *et al,* 2011). Interestingly, several of these candidates were affected in the *crp* and *csrA* mutants. For example, the gene encoding the pyruvate dehydrogenase regulator protein (*pdhR*) was specifically downregulated in the *Y. pseudotuberculosis crp* mutant. PdhR acts as a transcriptional regulator in a pyruvate-dependent manner to control central metabolic fluxes, e.g., during the transition from anaerobic to microaerobic conditions (Göhler *et al,* 2011; Trotter *et al,* 2011). The expression of another key regulator of the TCA cycle, i.e., ArcA, was repressed in the Δ*csrA* strain. This global regulator is involved in the reprogramming of metabolism according to O_2 concentration (Spiro & Guest, 1991). The impact of this transcription factor is further supported by the fact that several genes (*cydAB, ptsG, sucBCD, poxB, cmk*, and *fadBA*) known to be under the control of ArcA in *E. coli* or *Salmonella* (Iuchi & Lin, 1988; Liu & De Wulf, 2004; Evans *et al,* 2011) were also controlled by CsrA and/or Crp in *Y. pseudotuberculosis* (Table 13).

In addition to ArcA and PdhR, which were among the Crp- and CsrA-dependent genes, PtsN and PykF appeared to be promising candidates to modulate the pyruvate-TCA cycle node in *Y. pseudotuberculosis* based on their impact in *E. coli*. A recent study showed that the second phosphotransferase system of *E. coli*, denoted as nitrogen-PTS (PTS^{Ntr}), controls fluxes in the central metabolism, especially at the pyruvate-TCA cycle node (Commichau *et al,* 2006; Jahn *et al,* 2013). The identified PTS^{Ntr}-dependent genes include multiple TCA cycle genes, which are differentially expressed in the *Y. pseudotuberculosis csrA* and/or *crp* mutant strains (*gltAB, sucB, sdhD*, and *aceA*) (Figure 18), indicating a close link between these global regulatory systems. In support of this assumption, expression of the *kdpFABC* operon, a well-known target of PTS^{Ntr} in *E. coli* (Lüttmann *et al,* 2009), was found to be upregulated in the Crp-deficient mutant (Table 13). The phosphorylation state of $EIIA^{Ntr}$ (PtsN) is

influenced by the activity of the sugar PTS through crosstalk (e.g., by competition for PEP); thus, alterations in the PTS^{Glc} components in the Crp- and CsrA-deficient strains (e.g., repression of *ptsG* and *ptsIH* in a *crp* mutant) might also affect the flux through the pyruvate-acetyl-CoA node and the TCA cycle via alteration of the PTS^{Ntr} activity. Utilization as well as strong upregulation of the sugar PTS (e.g., *ptsG* induction in the presence of Crp) might drain the phosphoryl groups of PEP towards the $EIIA^{Glc}$, leading to preferentially dephosphorylated $EIIA^{Ntr}$.

During growth on glucose, pyruvate is generated from PEP as a product of PTS^{Glc} and by the pyruvate kinase isoenzymes (PykA and PykF). To specifically target the pyruvate–TCA cycle node, it seemed appropriate to also directly perturb a particular enzyme of this metabolic control point. The deletion of pyruvate kinase in *E. coli* results in rerouting of a local flux through the combined reactions of PEP carboxylase and malic enzyme (Emmerling *et al,* 2002; Al Zaid Siddiquee *et al,* 2004). Of the two pyruvate kinase enzymes (PykA and PykF), PykF was selected because it is highly active during growth on glucose in *E. coli*, whereas PykA has a much lower activity (Al Zaid Siddiquee *et al,* 2004; Meza *et al,* 2012).

In this regard, single mutants of *arcA, pykF, ptsN*, and *pdhR* were constructed to study their impact on virulence. The first characterization of their growth physiology under laboratory conditions revealed that the glucose uptake was comparable to that of the wild type, suggesting the absence of any major effect on the biological fitness of the pathogen. In contrast, the pyruvate-derived by-products differed significantly, indicating that the fluxes around the pyruvate-TCA cycle node were affected. Each mutant showed a unique metabolic phenotype (Table 7).

Table 7. Growth characteristics of the *Y. pseudotuberculosis* wild type strain (YPIII) and the mutants YP49 (Δ*arcA*), YP252 (Δ*ptsN*), YP253 (Δ*pykF*), and YP274 (Δ*pdhR*). The data comprise the specific growth rate (μ), the specific rate of glucose uptake (q_{Glc}), and yields on glucose for biomass ($Y_{X/S}$), pyruvate ($Y_{Pyr/S}$), lactate ($Y_{Lac/S}$), acetate ($Y_{Ace/S}$), formate ($Y_{Form/S}$), succinate ($Y_{Suc/S}$), fumarate ($Y_{Fum/S}$), ethanol ($Y_{EtOH/S}$), and α-ketoglutarate ($Y_{Akg/S}$). The values represent the mean of three biological replicates and the corresponding standard deviations.

Strain	μ	q_{Glc}	$Y_{X/S}$	$Y_{Pyr/S}$	$Y_{Lac/S}$	$Y_{Ace/S}$	$Y_{Form/S}$	$Y_{Suc/S}$	$Y_{Fum/S}$	$Y_{EtOH/S}$	$Y_{Akg/S}$
	[h^{-1}]	[mmol g^{-1} h^{-1}]	[g mol^{-1}]	[molar percentage of the specific glucose uptake rate]							
YPIII (Wt)	0.32 ± 0	7.1 ± 0.3	45.2 ± 2.0	46.4 ± 1.4	7.1 ± 0.6	6.7 ± 0.3	3.0 ± 0.4	0.2 ± 0	0.1 ± 0	3.3 ± 0.7	1.1 ± 0.1
YP253 (Δ*pykF*)	0.26 ±0	5.5 ±0	46.4 ±1.4	36.5 ±2.8	16.2 ±1.3	3.5 ±0.4	0.4 ± 0.1	0.8 ± 0.1	0.6 ± 0	3.8 ±0.8	1.4 ±0.1
YP252 (Δ*ptsN*)	0.23 ±0	6.4 ±0.4	35.9 ±2.9	64.5 ±4.1	3.4 ±0.5	5.4 ±0.3	0.5 ± 0	0.3 ± 0.1	0.2 ± 0	5.8 ±0.3	1.7 ±0.1
YP274 (Δ*pdhR*)	0.19 ±0	6.3 ±0.3	32.3 ±1.5	70.7 ±5.4	2.6 ±0.5	16.4 ±1.1	<0.1	<0.1	0.2 ±0	3.4 ±0.4	1.3 ±0.1
YP49 (Δ*arcA*)	0.31 ±0.01	6.4 ±0.3	48.2 ±1.6	41.5 ±2.1	4.0 ±0.3	13.5 ±0.3	0.5 ±0.1	<0.1	<0.1	4.5 ±0.9	1.1 ±0.1

Values below 0.1% for the by-product yields were below the detection limit.

5.1.9 Perturbations of the metabolic core machinery at the pyruvate-TCA cycle node reduce *Yersinia* virulence

To examine whether the pyruvate-TCA cycle node represents a focal point of virulence control, co-infection experiments with the wild type and the mutant strains YP49 (Δ*arcA*), YP252 (Δ*ptsN*), YP253 (Δ*pykF*), and YP274 (Δ*pdhR*) were performed. Groups of BALB/c mice were orally infected with approximately 10^7 bacteria in an inoculum comprised of an equal mixture of the wild type and the isogenic mutant strains. The number of bacteria present in the Peyer's patches (PPs), the mesenteric lymph nodes (MLN), the liver, and the spleen were quantified five days post-infection (Figure 19). The loss of *pykF, ptsN*, and *arcA* resulted in a strong reduction of *Y. pseudotuberculosis* virulence, and a mild effect was observed for the *pdhR* mutant. The absence of PdhR and ArcA significantly reduced the initial colonization of the PPs early in the infection. The subsequent dissemination of the pathogen into the MLNs was significantly decreased or totally abolished in the *arcA*, *pykF*, and *ptsN* mutants (Figure 19).

Our experiments further revealed that PykF and PtsN functioning was crucial for colonization and/or persistence in deeper tissues, such as the liver and spleen. These results clearly indicate that the presence of the pyruvate-TCA cycle node-modulating factors ArcA, PtsN, and PykF is particularly important for the pathogenesis of *Y. pseudotuberculosis*, whereby the individual modulators seem to participate at different stages during the course of the infection. The observed effects are not based on a general growth defect of the investigated mutants because each mutant had an overall glucose uptake rate comparable to that of the wild type (Table 7) and a similar colonization rate in at least one of the tested tissues (Figure 19).

Figure 19►. Influence of a perturbation of the pyruvate-TCA cycle node on the virulence of *Y. pseudotuberculosis*. BALB/c mice were orally infected with an equal mixture of 10^7 CFU of wild type *Y. pseudotuberculosis* (YPIII) and one isogenic mutant strain, i.e., YP49 (Δ*arcA*), YP252 (Δ*ptsN*), YP253 (Δ*pykF*), or YP274 (Δ*pdhR*). After 5 days of infection, the mice were sacrificed, and the number of bacteria in homogenized host tissues and organs (Peyer's patches (PPs), mesenteric lymph nodes (MLNs), spleen, and liver) was determined by plating. Data from two independent experiments (10 mice/group) are represented in scatter plots of the CFU per gram as determined by the counts of viable bacteria on the plates (upper panel). Each spot represents the CFU count in the indicated tissue samples from one mouse. The log (CFU/gr.) of 10^2 bacteria marks the limit of detection. The statistical significances between the wild type and the mutants were determined by a Mann-Whitney test. P-values: n.s.: not significant; *: <0.05; **: <0.01; ***: <0.001. Lower panel: Data are graphed as competitive index values for tissue samples from one mouse. The bars represent the medians of the competitive index values. A competitive index score of 1 denotes no difference in virulence compared to that of YPIII.

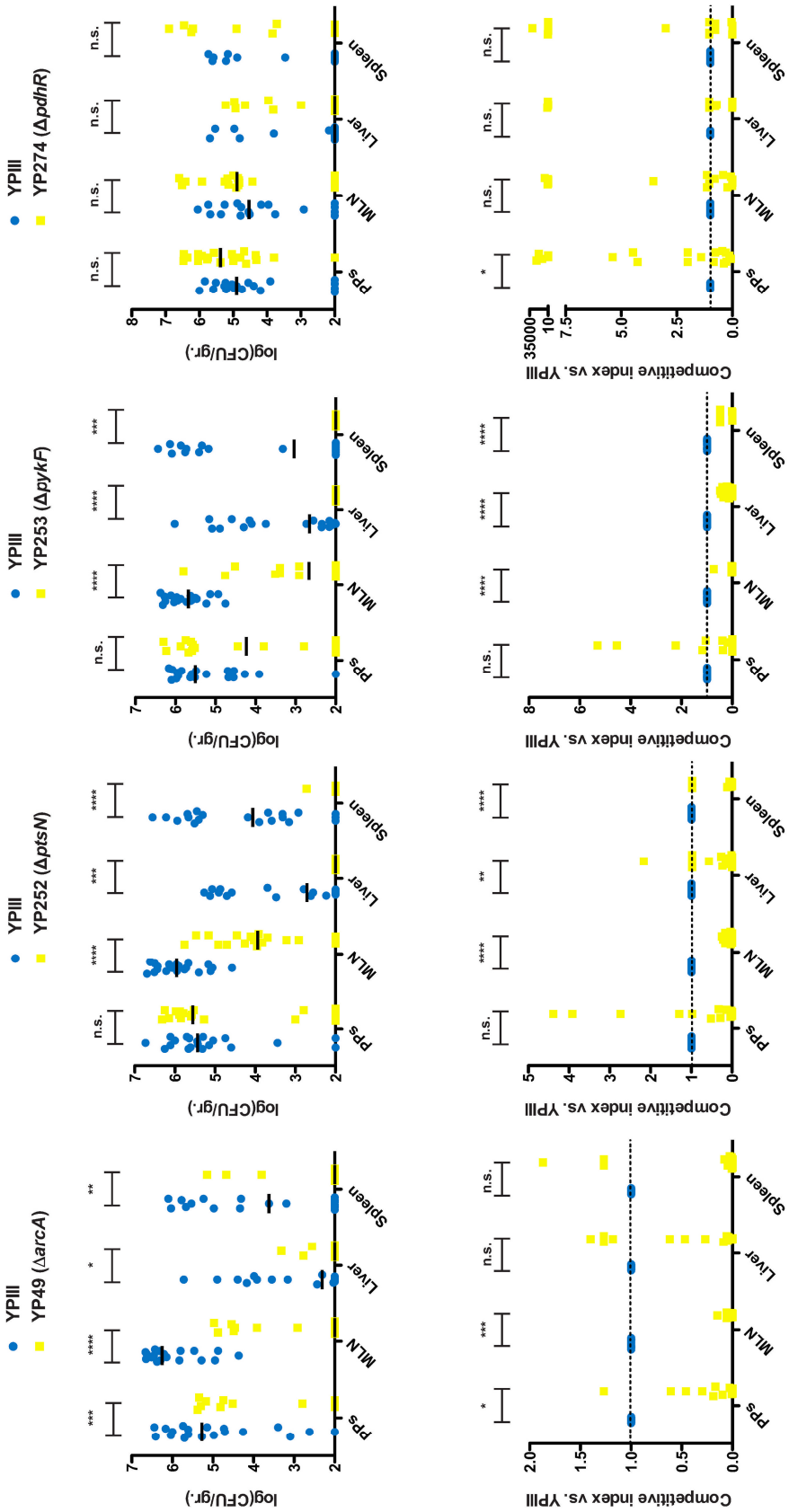
YPIII
YP49 (ΔarcA)
YPIII
YP252 (ΔptsN)
YPIII
YP253 (ΔpykF)
YPIII
YP274 (ΔpdhR)
log(CFU/gr.)
Competitive index vs. YPIII
PPs
MLN
Liver
Spleen
n.s.
*
**
***
****

5.1.10 Post-transcriptional control of flux as a crucial strategy for virulence

The present work, using a systems biology approach that integrates transcriptional control (transcriptome) with functional network operation (fluxome) in the human pathogen *Y. pseudotuberculosis*, elucidated a close link between the metabolic core machinery and pathogenic traits. It was shown that the virulence-promoting regulators RovA, CsrA, and Crp strongly affect the intracellular carbon fluxes (Figure 15, Figure 16) and the expression of multiple metabolic and virulence genes of *Y. pseudotuberculosis* (Figure 17, Figure 18). In particular, pyruvate metabolism and the TCA cycle emerged as focal points of control (Figure 21). Among the large set of metabolic flux changes, only a subset can be explained by transcriptional control (Figure 20).

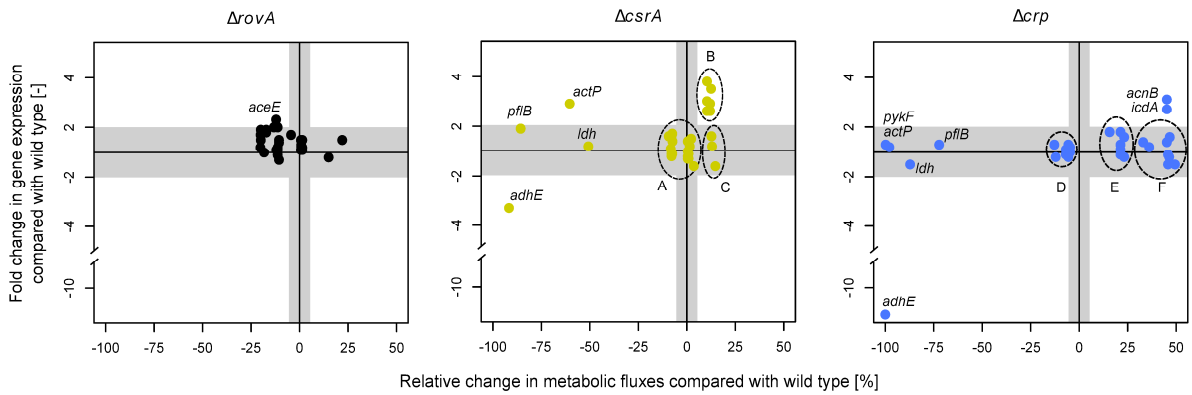

Figure 20. Quantitative correlation of the fluxome and transcriptome in the central carbon metabolism of *Y. pseudotuberculosis*. The integrated data are given as the relative change in the virulence mutants YP3 (Δ*rovA*), YP53 (Δ*csrA*), and YP89 (Δ*crp*) compared with the wild type YPIII. Abbreviations: *actP*, acetate permease; *adhE*, alcohol dehydrogenase; *pflB*, formate acetyl-transferase; *ldh*, lactate dehydrogenase; *acnB*, aconitase; *icdA*, isocitrate dehydrogenase; *pykF*, pyruvate kinase; A/D, Embden-Meyerhof-Parnas pathway and pentose phosphate pathway; B, tricarboxylic acid cycle; C, fumarase and malate dehydrogenase; E, pentose phosphate pathway; F, tricarboxylic acid cycle, pyruvate dehydrogenase and phosphoenolpyruvate carboxylase.

Obviously, the carbon fluxome of *Y. pseudotuberculosis* is largely under post-transcriptional control. Similarly, the primary metabolism of other bacteria is mainly

controlled by post-transcriptional mechanisms (Schilling *et al,* 2007; Haverkorn van Rijsewijk *et al,* 2011; Chubukov *et al,* 2013), which typically involve direct regulation of flux at the enzyme level by allosteric control (Link *et al,* 2013). Such a strategy seems crucial for the ability of pathogenic bacteria, such as *Y. pseudotuberculosis*, to cope with the rapidly changing environments that they face during their infection cycle.

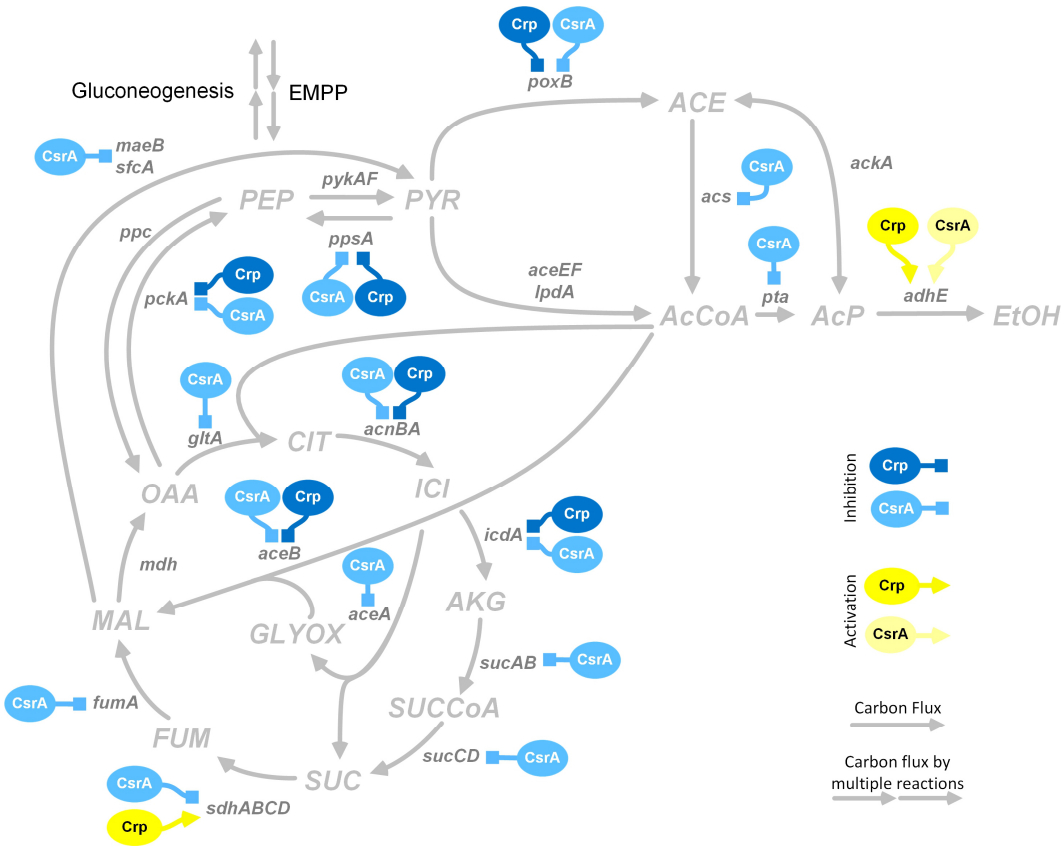

Figure 21. The pyruvate-TCA cycle node as the central control switch in the host-adapted control of metabolism and virulence in *Y. pseudotuberculosis*. The reaction arrows point in the physiological direction. The transcriptional control of genes by CsrA and Crp, which were identified by gene expression analysis (Table 13), is indicated. Bluish squares denote inhibition, yellowish arrows denote activation. Abbreviations: *pykF/pykA*, pyruvate kinases; *ppsA*, phosphoenolpyruvate synthase; *poxB,* pyruvate oxidase; *acs*, acetyl-CoA synthetase; *ackA*, acetate kinase; *adhE*, alcohol dehydrogenase; *pta*, phosphate acetyltransferase; *gltA*, citrate synthase; *acnBA*, aconitase; *icdA*, isocitrate dehydrogenase; *sucAB*, alpha-ketoglutarate dehydrogenase; *sucCD*, succinyl-CoA synthetase; *sdhABCD*, succinate dehydrogenase; *fumA*, fumarate hydratase; *mdh*, malate dehydrogenase; *aceA*, isocitrate lyase; *aceB*, malate synthase; *ppc,* PEP carboxylase; *pckA,* PEP carboxykinase; *aceEF*/*lpdA*, pyruvate dehydrogenase; *maeB*, *sfcA*, malic enzymes.

5.1.11 The secretion of high amounts of pyruvate by *Y. pseudotuberculosis* is unique among pathogens

The present study showed that *Y. pseudotuberculosis* released large amounts of pyruvate into the medium during growth on glucose. Excretion of pyruvate to this extent (46% of the glucose uptake) under these conditions is uncommon among related bacteria and primarily seems to be a transient phenomenon triggered during specific metabolic shifts, e.g., from aerobic to anaerobic growth (Trotter *et al,* 2011). Metabolically, the pyruvate secretion is somewhat intriguing at a first glance because its synthesis does not yield additional ATP or contribute to redox balancing, as in the case of pyruvate-derived acetate or lactate formation. The observed high fluxes for glucose uptake and glycolysis could induce pyruvate secretion due to a metabolic bottleneck downstream of this node. However, a limitation of the respiratory capacity can be excluded as a trigger for the pronounced pyruvate overflow due to the fully aerobic conditions during growth. Alternatively, the excretion of pyruvate could be important for the bacteria to avoid glucose-phosphate stress. High rates of nutrient uptake, in particular readily metabolizable PTS sugars, provide an advantage in the gut environment because these high rates reduce the availability of carbon nutrients for competing strains and organisms. However, an intracellular accumulation of phosphorylated sugar intermediates is growth inhibitory or bactericidal and induces a specific stress response (Vanderpool, 2007). Under this type of phosphate-sugar stress, *E. coli* induces the expression of the small regulatory RNA SgrS, which negatively controls the translation of *ptsG* mRNA, the mRNA that encodes the major glucose transporter $EIICB^{Glc}$, to reduce the substrate influx (Vanderpool & Gottesman, 2007). In fact, the *ptsG* transcript was found to be much less abundant in the *Y. pseudotuberculosis crp* mutant (Table 13), in which significantly lower amounts of pyruvate are secreted and glucose uptake is reduced (Figure 15 D, Table 4).

Additionally, pyruvate is a key signal in bacteria to program core metabolism (Trotter *et al,* 2011; Link *et al,* 2013); thus, the secretion might contribute to the fine adjustment of the intracellular level of this metabolite. Taken together, these findings indicate that pyruvate metabolism and export are likely used to control the biological fitness and virulence of *Yersinia*.

5.1.12 The pyruvate node and the TCA cycle are focal points of virulence control

The present study showed that the virulence-promoting metabolic regulators CsrA and Crp regulate the expression of multiple enzymes implicated in the control of the pyruvate-TCA cycle node (Table 13, Figure 21). Furthermore, it was demonstrated that modulators of this control point and, particularly, one of its enzymes (PykF) are crucial for *Y. pseudotuberculosis* virulence.

With regard to CsrA and Crp, both deletion mutants secreted much less or even no by-products; instead, these mutants channeled the carbon into the TCA cycle. This finding can be explained by the fact that CsrA and Crp act as repressors of multiple TCA cycle enzymes and associated pathway genes, and their deletion results in a moderate and strong derepression of the flux through the TCA cycle and the fuelling pathways (Figure 16, Figure 21, Table 13). Obviously, the control of the central carbon flow through the TCA cycle towards complete substrate oxidation seems to be important for optimizing overall fitness, reinforcing competitiveness, and adjusting the virulence functions of the pathogen. Recent work on the metabolic flux response in the commensal *E. coli* Nissle 1917 also revealed that CsrA has a strong influence on the central metabolism of glucose. However, in this case, strikingly lower fluxes via the TCA cycle were observed, which were accompanied by a 34% increase in acetate production (Revelles *et al,* 2013). This finding indicates significant differences

in the operation of central carbon metabolism between the commensal *E. coli* strain and the invasive enteropathogenic *Yersinia*, which most likely reflect different adaptation techniques of the colonized niches.

Pioneering systems biology studies of pathogenic *Yersinia* species, including *Y. pestis,* have reported that the metabolic core machinery is tightly regulated by virulence-associated environmental parameters in concert with virulence genes (Motin *et al,* 2004; Ansong *et al,* 2013). The first observations revealed the following: (i) an adjustment of many catabolic pathways for the metabolites available in mammals in response to a temperature shift from 26°C to 37°C (Motin *et al,* 2004); (ii) conserved post-transcriptional control of metabolism and (iii) the translational machinery, including the modulation of glutamate levels in *Yersinia* spp. (Ansong *et al,* 2013). Here, it was discovered that the pyruvate-TCA cycle node is a focal point of virulence control. It was demonstrated that regulators and enzymes modulating the fine adjustment of the pathway fluxes at this node affect important cellular components linked to metabolism and virulence in *Y. pseudotuberculosis*. The mouse infection data indicate that the discovered metabolic control point is of an utmost but previously unrecognized importance for the pathogenicity of this microorganism.

There are other interesting precedents tempt to speculate that the co-adjustment of metabolism and virulence through the pyruvate-TCA cycle node is not only crucial for the genus *Yersinia* but also constitutes a more general strategy in pathogenic bacteria. For instance, deletions in the pyruvate pathway have been shown to alter the SPI1-mediated gene expression and infectivity of the *Salmonella enterica* serovar Typhimurium (Abernathy *et al,* 2013). Furthermore, it has been reported that *Salmonella* mutants that are unable to convert malate to pyruvate and oxaloacetate are avirulent and immunogenic in BALB/c mice (Mercado-Lubo *et al,* 2009) and that

an incomplete TCA cycle increases the survival of *Salmonella* during infection (Bowden *et al,* 2010). Moreover, in *Pseudomonas aeruginosa*, mutations in TCA cycle enzymes have been shown to affect the type III secretion system of the pathogen (Dacheux *et al,* 2002), and regulators of *Staphylococcus aureus* responding to TCA cycle-associated metabolic changes have also been implicated in virulence control (Somerville & Proctor, 2009).

A more detailed investigation of the interplay between the pyruvate-TCA cycle node and the regulation of virulence factors in enteric and other pathogens promises a better understanding of the complex networks of host-adapted metabolism and may aid in the discovery of novel drug targets and in the design of more effective therapies against bacterial infections.

5.2 Antibiotic treatment

5.2.1 Response of core metabolism to antibiotic treatment

As shown, the virulence program of *Y. pseudotuberculosis* involves flux rearrangement at the pyruvate-TCA cycle node, probably to face the changing environments during its life cycle. Obviously, survival in the host is, at least, partly controlled and supported by metabolism. Therefore, it was tempting to see, to which extent metabolism is affected by standard antibiotic therapies and how *Y. pseudotuberculosis* responds to antibiotic stress. For this purpose, the carbon flux distribution of *Y. pseudotuberculosis* was analyzed at sub-inhibitory concentrations of erythromycin and tetracycline, two standard antibiotics of clinical therapies applied against infections. Shortly, the macrolide antibiotic erythromycin acts through reversible binding of the 50S ribosome subunit and subsequent inhibition of translocation (Mutschler *et al,* 2005). Erythromycin is a narrow-spectrum antibiotic, preferentially used for treatment against Gram-positive bacteria. The low susceptibility by Gram-negative bacteria to erythromycin is due to its high hydrophobicity (Köhler *et al,* 2001). The minimal inhibitory concentration (MIC) of erythromycin ranges from 16 to 128 mg L^{-1} for different *Y. pseudotuberculosis* strains (Stock & Wiedemann, 1999). Here, an intermediate concentration of 50 mg L^{-1} was used for metabolic flux analysis. In contrast, tetracycline is a broad-spectrum antibiotic with high efficiency against a set of Gram-negative bacteria. Furthermore, tetracycline is used against multiple infections of the gastro intestinal tract (Burger & Wachter, 1998). It acts through prohibition of the binding of aminoacyl-tRNA to the acceptor site of bacterial ribosomes (Mutschler *et al,* 2005). Here, reported inhibitory concentrations of tetracycline (0.5 – 2 mg L^{-1}) (Stock & Wiedemann, 1999) did not permit growth under tested conditions. Hence, a concentration of 0.1 mg L^{-1} was

used to enable growth. Taken together, the two chosen antimicrobial agents affect a similar target, but show distinct susceptibilities among bacterial genera.

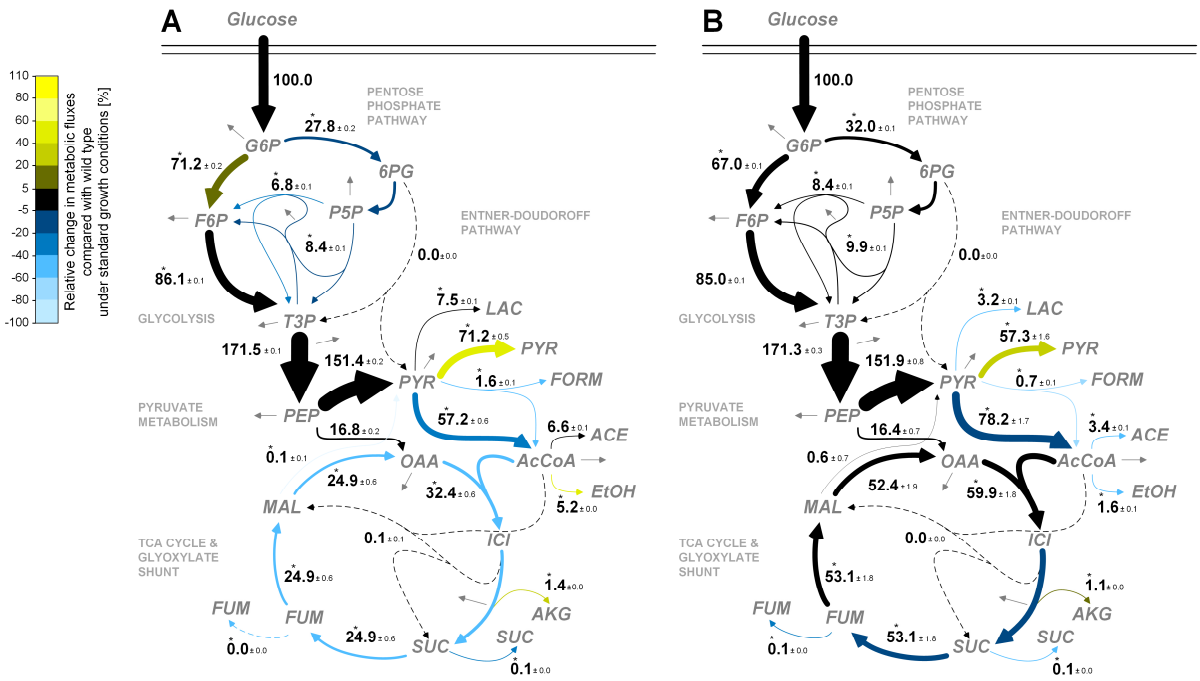

Figure 22. *In vivo* carbon flux distribution of glucose-grown *Y. pseudotuberculosis* wild type (YPIII) under administration of 50 mg L^{-1} erythromycin (**A**) and under administration of 0.1 mg L^{-1} tetracycline (**B**) estimated from the best fit to the experimental results using a comprehensive approach of combined metabolite balancing and ^{13}C tracer experiments with labeling measurements of proteinogenic amino acids. For flux analysis, cells were grown on [1-^{13}C] glucose as the tracer substrate. The cultures showed metabolic (Figure 23) and isotopic steady states (Figure 24). All fluxes are expressed as the molar percentage of the corresponding specific glucose uptake rate (6.0 mmol g^{-1} h^{-1} and 5.6 mmol g^{-1} h^{-1}), which was set as 100%. Significantly altered fluxes ($p<0.01$) are marked (*). Color indicates the relative change in metabolic fluxes compared with wild type under standard growth conditions. The errors represent 95% confidence intervals and were calculated by Monte-Carlo analysis.

When grown under antibiotics stress, *Y. pseudotuberculosis* showed a decreased specific growth rate and an altered flux distribution at the pyruvate-TCA cycle node. Administration of erythromycin lowered the growth rate by 9%, whereas the pyruvate efflux was increased by 53% (Table 8). The carbon to form the additional amount of pyruvate was mainly withdrawn from the TCA cycle (Figure 22A). The pyruvate efflux was increased even at the level of absolute fluxes (Figure 25B). Metabolic steady

state was verified by the constant stoichiometry of by-product formation (Figure 23) and isotopic steady state by the constant mass isotopomer distributions of nonlabeled (M_0), single labeled (M_1), and double labeled (M_2) *t*-butyl-dimethylsilyl derivates of proteinogenic amino acids (Figure 24). The excellent agreement between measured and simulated mass isotopomer distributions demonstrated high confidence in the obtained flux distribution (Table 9).

Table 8. Growth characteristics of *Y. pseudotuberculosis* wild type (YPIII) in *Yersinia* minimal medium (YMM) and under administration of the antimicrobial agent erythromycin (YMM+Ery) or tetracycline (YMM+Tet). The data comprise the specific growth rate (μ), the specific rate of glucose uptake (q_{Glc}), and yields on glucose for biomass ($Y_{X/S}$), pyruvate ($Y_{Pyr/S}$), lactate ($Y_{Lac/S}$), acetate ($Y_{Ace/S}$), formate ($Y_{Form/S}$), succinate ($Y_{Suc/S}$), fumarate ($Y_{Fum/S}$), ethanol ($Y_{EtOH/S}$), and α-ketoglutarate ($Y_{Akg/S}$), respectively. Values represent the mean of three biological replicates with corresponding standard deviations.

Condition	μ	q_{Glc}	$Y_{X/S}$	$Y_{Pyr/S}$	$Y_{Lac/S}$	$Y_{Ace/S}$	$Y_{Form/S}$	$Y_{Suc/S}$	$Y_{Fum/S}$	$Y_{EtOH/S}$	$Y_{Akg/S}$
	[h^{-1}]	[mmol g^{-1} h^{-1}]	[g mol^{-1}]	[molar percentage of the specific glucose uptake rate]							
YMM	0.32 ± 0	7.1 ± 0.3	45.2 ± 2.0	46.4 ± 1.4	7.1 ± 0.6	6.7 ± 0.3	3.0 ± 0.4	0.2 ± 0	0.1 ± 0	3.3 ± 0.7	1.1 ± 0.1
YMM+Ery	0.29 ± 0	6.0 ± 0.2	49.2 ± 2.3	70.9 ± 2.2	7.5 ± 0.3	6.7 ± 0.6	1.6 ± 0.4	0.2 ± 0	<0.1	5.1 ± 0.1	1.4 ± 0.1
YMM+Tet	0.26 ± 0.01	5.6 ± 0.4	46.5 ± 5.0	57.6 ± 5.1	3.2 ± 0.3	3.3 ± 0.6	0.8 ± 0.3	< 0.1	<0.1	1.6 ± 0.3	1.1 ± 0.1

Values below 0.1% for the by-product yields were below the detection limit.

The administration of tetracycline lowered the specific growth rate and the glucose uptake rate by approximately 20%, similar to what was observed for erythromycin (Table 8). In contrast, the relative carbon flux through glycolysis, PP pathway, and TCA cycle remained approximately at the values of the wild type under standard growth conditions. However, pyruvate efflux was increased by 24% at the expense of other by-products (Figure 22B). With regard to absolute flux, fluxes through central carbon metabolism were generally decreased (Figure 25B), whereas the pyruvate secretion rate was maintained at 3 mmol g^{-1} h^{-1}, as found for the wild type under standard growth conditions (Table 8, Figure 25B).

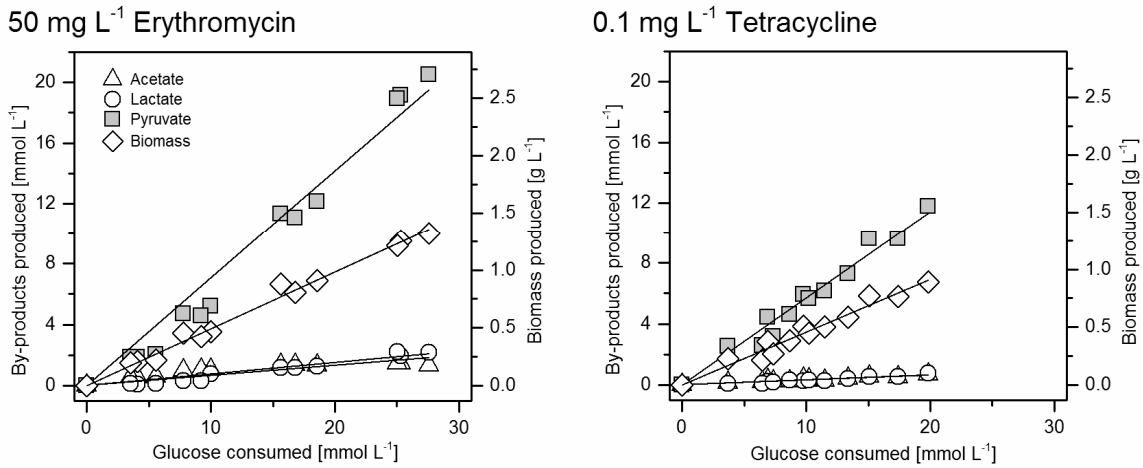

Figure 23. Stoichiometry of by-product formation during cultivation of the wild type of *Y. pseudotuberculosis* (YPIII) under administration of 50 mg L^{-1} erythromycin and 0.1 mg L^{-1} tetracycline. The linear correlation between formed pyruvate (*gray square*), acetate (*open triangle*), lactate (*open circle*), biomass (*open diamond*) and consumed glucose indicates metabolic steady state. All cultivations were performed in triplicate.

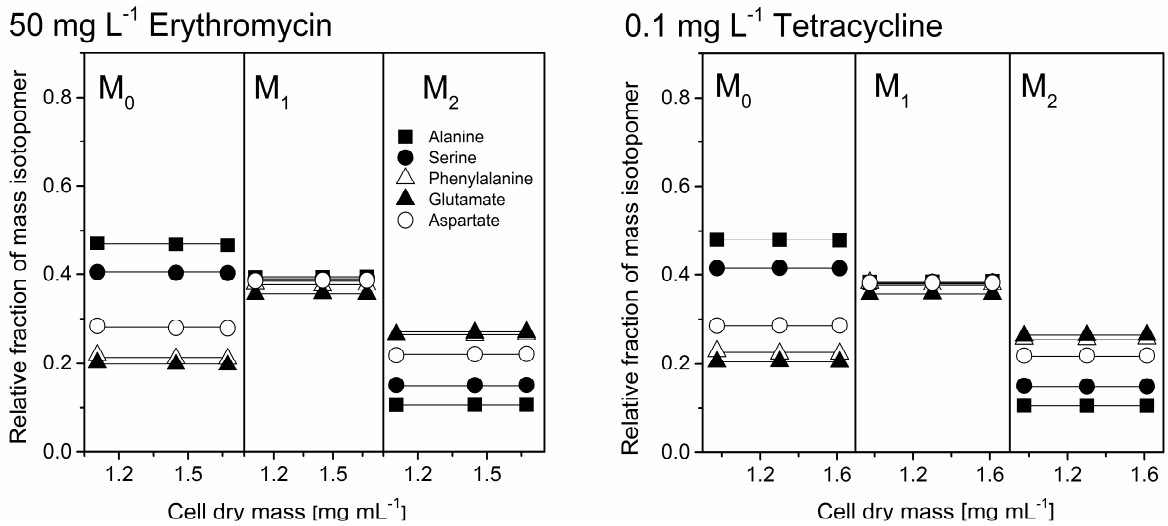

Figure 24. Verification of isotopic steady state during ^{13}C tracer studies of *Y. pseudotuberculosis* grown on 99% [1-^{13}C] glucose and under administration of either 50 mg L^{-1} erythromycin or 0.1 mg L^{-1} tetracycline by constant labeling patterns of proteinogenic amino acids at different cell dry mass concentrations, reflecting different cultivation time points. The data comprise the relative fractions of nonlabeled (M_0), single labeled (M_1), and double labeled (M_2) M-57 fragments of alanine (*black square*), serine (*black circle*), phenylalanine (*open triangle*), glutamate (*black triangle*), and aspartate (*open circle*).

5.2.2 Inherent erythromycin resistance of *Yersinia pseudotuberculosis* is accompanied by maintaining a highly active glycolysis

A recent study has demonstrated that erythromycin susceptibility by methicillin-resistant *Staphylococcus* was restored by inhibition of ATP delivering pyruvate kinase. Hereby, the tested *Staphylococcus* strains harbored multiple copies of a plasmid coding for the efflux pump MsrA that provides resistance against different macrolide antibiotics and obtains necessary energy by two ATP-binding motifs (Chan *et al,* 2013). According to this, the increased pyruvate secretion could be a viable strategy to maintain a high glycolytic flux under antibiotic stress to provide high amounts of ATP (Figure 22A). The ATP could then be used for inherent drug efflux pumps. ATP is further known as a crucial co-factor for enzymatic inactivation of antimicrobial macrolides (O'Hara *et al,* 1998). Concerning this, sufficient supply of ATP is at least crucial for two main strategies to overcome antimicrobial stress. Hence, simultaneous manipulation of glycolytic activity and administration of erythromycin implies the possibility to recover drug efficiency.

5.2.3 The high susceptibility for tetracycline is accompanied by the absence of major flux rerouting in *Yersinia pseudotuberculosis*

The administration of tetracycline led to an increased pyruvate efflux at the expense of other by-products (Figure 22B; Figure 25). However, a major decrease in TCA cycle flux, as observed for erythromycin, did not occur. This tempts to speculate that, a high TCA cycle flux is a crucial characteristic for maintenance of bacterial fitness under tetracycline induced stress. In general, efflux determinants are the most wide spread resistant factors in Gram-negative bacteria. At present, 38 tetracycline resistant determinants are described of which 23 act by efflux, 11 act by ribosomal protection, 3 act by enzymatic protection, and 1 acts by an unknown mode of mechanism (Roberts, 2005). Interestingly, tetracycline efflux is generally maintained

by a metal-tetracycline/H^+ antiporter with NADH as driving force (Yamaguchi *et al,* 1990; Chopra & Roberts, 2001). Assuming that the efflux of tetracycline by *Y. pseudotuberculosis* requires NADH, it seems reasonable that *Yersinia* maintains a high TCA cycle flux and concomitantly decreases the flux through NADH-consuming reactions, such as lactate dehydrogenase and alcohol dehydrogenase (Figure 22B, Figure 25).

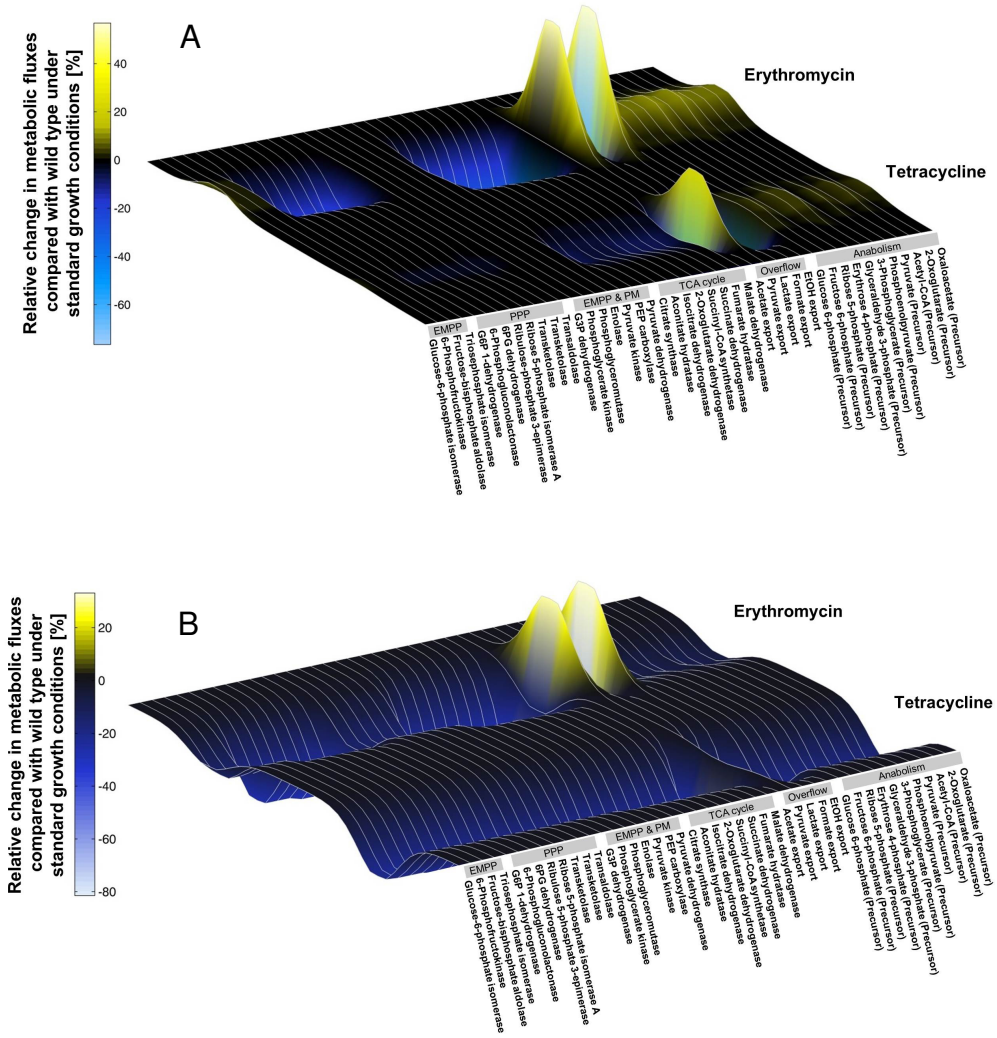

Figure 25. Relative (A) and absolute (B) flux changes in *Y. pseudotuberculosis* YPIII under administration of 50 mg L^{-1} erythromycin or 0.1 mg L^{-1} tetracycline, normalized to the flux distribution of the wild type without addition of antimicrobial agents.

Taken together, the chosen sub-inhibitory levels of antibiotics resulted in a similar slight reduction of bacterial fitness, at concentrations of 0.2 µmol L^{-1} and 68 µmol L^{-1}

for tetracycline and erythromycin, respectively (Table 8). However, *Y. pseudotuberculosis* responded differently on the level of intracellular fluxes. Whereas maintenance of a high glycolytic flux and ATP supply were the major benefits of the altered fluxes under treatment with erythromycin, tetracycline seemed to reduce NADH consuming pathways and to maintain a high TCA cycle flux. Both flux adaptations might be explained by the needs to specifically support efflux of the antibiotic, thus pointing at a possible role of metabolism to defend against antibiotic stress.

Table 9. Relative mass isotopomer fractions of *t*-butyl-dimethylsilyl derivates of proteinogenic amino acids used for ^{13}C metabolic flux analysis of *Y. pseudotuberculosis* YPIII cultivated on 99% [1-^{13}C] glucose and under administration of 50 mg L^{-1} erythromycin or 0.1 mg L^{-1} tetracycline. The data set comprises experimental values with deviations from replicate GC/MS measurement (Exp) and calculated values (Calc), predicted by the solution of the mathematical model that corresponded to the optimized set of fluxes.

		Erythromycin			**Tetracycline**		
		M_0	**M_1**	**M_2**	**M_0**	**M_1**	**M_2**
Ala (*m/z*) 260	Exp	0.467 (±0.01%)	0.394 (±0.03%)	0.106 (±0.04%)	0.479 (±0.04%)	0.384 (±0.05%)	0.105 (±0.05%)
	Calc	0.462	0.391	0.113	0.474	0.383	0.110
Val (*m/z*) 288	Exp	0.284 (±0.11%)	0.416 (±0.04%)	0.217 (±0.16%)	0.298 (±0.45%)	0.412 (±0.30%)	0.209 (±0.03%)
	Calc	0.282	0.412	0.219	0.297	0.411	0.210
Thr (*m/z*) 404	Exp	0.281 (±0.05%)	0.388 (±0.13%)	0.221 (±0.25%)	0.285 (±0.14%)	0.384 (±0.09%)	0.219 (±0.16%)
	Calc	0.282	0.382	0.221	0.286	0.380	0.220
Asp (*m/z*) 418	Exp	0.281 (±0.47%)	0.387 (±0.29%)	0.221 (±0.36%)	0.287 (±0.53%)	0.383 (±0.12%)	0.219 (±0.28%)
	Calc	0.282	0.381	0.221	0.285	0.379	0.220
Glu (*m/z*) 432	Exp	0.197 (±0.38%)	0.358 (±0.34%)	0.269 (±0.10%)	0.205 (±0.30%)	0.358 (±0.01%)	0.264 (±0.18%)
	Calc	0.197	0.355	0.268	0.204	0.356	0.264
Ser (*m/z*) 390	Exp	0.404 (±0.03%)	0.392 (±0.14%)	0.150 (±0.31%)	0.415 (±0.07%)	0.384 (±0.04%)	0.148 (±0.18%)
	Calc	0.408	0.387	0.150	0.418	0.381	0.148
Phe (*m/z*) 336	Exp	0.211 (±0.23%)	0.375 (±0.26%)	0.263 (±0.04%)	0.223 (±0.35%)	0.378 (±0.05%)	0.255 (±0.04%)
	Calc	0.209	0.375	0.267	0.224	0.380	0.259
Gly (*m/z*) 246	Exp	0.757 (±0.08%)	0.172 (±0.20%)		0.756 (±0.00%)	0.173 (±0.03%)	
	Calc	0.753	0.175		0.756	0.173	
Tyr (*m/z*) 466	Exp	0.185 (±1.21%)	0.344 (±0.08%)	0.270 (±0.06%)	0.198 (±0.09%)	0.348 (±0.49%)	0.263 (±0.31%)
	Calc	0.180	0.344	0.275	0.193	0.350	0.269

5.3 Control of virulence by temperature

5.3.1 Impact of temperature on virulence of *Y. pseudotuberculosis*

As shown, the abundance of the global virulence regulator RovA in *Y. pseudotuberculosis* is mediated by the nutrient environment (Table 3), which reflects a fine-tuned adaptation of the pathogen to respond to the different environment inside and outside of its host. Similarly, also temperature strongly affects the level of RovA. The regulator of virulence shows decreased stability and only little autoactivation at 37°C (Herbst *et al,* 2009). So far, the temperature dependence of RovA expression is only known as qualitative phenomenon. Towards a better understanding and model-based description, it appeared straightforward to study this on a quantitative basis, which, however, required precise and defined experimental handling. For this purpose, *Y. pseudotuberculosis,* expressing green fluorescent protein (GFP) under control of the *rovA* promoter, should be cultivated in a small scale continuously operated reactor. Coupled to fluorescence-activated cell sorting and Western blot analysis, this provided the possibility to precisely analyze the gene expression of RovA as function of temperature and time.

5.3.2 Development of a reactor setup for precise temperature profiles

The analysis of temperature dependence of RovA expression is limited, when performed in shake flasks. Particularly, accurate and fast step changes of temperature are not feasible in standard incubators, so that it is impossible to uncover common phenomena such as bistability and hysteresis, as intended here. Accordingly, a continuous reactor set-up was used for temperature shift experiments. First tests with the conventional reactor system revealed that the commercial heating system, based on a heating element, did not allow fast changes of broth temperature, but that it took up to 15 minutes until a desired temperature was reached. This was

not suitable for the planned experiments. To this end, the built-in heating rod was combined with temperature control by a water-filled jacket around the reactor to control temperature. For fast and precise temperature up-shifts, the temperature of water in the jacket was set to a value slightly below the target temperature. Using this procedure, temperature overshooting, otherwise observed, was avoided. Almost intermediate temperature down-shifts were realized by adding ice chilled water to the water cycle, so that the temperature of the cooling jacket was temporally far below the desired one. The interplay of cooling water and heating rod then provided exact temperature control.

5.3.3 Determination of an appropriate dilution rate for RovA synthesis

In batch culture of *Y. pseudotuberculosis*, *rovA* transcription starts at mid-log phase and reaches a peak during stationary phase (Nagel *et al,* 2001). Obviously, RovA expression is promoted under reduced rates of growth. Hence, a relatively low dilution rate representing this growth phase seemed favorable for the planned continuous culture. Initial growth experiments were conducted at 25°C and 37°C, respectively, to determine the process window with regard to suitable specific growth rates. These were carried out in 100 mL baffled shake flasks with a working volume of 10 mL of LB broth. Specific growth rates, obtained from differentiation of data on cell concentration, varied between 0.6 h^{-1} and 0.2 h^{-1} at both temperatures (Figure 26). From this, a dilution rate of about 0.3 h^{-1} seemed appropriate for continuous cultivation, because it is significantly below the maximum specific growth rate (μ_{max}). Moreover, the resulting hydrodynamic residence time of 3.3 hours is relatively short and, thus, reduces the time necessary for achieving steady state.

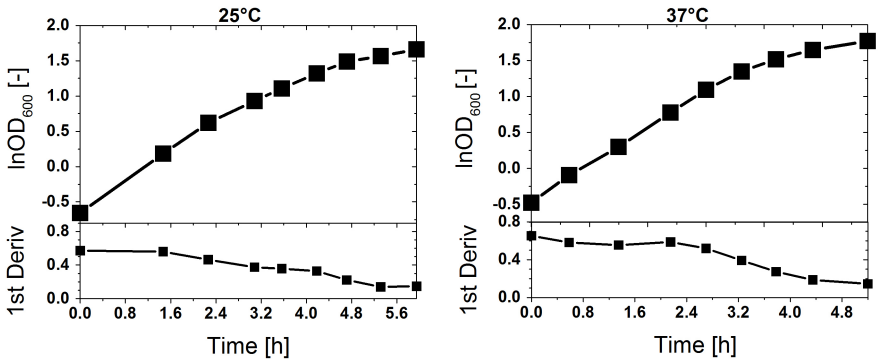

Figure 26. Initial growth experiments of *Yersinia pseudotuberculosis* (YPIII) harboring plasmid pkH70 at 25°C and 37°C, respectively, to determine the process window with regard to suitable specific growth rates for subsequent continuous cultivations. Experiments were taken out in 10 mL selective LB broth in 100 mL baffled shake flasks in triplicate. The first derivation (1st Deriv) equals the specific growth rate [h^{-1}] and was calculated for discrete points by the average of the slopes between the point and its two closest neighbors as performed by the data analysis software OriginPro 9 (OriginLab, Northampton, US).

5.3.4 Temperature up-shift mimicking the entrance of *Y. pseudotuberculosis* into the host

An initial batch phase of approximately five hours was performed at 25°C, and then the reactor was switched to continuous operation (D = 0.32 h^{-1}). For an ideal stirred tank reactor, volume exchange is 95% and more than 99% after three and five residence times, respectively (Dunn *et al,* 2003). After 15.2 hours, equal to 3.2 hydrodynamic residence times, the culture reached constant states regarding cell concentration and pH-value (Figure 27). At this point, however, the dissolved oxygen level had reached a minimum (29%) and started to increase to a constant level of 53% within the next six hours. Hence, steady state was accomplished after 5.1 residence times. Then, defined step changes of the temperature were realized: the temperature was increased from the initial value of 25°C, to 28°C, 30°C, 32°C, 34°C, and 37°C, linked to periodic sampling of cells from the reactor outlet for monitoring of

cell concentration and subsequent fluorescence-activated cell sorting and Western blotting.

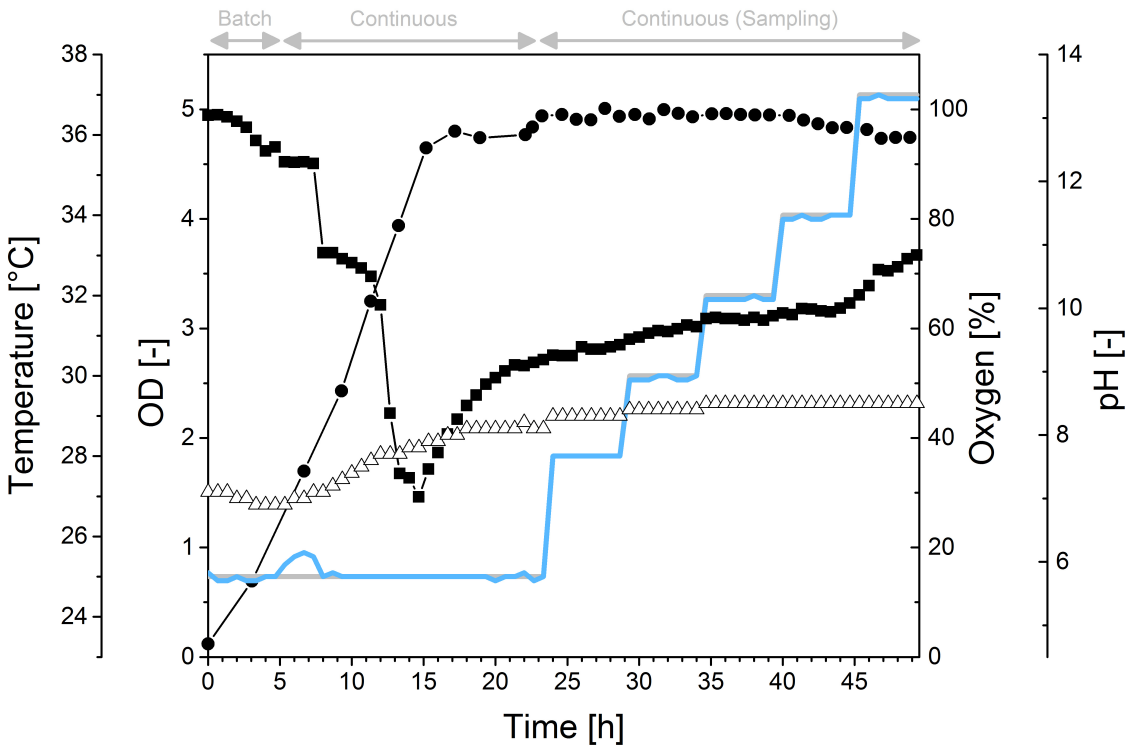

Figure 27. Cultivation profile of *Yersinia pseudotuberculosis* YPIII harboring plasmid pkH70. The given temperature up-shift mimics the entrance into the host. Optical density (OD) at 600 nm is given as filled circles (●), oxygen saturation as filled squares (■), pH as empty triangles (△), actual and target temperature as blue and gray lines, respectively.

5.3.5 Temperature down-shift mimicking release from the host

An initial batch phase at 25°C was performed. After five hours, the reactor was switched to continuous mode. A constant optical density and pH value was achieved within 15 hours post inoculation. The oxygen saturation reached a constant value after 21 hours. Thus, the process showed high consistence with the previous cultivation (Figure 27 and Figure 29). In contrast to the up-shift experiment, a drastic down-shift without any interim steps was performed. This was due to the fact that a preliminary study revealed that the restart of RovA synthesis only occurs at ambient temperatures. The fraction of fluorescing cells, representing an active RovA transcription, was far below 1% until the temperature was set to 25°C (Figure 28).

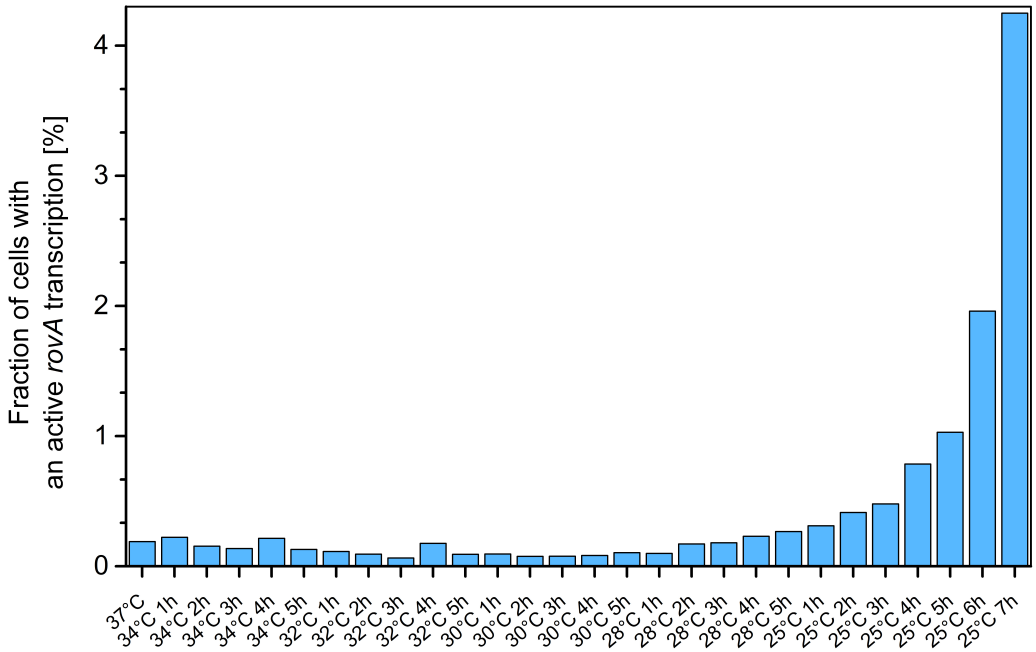

Figure 28. Preliminary study on reactivation of *rovA* transcription as function of time and temperature. The decreasing temperature mimics the release of *Yersinia pseudotuberculosis* from the host. Data represent the relative fractions of fluorescing *Yersinia pseudotuberculosis* YPIII harboring plasmid pkH70 (expressing the green fluorescent protein under control of the *rovA* promoter), estimated by FACS analysis. Samples were taken at different temperatures and after certain time intervals from the outlet of a continuous cultivation at a dilution rate of 0.32 h^{-1}.

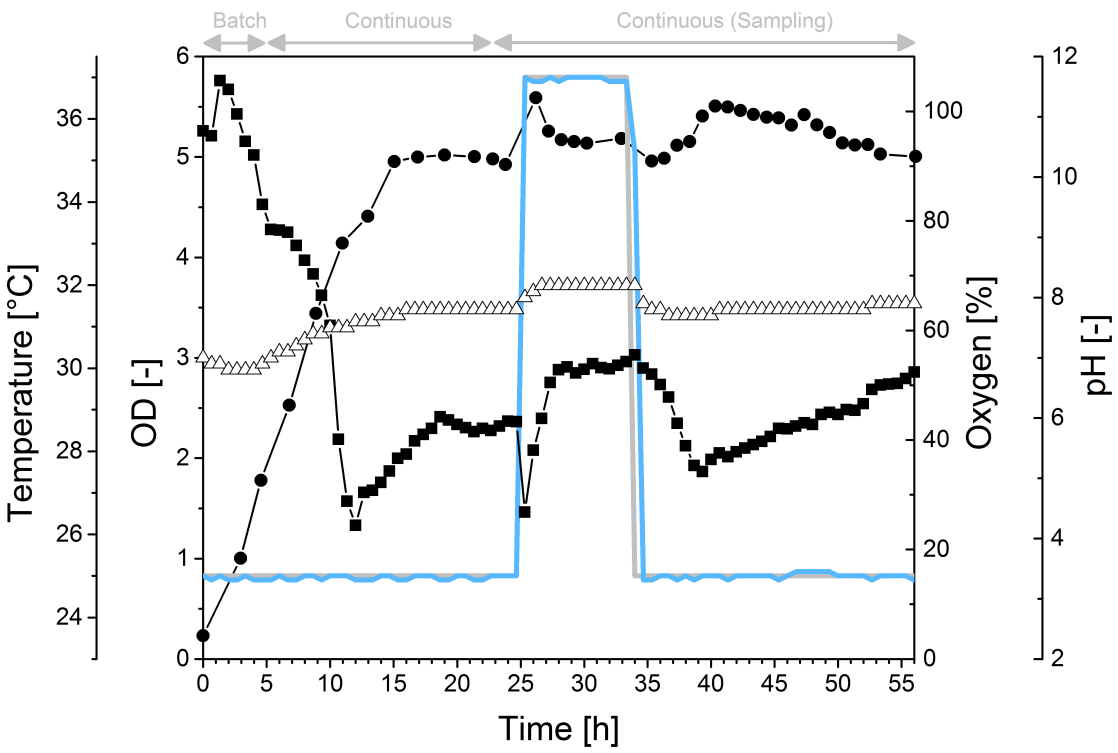

Figure 29. Cultivation profile of *Yersinia pseudotuberculosis* YPIII harboring plasmid pkH70. The temperature down-shift mimics the release from the host. Optical density (OD) at 600 nm is given as filled circles (●), oxygen saturation as filled squares (■), pH as empty triangles (△), actual and target temperature as blue and gray lines, respectively.

5.3.6 Fluorescence-activated cell sorting correlates with Western blot analysis

The fraction of green fluorescent positive (GFP+) *Yersinia* cells possess an active *rovA* transcription (Figure 30A). Simultaneously processed Western blot analysis illustrates the correlation of transcription and actual protein availability (Figure 30B).

5.3.7 Silencing and activation of *rovA* transcription follow different kinetics

The entire data set from fluorescence-activated cell sorting of the continuous reactor cultures is given in Figure 30 and Table 10. Within the first hours (25°C - 28°C, 5h), the amount of GFP+ cells, i.e., cells that expressed RovA, did not alter significantly. The increase of temperature to 30°C and to 32°C, respectively, induced a slow but steady decrease of the traceable *rovA* transcription to 88% (after five hours at 32°C).

The switch from 32°C to 34°C then induced a strong decrease of the RovA level (63% GFP+ cells, after five hours at 34°C). The decrease of RovA was even more pronounced at 37°C, the temperature reflecting the host of the pathogen. After growth of *Y. pseudotuberculosis* for one hour at this temperature, the amount of GFP+ cells was reduced to 32%, and it further decreased within the next two hours to only 2% (Figure 30). The direct comparison of transcriptional activity (GFP expression) and traceable RovA levels (Western blot) at 37°C showed that, although 32% of *Yersinia* cells remained in the GFP+ state and obviously still expressed *rovA*, no RovA was detected in the prepared cell lysates. During the temperature up-shift, *Yersinia* showed similar changes of *rovA* expression and RovA level. This is consistent with post-transcriptional control of RovA by temperature induced conformational change that makes the protein more susceptible to degradation by proteases (Herbst *et al,* 2009). From the fact that the number of GFP+ cells decreased significantly slower than the actual amount of RovA, it is tempting to speculate that delayed inactivation of *rovA* transcription is favorable for survival of the population during the infection.

After transcription of *rovA* was completely halted at 37°C, the re-activation of transcription after cooling down of the population to 25°C was markedly prolonged. Temperatures above 25°C did not favor re-activation (Figure 28). At 25°C, it took more than six hours to reach significant amounts of GFP+ cells (4.1% ± 3.4%). Even after 17 hours at 25°C, only half of the population (46% ± 12%) showed active *rovA* transcription (Figure 30, Table 10). Additionally, the standard deviation of FACS analyses increased significantly compared to the up-shift experiments, which might indicate a certain degree of culture heterogeneity due to statistical probability of the process of reactivation.

5.3.8 Bistability can explain the observed RovA expression pattern

Taken together, the progression of RovA expression indicates bistability: a genetically homogenous population that diverges into two phenotypically different subpopulations without genetic changes (Smits *et al,* 2005; Dubnau & Losick, 2006; Casadesus & Low, 2013). Since the environmental conditions were equal for every cell within the bioreactor, the stochastically driven re-activation of *rovA* transcription (Figure 30) seems an indicator of such a behavior. Additionally, evidence for bistability was the observed hysteresis (Figure 30), an inevitable property of bistability (Ferrell, 2002). Hysteresis describes the fact that the time profile of the switch between two states differs depending on whether the system is switched forward or backward (Smits *et al,* 2006). It is known that population heterogeneity, mediated by bistability, provides an efficient way to prepare for different circumstances and maximize the chance for survival (Dubnau & Losick, 2006).

5.3.9 Does RovA expression fit with known models of bistability?

Two mechanisms are known to mediate bistability, i.e., bifurcation of an isogenic population. The first mechanism is based on positive, non-linear auto-regulation and the second mechanism is based on two mutually repressing regulators (Gardner *et al,* 2000; Dubnau & Losick, 2006). Previously, the activity of the *rovA* promoter was found to correlate with the amount of the RovA protein (Heroven *et al,* 2004; Nagel *et al,* 2001) and, hence, to be subjected to auto-regulation. Moreover, the experimental data in this work show striking parallels to an auto-regulated bistable system in *B. subtilis*. The progression of RovA during the down-shift from 37°C to 25°C (Figure 30) matches the bistable response of *Bacillus subtilis* during developing competence (Smits *et al,* 2005). Auto-regulation and stochastic fluctuation of an activator protein were found as crucial elements to mediate bistability in *Bacillus subtilis*. Additionally identified regulatory elements were found to influence the properties of bistability in

controlling the basal level of the activating transcription factor and the threshold at which auto-regulation is initiated (Smits *et al,* 2005). In *B. subtilis* the auto-regulator ComK (transcription regulator of competence) is proteolyzed during exponential growth, whereas at stationary phase, a signal cascade inhibits the involved proteases and prevents degradation of ComK. As a consequence, individual cells have a certain probability to reach the threshold concentration of ComK, at which the auto-regulation starts. In *Yersinia,* RovA is constitutively expressed, but undergoes a conformational change at 37°C, which makes it inactive and susceptible to proteolysis. At decreasing temperature, RovA switches back to the stable form and starts to compete with the RovA repressor H-NS (Herbst *et al,* 2009).

In summary, the quantitative analysis of RovA by defined temperature variations in continuous culture revealed a bistable behavior of this global virulence regulator. Hence, heterogeneity in RovA expression will lead to at least two fundamentally different subpopulations. As RovA affects a wide range of metabolic, stress, and virulence genes (Herbst *et al,* 2009), this probably has fundamental effects on cellular physiology of *Y. pseudotuberculosis*. Bistability seems an important phenomenon in the lifestyle of the pathogen. The experimental data, together with additional studies will provide the basis for a further investigation of the underlying mechanisms and kinetics of virulence control.

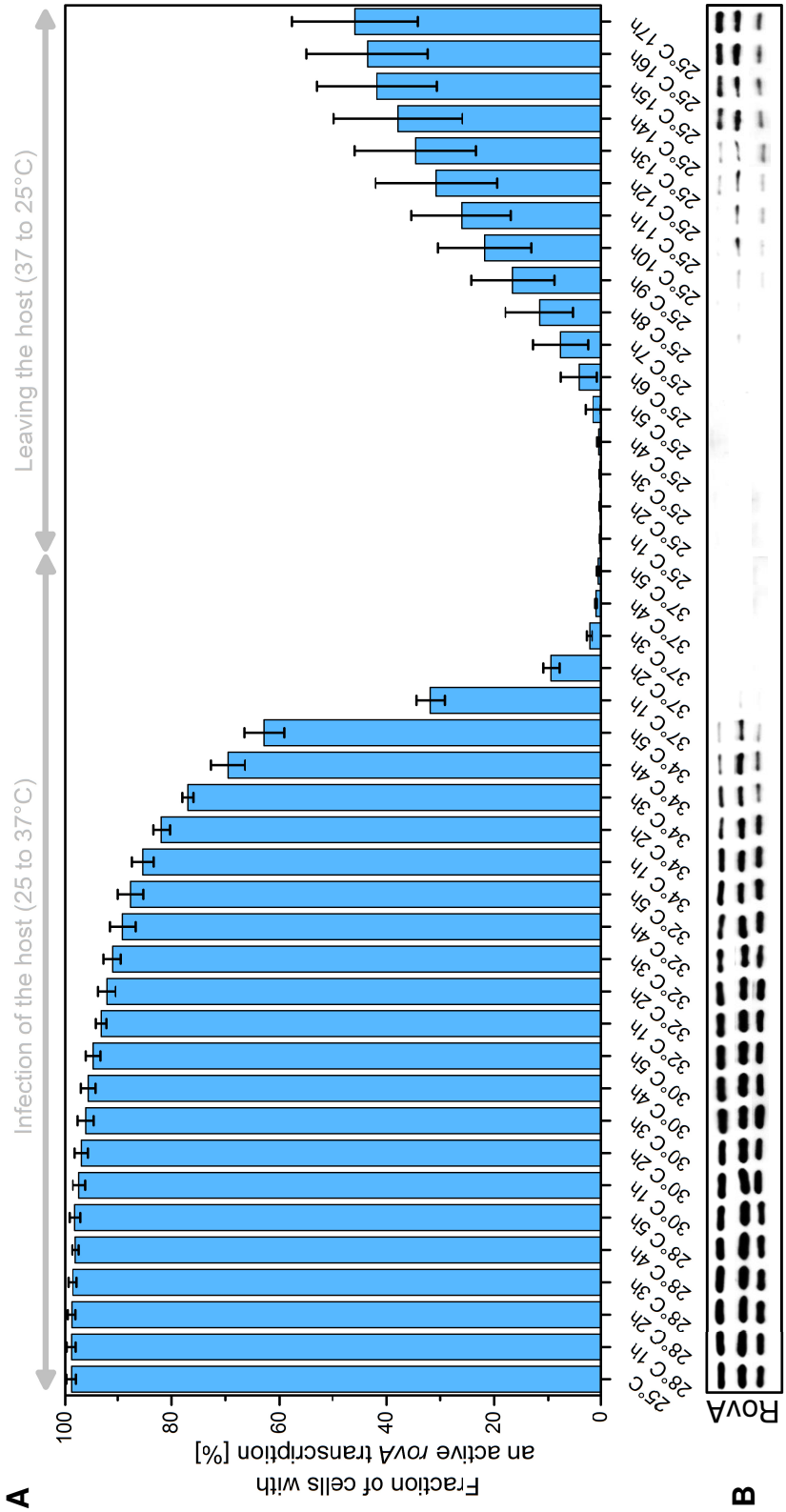

Figure 30. Relative fractions of fluorescing *Yersinia pseudotuberculosis* YPIII with plasmid pkH70 (expressing the green fluorescent protein under control of the *rovA* promoter), estimated by FACS analysis (**A**). The temperature up-shift to 37°C mimics the entrance of *Yersinia* into the host and the subsequent down-shift to 25°C mimics the release from the host. The data represent the means and deviations of three independent biological replicates. In parallel, the actual RovA concentration of each replicate was measured by Western blot analysis (**B**). All samples were taken from a continuous cultivation at a dilution rate of 0.32 h^{-1}.

Table 10. Fractions of fluorescing *Yersinia pseudotuberculosis* YPIII with plasmid pkH70 (expressing the green fluorescent protein under control of the *rovA* promoter). Samples were taken at different temperatures and after certain time intervals from the outlet of a continuous cultivation at a dilution rate of 0.32 h^{-1} performed in triplicate. The evaluation of 100,000 counted cells per run was performed to ensure statistical certainty.

Program step	Replicate 1 GFP+ [%]	Replicate 2 GFP+ [%]	Replicate 3 GFP+ [%]	Mean GFP+ [%]	Standard deviation [%]
25°C	99.6	99.1	97.8	98.8	0.9
28°C 1h	99.5	99.2	97.8	98.8	0.9
28°C 2h	99.4	99.0	97.9	98.8	0.8
28°C 3h	99.2	98.9	97.7	98.6	0.8
28°C 4h	98.8	97.7	97.6	98.0	0.7
28°C 5h	99.3	97.8	97.3	98.1	1.0
30°C 1h	98.7	96.9	96.5	97.4	1.2
30°C 2h	98.3	96.4	96.0	96.9	1.2
30°C 3h	97.6	96.1	94.6	96.1	1.5
30°C 4h	97.1	95.4	94.4	95.6	1.4
30°C 5h	96.2	94.5	93.5	94.7	1.4
32°C 1h	94.3	93.0	92.4	93.2	1.0
32°C 2h	94.1	91.1	91.3	92.2	1.7
32°C 3h	93.0	90.7	89.7	91.1	1.7
32°C 4h	91.9	88.4	87.2	89.2	2.4
32°C 5h	90.4	86.3	86.3	87.7	2.4
34°C 1h	87.7	84.3	84.2	85.4	2.0
34°C 2h	83.4	80.2	82.0	81.9	1.6
34°C 3h	77.6	75.9	77.6	77.0	1.0
34°C 4h	69.4	66.4	72.7	69.5	3.2
34°C 5h	61.3	60.1	67.0	62.8	3.7
37°C 1h	30.4	30.2	34.9	31.8	2.7
37°C 2h	11.1	8.0	8.9	9.4	1.6
37°C 3h	2.8	1.7	2.1	2.2	0.5
37°C 4h	0.7	0.9	1.1	0.9	0.2
37°C 5h	0.2	0.6	0.7	0.5	0.3
25°C 1h	0.1	0.2	0.2	0.2	0.1
25°C 2h	0.1	0.1	0.2	0.2	0.1
25°C 3h	0.2	0.2	0.2	0.2	0.0
25°C 4h	0.7	0.2	0.2	0.4	0.3
25°C 5h	3.2	0.8	0.5	1.5	1.5
25°C 6h	8.1	2.5	1.9	4.1	3.4
25°C 7h	13.5	5.4	4.0	7.6	5.1
25°C 8h	18.7	8.9	7.1	11.6	6.3
25°C 9h	25.3	13.2	10.9	16.5	7.7
25°C 10h	31.5	18.7	15.0	21.7	8.7
25°C 11h	36.5	23.3	18.5	26.1	9.3
25°C 12h	43.6	26.6	22.1	30.8	11.3
25°C 13h	47.2	31.4	25.3	34.6	11.3
25°C 14h	51.3	33.7	28.6	37.9	11.9
25°C 15h	54.5	37.4	33.5	41.8	11.2
25°C 16h	56.5	39.0	35.3	43.6	11.3
25°C 17h	59.1	41.7	36.9	45.9	11.7

6 CONCLUSION AND OUTLOOK

The interaction of pathogens with the human host has been studied for more than 200 years (Brown *et al,* 2008) and, since then, a lot of information about virulence has been obtained. Although the human host is even considered as a chemostat that provides specific nutritional conditions for different infection sites (Brown *et al,* 2008), the complex interplay between nutritional status, metabolism, and virulence is still not understood, and the metabolic requirements of *Yersinia* for adapting to and surviving in different host niches are largely unknown. In this work, a systems biology approach was utilized to address this question with a focus on central carbon metabolism. In particular, the link between virulence and metabolism was investigated in the wild type and in specific mutants lacking the key virulence regulators CsrA, Crp, and RovA that coordinate virulence and metabolism. To this end, transcriptome and ^{13}C based fluxome analyses were integrated. The latter involved ^{13}C tracer studies, mass spectrometric labeling analysis, and comprehensive computer models to assess the pathway flux (Sauer, 2006; Kohlstedt *et al,* 2010). This work provided quantitative insight into the molecular fluxes of *Y. pseudotuberculosis*. Derived data sets were integrated into a carefully curated concept, which identified the pyruvate-TCA cycle node as a focal point of virulence control. Second generation mutants with knock-outs in regulatory genes of this metabolic branch point, i.e., Δ*arcA*, Δ*ptsN*, and Δ*pdhR* and of its central enzyme, i.e., pyruvate kinase, were constructed and tested in an oral mouse infection model. The loss of each factor resulted in significant reduction of *Yersinia* virulence. Since the glucose uptake rate of all new mutants was comparable to that of the wild type, and a similar colonization rate in at least one of the tested mouse tissues was observed, a reduction of virulence based on a growth defect could be excluded. In summary, this work proved integrated transcriptome and ^{13}C fluxome studies as a powerful tool to provide new insights into the life style of

pathogens and point at the pyruvate-TCA cycle node as a focal point of virulence control in *Yersinia pseudotuberculosis*.

Different directions of research appear particularly promising to further explore the life style of the pathogen. A closer view to the real infection process might be obtained by applying ^{13}C metabolic flux analysis, i.e., investigation of the actual phenotype of the cell at the level of pathway flux, to a host model using a prepared mouse intestine as culture vessel. This would allow to directly correlate tissue integrity and data from the in-depth profiling of virulence mutants. In addition, *in vitro* experiments mimicking organ-specific growth environments will further help to decipher the control mechanisms of the identified pyruvate-TCA cycle node. One way to approach this task is to determine the metabolic phenotype in the presence of alternative carbon sources (e.g., pyruvate, glucose, acetate, or glutamine) as the access to these metabolites differs throughout the host (Sugimoto *et al,* 2012).

As shown, the effect of erythromycin and tetracycline on the metabolic phenotype was analyzed. The observed effect on carbon flux distribution was different even though both antibiotics inhibit translocation. Administration of erythromycin, e.g., increased the pyruvate efflux by 53% at the expense of TCA cycle flux. An increased pyruvate efflux could be a viable strategy to provide high amounts of ATP and thus favors ATP driven macrolide efflux (Chan *et al,* 2013). In contrast, active tetracycline secretion is a NADH driven process (Yamaguchi *et al,* 1990; Chopra & Roberts, 2001) and in accordance therewith, *Yersinia* maintains a high TCA flux under tetracycline therapy. Thereby, both flux adaptions might be explained by the needs to specifically support efflux of the antibiotic. Hence, analysis of a *Yersinia* mutant with an altered pyruvate kinase activity, e.g., the single gene deletion mutant YP253 (Δ*pykF*), seems interesting to further investigate the role of metabolism under administration of the tested antibiotics.

Finally, the abundance of the global regulator RovA is an indicator for virulence promoting conditions and was shown to be mediated by the nutrient environment. The fine-tuned adaption of the pathogen to respond to different conditions inside and outside the host is further mediated by temperature (Herbst *et al,* 2009). Thus far, RovA abundance as a function of temperature was mainly analyzed qualitatively. In this work, RovA abundance was determined quantitatively using fluorescence-activated cell sorting and Western blot analysis. A continuous culture with defined temperature variations was used to mimic the infection process. In summary, the measured progression of RovA expression showed stochastically driven re-activation and hysteresis as a characteristic property of bistability (Ferrell, 2002). As a wide range of metabolic, stress, and virulence genes (Herbst *et al,* 2009) is controlled by RovA, bistability probably leads to fundamentally different subpopulations. The resulting heterogeneity prepares the population best for different challenges and thus maximizes survival (Dubnau & Losick, 2006). The experimental data is an excellent basis for further analyses and will help to investigate the underlying mechanisms and kinetics of virulence control towards dynamic models.

7 APPENDIX

7.1 Abbreviations

3,4-DHB	3,4-Dihydroxybenzoic acid
B and BT (suffix)	Metabolite serves as biomass precursor
EX (suffix)	Secreted metabolite
Δ	Indicates a gene deletion
1st Deriv	First derivation
3PG	3-Phosphoglycerate
6PG	6-Phosphogluconate
accA	Gene encoding acetyl-CoA carboxylase, carboxyl transferase, alpha subunit
AcCoA/ACCOA/Acetyl-CoA	Acetyl coenzyme A
Ace or ACE	Acetate
aceA	Gene encoding isocitrate lyase
aceB	Gene encoding malate synthase A
aceEF, lpdA	Genes encoding pyruvate dehydrogenase
ackA	Gene encoding acetate kinase
acnA, acnB	Genes encoding aconitate hydratase 1 and 2
acs	Gene encoding acetyl-CoA synthetase
actP	Gene encoding acetate permease
adhE	Gene encoding acetaldehyde/alcohol dehydrogenase
ailA	Gene encoding virulence-related outer membrane protein
Akg or AKG	α-Ketoglutaric acid
Ala/ALA	Alanine
Asp/APSX	Aspartate
ArcA	Transcriptional regulator of aerobic respiratory control
arcA	Gene encoding transcriptional regulator of aerobic respiratory control
ATP	Adenosine triphosphate
B. subtilis	*Bacillus subtilis*
BALB/c mice	Bagg albino c inbred mice strain
BP	Bisphosphate
bp	Base pairs
Calc	Calculated values
cdd	Gene encoding cytidine deaminase
CDM	Cell dry mass
CDW	Cell dry weight
CFU	Colony-forming units
cheA	Gene encoding CheA signal transduction histidine kinase
cheD	Gene encoding methyl-accepting chemotaxis sensory transducer
cheW	Gene encoding CheW protein
CHRM	Chorismate
CI	Confidence interval
CIT	Citrate
clpA	Gene encoding ATP-dependent Clp protease, ATP-binding subunit clpA
cmk	Gene encoding cytidylate kinase
CO2	Carbon dioxide
CoA	Coenzyme A
cog	Clusters of orthologous groups of proteins
ComK	Transcriptional regulator of competence
Crp	Catabolite repression protein
crp	Gene encoding catabolite repression protein
cspA-D	Genes encoding cold-shock DNA-binding domain proteins
CsrA	Carbon storage regulator A
csrA	Gene encoding carbon storage regulator A
CsrB and CsrC	Regulatory RNAs of the Carbon storage regulator system
cstA	Gene encoding carbon starvation protein CstA
cTrans	Carbon transitions
cydA	Gene encoding cytochrome bd ubiquinol oxidase subunit I
cydB	Gene encoding cytochrome d ubiquinol oxidase, subunit II
ddp genes	Genes encoding peptide transport factors
DHAP	Dihydroxyacetone phosphate
DMEM	Dulbecco's Modified Eagle Medium (Commercial nutrient mixture)
DNA	Deoxyribonucleic acid
E. coli	*Escherichia coli*
E4P	Erythrose 4-phosphate
ED pathway	Entner-Doudoroff pathway
EDTA	Ethylenediaminetetraacetic acid
EMP pathway/EMPP	Embden-Meyerhof-Parnas pathway
Ery	Erythromycin
EtOH	Ethanol
Exp	Experimental values

F16BP	Fructose 1,6-bisphosphate
F6P	Fructose 6-phosphate
FACS	Fluorescence-activated cell sorting
fadA	Gene encoding acetyl-CoA C-acyltransferase FadA
fadB	Gene encoding fatty oxidation complex, alpha subunit FadB
fadI	Gene encoding *acetyl-CoA C-acyltransferase FadI*
fadJ	Gene encoding fatty acid oxidation complex, alpha subunit FadJ
fadL	Gene encoding membrane protein involved in aromatic hydrocarbon degradation
FELASA	Federation of Laboratory Animal Science Associations
flhDC	Operon encoding flagellar transcriptional activators
fli, flg, flh genes	Genes encoding the flagella apparatus
Form or FORM	Formate
fruB	Gene encoding phosphocarrier, HPr family (fructose uptake)
fruK	Gene encoding 1-phosphofructokinase (fructose uptake)
Fum or FUM	Fumarate
fumA	Gene encoding hydrolyase, Fe-S type, tartrate/fumarate subfamily, beta subunit
Fur	Ferric uptake regulator
G3P	Glyceraldehyde 3-phosphate
G6P	Glucose 6-phosphate
GAP	Glyceraldehyde 3-phosphate
gapA	Gene encoding glyceraldehyde 3-phosphate dehydrogenase
GC content	Guanine-cytosine content
GC-MS	Gas chromatography-mass spectrometry
Gene::Kan^R	Disrupted gene by insertion of kanamycin resistance gene
GEO	Gene Expression Omnibus database
GFP	Green fluorescent protein
GFP+/-	Green fluorescent positive/negative
Glc	Glucose
GLC6P	Glucose 6-phosphate
glgXAP	Genes encoding glycogen debranching enzyme GlgX, glycogen/starch synthase and glycogen/starch/alpha-glucan phosphorylase
glnH	Gene encoding cationic amino acid ABC transporter, periplasmic binding protein
glnP	Gene encoding polar amino acid ABC transporter, inner membrane subunit
glnQ	Gene encoding ABC transporter
glpFK	Genes encoding MIP family channel protein and glycerol kinase (glycerol uptake)
GlpR	DNA-binding transcriptional repressor GlpR, glycerol metabolism
gltA	Gene encoding citrate synthase I
gltB	Gene encoding glutamate synthase (ferredoxin)
Glu/GLUX	Glutamate
Gly/GLY	Glycine
GLYO/GLYOX	Glyoxylate
gnd	Gene encoding 6-phosphogluconate dehydrogenase
gpt	Gene encoding xanthine phosphoribosyltransferase
gr.	Gram
groEL, groES	Genes encoding chaperonin GroEL and Cpn10
GV-SOLAS	Gesellschaft für Versuchstierkunde / Society for Laboratory Animals Science
H	Proton
HAM's F-12	Commercial nutrient mixture
HdfR	Transcriptional Regulator (flagella formation)
H-NS	Nucleoid-associated protein
HPLC	High performance liquid chromatography
htrA	Gene encoding protease Do
ibpAB	Genes encoding for heat shock protein Hsp20
icdA	Gene encoding isocitrate dehydrogenase
ICI or ICIT	Isocitrate
IhfA/B	Integration host factor
invA	Gene encoding invasin region 3
kan	Gene encoding kanamycin resistance
katA	Gene encoding catalase
katY	Gene encoding catalase/peroxidase HPI
kdpFABC	Genes encoding potassium transport factors
Lac/LAC	Lactate
LB	Lysogeny broth (microbial growth medium)
ldh	Gene encoding lactate dehydrogenase
luxS	Gene encoding quorum-sensing autoinducer 2 (AI-2), LuxS
M cells	Microfold cells
M_0	Relative mass isotopomer fraction of nonlabeled *t*-butyl-dimethylsilyl-derivatized amino acids
M_1	Relative mass isotopomer fraction of single labeled *t*-butyl-dimethylsilyl-derivatized amino acids
M_2	Relative mass isotopomer fraction of double labeled *t*-butyl-dimethylsilyl-derivatized amino acids
maeB	Gene encoding malic enzyme
MAL	Malate
manXZ	Genes encoding PTS system for mannose/fructose/sorbose
mdh	Genes encoding malate dehydrogenase
MDV	Mass isotopomer distribution vector
mglBAC	Genes encoding periplasmic binding protein/LacI transcriptional regulator, ABC transporter related and ABC transporter related (galactose uptake)

MIC	Minimal inhibitory concentration
mid-log phase	In the middle of the logarithmic growth phase
MLNs	mesenteric lymph nodes
motA	Gene encoding chemotaxis protein MotA
motB	Gene encoding chemotaxis protein MotA
mRNA	Messenger ribonucleic acid
MsrA	Macrolide efflux pump
MTHF	5,10-Methylenetetrahydrofolate
n.s.	not significant
NAD(H)	Nicotinamide adenine dinucleotide
NADP(H)	Nicotinamide adenine dinucleotide phosphate
NCBI	National Center for Biotechnology Information
ndk	Gene encoding nucleoside-diphosphate kinase
nt	Nucleotides
nupC1	Nucleoside transporter
OAA	Oxaloacetate
oppAB	Gene encoding for extracellular solute-binding protein family 5 and alkaline phosphatase (amino acid peptide transport)
P	Phosphate
p	p-value
P5P	Ribulose 5-phosphate / Ribose 5-phosphate
PBS	Phosphate buffered saline
pckA	Gene encoding phosphoenolpyruvate carboxykinase
PCR	Polymerase chain reaction
PDHR	Pyruvate dehydrogenase regulator
pdhR	Gene encoding pyruvate dehydrogenase regulator
PEP	Phosphoenolpyruvate
pflB	Gene encoding formate acetyl-transferase
PGA	Glycerate 3-phosphate
pgk	Gene encoding phosphoglyceratekinase
Phe/PHEX	Phenylalanine
PM	Pyruvate metabolism
poxB	Gene encoding quinone-reducing pyruvate dehydrogenase
PP pathway	Pentose phosphate pathway
ppc	Gene encoding phosphoenolpyruvate carboxylase
PPs	Peyer's patches
ppsA	Gene encoding phosphoenolpyruvate synthase
psaA	Gene encoding pH 6 antigen precursor (antigen 4, adhesin)
psaB	Gene encoding pili assembly chaperone
pta	Gene encoding phosphate acetyltransferase
PTS	Phosphotransferase systems
ptsG	Gene encoding EIIBC subunit of the glucose phosphotransferase system
PTS^{Glc}	Glucose-phosphotransferase system
ptsH	Gene encoding phosphotransferase system, phosphocarrier protein HPr
ptsI	Gene encoding phosphoenolpyruvate-protein phosphotransferase
ptsN	Gene encoding for $EIIA^{Ntr}$ (part of the phosphotransferase system)
PtsN	$EIIA^{Ntr}$ (part of the phosphotransferase system)
PTS^{Ntr}	Nitrogen-phosphotransferase system
PykA	Pyruvate kinase A
pykAF	Genes encoding pyruvate kinases
PykF	Pyruvate kinase F
Pyr/PYR	Pyruvate
pyrD	Gene encoding dihydroorotate oxidase
R	Software environment for statistical computing and graphics
R5P	Ribose 5-phosphate
RES	Resuspension buffer of the NucleoBond Xtra kit
RNA	Ribonucleic acid
RovA	Regulator of virulence A
rovA	Gene encoding the regulator of virulence A
RovM	Regulator of virulence M
rpm	Revolutions per minute
rRNA	Ribosomal ribonucleic acid
rxnEQ	Reaction equations
S7P	Sedoheptulose 7-phosphate
*Sac*I	Restriction enzyme from *Streptomyces achromogenes*
sdhABCD	Genes encoding succinate dehydrogenase
SDS	Sodium dodecyl sulfate
Ser/SER	Serine
sfcA	Gene encoding malate dehydrogenase (oxaloacetate-decarboxylating)
SgrS	Regulatory RNA that negatively controls the translation of *ptsG* mRNA
SHKM	Shikimate
soda, sodC	Genes encoding superoxide dismutases
SPI1	Salmonella pathogenicity island 1
spp.	Species
Suc or SUC	Succinate
sucAB	Genes encoding α-ketoglutarate dehydrogenase
sucCD	Genes encoding succinyl-CoA synthetase

T3P	Triose 3-phosphates
tau	Genes encoding taurine transport proteins
TCA cycle	Tricarboxylic acid cycle
Tet	Tetracycline
Thr/THR	Threonine
Tris	Tris(hydroxymethyl)aminomethane
tRNA	Transfer ribonucleic acid
Tyr/TYRX	Tyrosine
udp	Gene encoding uridine phosphorylase
uhpC	Gene encoding phosphoglycerate transporter
ulaABC/*sgaTBA*	Genes encoding putative ascorbate PTS system
UV	Ultraviolet (light)
UvrY	Response regulator of the two-component signal transduction system BarA/UvrY
Val/VAL	Valine
Wt	Wild type
X	Denotes genes without classification according to the clusters of orthologous groups of proteins
xanP	Gene encoding uracil-xanthine permease
Y. pestis	*Yersinia pestis*
Y. pseudotuberculosis	*Yersinia pseudotuberculosis*
yadA	Gene encoding adhesin YadA
YMM	*Yersinia* minimal medium
yop genes	Genes encoding for Yersinia outer proteins
ysc genes	Genes encoding type III secretion protein
yspI, ypsI	Genes encoding autoinducer synthesis proteins
yspR, ypsR	Genes encoding transcriptional regulators, LuxR family
zwf	Gene encoding glucose 6-phosphate dehydrogenase

7.2 Symbols

μ	Specific growth rate	[h^{-1}]
OD_{600}	Optical density at 600 nm	[-]
vvm	Volume of gas per volume of liquid and minute	[$L\ L^{-1}\ min^{-1}$]
m/z	Mass-to-charge ratio	[-]
q_{Glc}	Specific rate of glucose uptake	[$mmol\ g_{CDW}^{-1}\ h^{-1}$]
$Y_{X/S}$	Yield on glucose for biomass	[$g\ mol^{-1}$]
$Y_{P/S}$	Yields on glucose for by-products given as the molar percentage of the specific glucose uptake rate	[%]
D	Dilution rate	[h^{-1}]

7.3 Data from ^{13}C metabolic flux analysis

Table 11. Metabolic network and calculated fluxes with 95% confidence intervals (CI) of glucose-grown *Yersinia pseudotuberculosis* wild type (YPIII), the single gene deletion mutants YP3 (Δ*rovA*), YP53 (Δ*csrA*), YP89 (Δ*crp*) and of the wild type under administration of 50 mg L^{-1} erythromycin or 0.1 mg L^{-1} tetracycline. The network consists of reaction equations (rxnEQ) and of carbon transitions (cTrans) for metabolite and isotopomer balancing, respectively (Wittmann & Heinzle, 2002; Krömer *et al,* 2004). All fluxes are expressed as a molar percentage of the corresponding specific glucose uptake rate, which was set as 100%. Abbreviations: GLC, glucose; PEP, phosphoenolpyruvate; GLC6P, glucose 6-phosphate; PYR, pyruvate; F6P, fructose 6-phosphate; F16BP, fructose 1,6-bisphosphate; DHAP, dihydroxyacetone phosphate; G3P, glyceraldehyde 3-phosphate; 6PG, 6-phosphogluconate; P5P, ribulose 5-phosphate / ribose 5-phosphate; CO2, carbon dioxide; S7P, sedoheptulose 7-phosphate; E4P, erythrose 4-phosphate; 3PG, 3-phosphoglycerate; SER, serine; GLY, glycine; MTHF, 5,10-Methylenetetrahydrofolate; OAA, oxaloacetate; ACCOA, acetyl coenzyme A; CIT, citrate; ICIT, isocitrate; AKG, α-ketoglutarate; SUC, succinate; GLYO, glyoxylate; MAL, malate; FUM, fumarate; ACE, acetate; FORM, formate; EtOH, ethanol; LAC, lactate; VAL, valine; SHKM, shikimate; CHRM, chorismate; PHEX, phenylalanine, TYRX, tyrosine; ASPX, aspartate; GLUX, glutamate; THR, threonine; _B/_BT, metabolite serves as biomass precursor; _EX, secreted metabolite. Possible reaction types: F, irreversible; F(X), irreversible and assigned as a free flux; FR, reversible; B, reaction that is exluded from isotopomer modeling; S, reaction that is only used for isotopomer modeling.

			Wild type		YP3 (Δ*rovA*)		YP53 (Δ*csrA*)		YP89 (Δ*crp*)		Erythromycin		Tetracycline	
rxnEQ	**cTrans**	**Type**	**Flux**	**CI**	**Flux**	**CI**	**Flux**	**CI**	**Flux**	**CI**	**Flux**	**CI**	**Flux**	**CI**
GLC_EX + PEP = GLC6P + PYR	abcdef + ghi = abcdef + ghi	F	100.0	-	100.0	-	100.0	-	100.0	-	100.0	0.0	100.0	-
GLC6P = F6P	abcdef = abcdef	F	66.6	0.1	70.0	0.1	69.0	0.1	58.5	0.1	71.2	0.2	67.0	0.1
F6P = F16BP	abcdef = abcdef	F	84.9	0.1	86.1	0.1	85.7	0.0	80.2	0.1	86.1	0.1	85.0	0.1
F16BP = DHAP + G3P	abcdef = cba + def	F	84.9	0.1	86.1	0.1	85.7	0.0	80.2	0.1	86.1	0.1	85.0	0.1
DHAP = G3P	abc = abc	F	84.9	0.1	86.1	0.1	85.7	0.0	80.2	0.1	86.1	0.1	85.0	0.1
GLC6P = 6PG	abcdef = abcdef	F(X)	32.5	0.1	29.1	0.1	30.1	0.1	40.1	0.1	27.8	0.2	32.0	0.1
6PG = P5P + CO2	abcdef = bcdef + a	F	32.5	0.1	29.1	0.1	30.1	0.1	40.1	0.1	27.8	0.2	32.0	0.1
6PG = PYR + G3P	abcdef = abc + def	F(X)	0.0	0.0	0.0	0.0	0.0	0.0	0.0	0.0	0.0	0.0	0.0	0.0
P5P + P5P = S7P + G3P	abcde + fghij = fgabcde + hij	FR	10.1	0.0	8.9	0.0	9.3	0.0	12.2	0.1	8.4	0.1	9.9	0.1
S7P + G3P = E4P + F6P	abcdefg + hij = defg + abchij	FR	10.1	0.0	8.9	0.0	9.3	0.0	12.2	0.1	8.4	0.1	9.9	0.1
E4P + P5P = F6P + G3P	abcd + efghi = efabcd + ghi	FR	8.6	0.0	7.5	0.0	7.8	0.0	9.9	0.1	6.8	0.1	8.4	0.1
G3P = 3PG	abc = abc	F	177.8	0.1	179.0	0.1	178.6	0.1	169.4	0.1	178.4	0.1	177.7	0.2
3PG = PEP	abc = abc	F	171.4	0.1	172.8	0.2	172.3	0.1	159.6	0.2	171.5	0.1	171.3	0.3
3PG_B = SER	abc = abc	F	1.3	0.3	1.4	0.3	1.6	0.3	1.3	0.4	1.4	0.3	1.5	0.3
SER = GLY + MTHF	abc = ab + c	F	1.3	0.3	1.4	0.3	1.6	0.3	1.3	0.4	1.4	0.3	1.5	0.3

PEP = PYR	abc = abc	F	51.5	0.9	53.7	0.3	53.8	0.6	32.1	0.7	51.4	0.2	51.9	0.8
PEP + CO2 = OAA	abc + d = abcd	FR	16.9	1.0	16.2	0.3	15.5	0.6	23.0	0.7	16.8	0.2	16.4	0.7
PYR = ACCOA + CO2	abc = bc + a	F	83.5	0.4	73.3	1.0	85.2	0.8	111.0	0.4	57.2	0.6	78.2	1.7
ACCOA + OAA = CIT	ab + cdef = fedbac	F	62.8	0.5	52.0	1.1	69.3	0.8	91.1	0.4	32.4	0.6	59.9	1.8
CIT = ICIT	abcdef = abcdef	F	62.8	0.5	52.0	1.1	69.3	0.8	91.1	0.4	32.4	0.6	59.9	1.8
ICIT = AKG + CO2	abcdef = abcde + f	F	62.8	0.5	52.0	1.1	69.3	0.8	91.1	0.4	32.4	0.6	59.9	1.8
ICIT = 0.5 SUC + 0.5 SUC + GLYO	abcdef = 0.5 edcf + 0.5 fcde + ab	F(X)	0.0	0.0	0.0	0.0	0.0	0.1	0.0	0.0	0.1	0.1	0.0	0.0
GLYO + ACCOA = MAL	ab + cd = abdc	F	0.0	0.0	0.0	0.0	0.0	0.1	0.0	0.0	0.1	0.1	0.0	0.0
AKG = 0.5 SUC + 0.5 SUC + CO2	abcde = 0.5 bcde + 0.5 edcb + a	F	56.2	0.5	44.9	1.1	62.9	0.8	81.9	0.5	25.0	0.7	53.2	1.8
SUC = FUM	abcd = abcd	F	56.0	0.5	44.7	1.1	63.0	0.8	81.9	0.5	24.9	0.6	53.1	1.8
FUM = MAL	abcd = abcd	F	55.9	0.5	44.6	1.1	63.0	0.8	81.9	0.5	24.9	0.6	53.1	1.8
MAL = OAA	abcd = abcd	F(X)	54.3	1.2	44.4	1.0	62.3	1.1	81.2	0.8	24.9	0.6	52.4	1.9
MAL = PYR + CO2	abcd = abc + d	F	1.5	0.9	0.2	0.3	0.7	0.6	0.8	0.6	0.1	0.1	0.6	0.7
ACCOA = ACE	ab = ab	F	10.1	0.2	10.7	0.3	3.0	0.3	0.1	0.0	11.8	0.1	5.0	0.2
PYR = FORM + ACCOA	abc = a + bc	F	2.9	0.1	2.6	0.0	0.4	0.1	0.8	0.0	1.6	0.1	0.7	0.1
ACE = ETOH	ab = ab	F	3.3	0.2	3.8	0.2	0.3	0.1	0.0	0.0	5.2	0.0	1.6	0.1
PYR = LAC	abc = abc	F	7.2	0.2	8.3	0.2	3.5	0.1	0.9	0.0	7.5	0.1	3.2	0.1
CO2 = CO2_EX	a = a	FR	221.2	1.5	185.1	3.2	234.8	2.4	303.5	1.5	127.2	1.8	209.5	5.4
AKG = AKG_EX		B	1.1	0.0	1.5	0.0	0.9	0.0	0.8	0.0	1.4	0.0	1.1	0.0
PYR = PYR_EX		B	46.5	0.4	56.7	1.0	52.5	0.7	0.1	0.0	71.2	0.5	57.3	1.6
SUC = SUC_EX		B	0.2	0.0	0.2	0.0	0.0	0.0	0.0	0.0	0.1	0.0	0.1	0.0
LAC = LAC_EX		B	7.2	0.2	8.3	0.2	3.5	0.1	0.9	0.0	7.5	0.1	3.2	0.1
FORM = FORM_EX		B	2.9	0.1	2.6	0.0	0.4	0.1	0.8	0.0	1.6	0.1	0.7	0.1
FUM = FUM_EX		B	0.1	0.0	0.1	0.0	0.0	0.0	0.0	0.0	0.0	0.0	0.1	0.0
ACE = ACE_EX		B	6.8	0.1	6.8	0.2	2.7	0.3	0.1	0.0	6.6	0.1	3.4	0.1
ETOH = ETOH_EX		B	3.3	0.2	3.8	0.2	0.3	0.1	0.0	0.0	5.2	0.0	1.6	0.1
GLC6P = GLC6P_B		B	0.9	0.0	0.9	0.0	0.9	0.0	1.4	0.0	1.0	0.0	0.9	0.0
F6P = F6P_B		B	0.3	0.0	0.3	0.0	0.3	0.0	0.5	0.0	0.3	0.0	0.3	0.0
P5P = P5P_B	abcde = abcde	F	3.8	0.0	3.8	0.1	3.8	0.0	5.7	0.1	4.1	0.1	3.8	0.1
E4P = E4P_B	abcd = abcd	F	1.5	0.0	1.5	0.0	1.5	0.0	2.3	0.0	1.6	0.0	1.5	0.0
G3P = G3P_B		B	0.6	0.0	0.6	0.0	0.6	0.0	0.9	0.0	0.6	0.0	0.6	0.0
3PG = 3PG_B	abc = abc	F	6.4	0.1	6.3	0.1	6.4	0.0	9.8	0.1	6.9	0.1	6.4	0.2
PEP = PEP_B	abc = abc	F	2.9	0.0	2.9	0.1	2.9	0.0	4.4	0.1	3.2	0.0	3.0	0.1
PYR = PYR_B	abc = abc	F	13.0	0.2	12.9	0.2	12.9	0.1	20.1	0.2	14.0	0.2	13.1	0.4
ACCOA = ACCOA_B	ab = ab	F	13.5	0.1	13.3	0.2	13.3	0.1	20.5	0.2	14.5	0.2	13.9	0.4
AKG = AKG_B		B	5.5	0.1	5.5	0.1	5.5	0.0	8.4	0.1	6.0	0.1	5.6	0.1
OAA = OAA_B	abcd = abcd	F	8.5	0.1	8.6	0.1	8.5	0.0	13.1	0.2	9.3	0.1	8.8	0.2
PYR_B + PYR_B = VAL + CO2	abc + def = abefc + d	F	0.9	0.2	1.0	0.2	1.1	0.2	0.9	0.3	1.0	0.2	1.0	0.2
E4P_B + PEP_B = SHKM	abcd + efg = efgabcd	F	0.7	0.2	0.8	0.2	0.9	0.1	0.7	0.2	0.8	0.2	0.8	0.1
SHKM + PEP_B = CHRM	abcdefg + hij = abcdefghij	F	0.7	0.2	0.8	0.2	0.9	0.1	0.7	0.2	0.8	0.2	0.8	0.1
CHRM = PHEX + CO2	abcdefghij = hijbcdefg + a	F	0.5	0.1	0.5	0.1	0.6	0.1	0.5	0.1	0.5	0.1	0.5	0.1
CHRM = TYRX + CO2	abcdefghij = hijbcdefg + a	F	0.3	0.1	0.3	0.1	0.3	0.0	0.3	0.1	0.3	0.1	0.3	0.0
OAA_B = OAA_BT		B	8.5	0.1	8.6	0.1	8.5	0.0	13.1	0.2	9.3	0.1	8.8	0.2
E4P_B = E4P_BT		B	0.7	0.2	0.7	0.2	0.5	0.1	1.5	0.2	0.8	0.2	0.7	0.1
P5P_B = P5P_BT		B	3.8	0.0	3.8	0.1	3.8	0.0	5.7	0.1	4.1	0.1	3.8	0.1
PYR_B = PYR_BT		B	11.2	0.5	11.0	0.4	10.6	0.3	18.3	0.6	12.1	0.4	11.1	0.6
PEP_B = PEP_BT		B	1.5	0.3	1.4	0.3	1.1	0.3	3.0	0.4	1.7	0.3	1.4	0.3
ACCOA_B = ACCOA_BT		B	13.5	0.1	13.3	0.2	13.3	0.1	20.5	0.2	14.5	0.2	13.9	0.4
3PG_B = 3PG_BT		B	5.1	0.3	4.9	0.3	4.7	0.3	8.5	0.4	5.6	0.3	5.0	0.4

0.333 VAL + 0.483 GLY + 0.180 PHEX + 0.091 TYRX = BIOMASS	B	2.7	0.6	2.9	0.6	3.4	0.5	2.7	0.8	2.9	0.6	3.0	0.5
PYR = ALA	S												
OAA = ASPX	S												
AKG = GLUX	S												
OAA = THR	S												

Table 12. Additional inputs required to perform ^{13}C metabolic flux analysis with OpenFlux. The list Excluded Metabolites contains metabolites that are not used for metabolite balances. The list Simulated MDVs contains metabolites that are used for isotopomer modeling. The binary code defines the availability of carbon atoms within the backbone of the metabolite according to the rules of OpenFlux (Quek *et al,* 2009).

Excluded Metabolites	Simulated MDVs	Input substrates
MTHF	ALA#111	GLC_EX
FUM_EX	VAL#11111	CO2_EX
PYR_EX	THR#1111	
ACE_EX	ASPX#1111	
ETOH_EX	GLUX#11111	
SUC_EX	SER#111	
FORM_EX	PHEX#111111111	
GLC_EX	GLY#11	
AKG_EX	TYRX#111111111	
AKG_B		
LAC_EX		
GLC6P_B		
F6P_B		
P5P_BT		
E4P_BT		
G3P_B		
3PG_BT		
PYR_BT		
OAA_BT		
ACCOA_BT		
CO2_EX		
BIOMASS		
PEP_BT		

7.4 Data from gene expression analysis

Table 13. Transcriptional profile of glucose-grown single gene deletion mutants *Y. pseudotuberculosis* YP3 (Δ*rovA*), YP53 (Δ*csrA*), and YP89 (Δ*crp*). Data are given as the fold change in expression compared with *Y. pseudotuberculosis* wild type (YPIII). The data were obtained from three biological replicates, each with three samples. The set of differentially expressed genes was filtered by the fold change (|log2FC| >=0.8). All array data generated in this study were deposited in the Gene Expression Omnibus (GEO) database and are available under accession number GSE54547.

Locus	Gene name	Product, desciption	Fold Change		
			Δ*crp*	**Δ*csrA***	**Δ*rovA***
VIRULENCE GENES					
pYV0013	*yadA*	adhesin YadA	1.60	**-2.06**	**2.72**
pYV0020	*sycH*	YopH targeting protein	-1.33	**-2.17**	-1.56
pYV0024	*sycE, yerA*	YopE chaperone	**-1.96**	**-2.00**	-1.58
pYV0025	*yopE*	outer membrane virulence protein	-1.29	**-1.89**	-1.13
pYV0040	*yopK/yopQ*	Yop targeting protein YopK, YopQ	**-2.67**	**-3.43**	-1.69
pYV0055	*yopB*	Yop targeting protein	**2.01**	1.15	**1.79**
pYV0057	*lcrV*	V antigen, antihost protein/regulator	-1.24	**-2.66**	-1.15
pYV0058	*lcrG*	Yop regulator	-1.29	**-2.77**	-1.31
pYV0062	*yscX*	type III secretion protein	**1.75**	1.55	1.64
pYV0063	*sycN*	type III secretion protein	**2.20**	**1.78**	1.61
pYV0064	*tyeA*	Yop secretion and targeting protein	**2.36**	**1.75**	1.64
pYV0065	*yopN, lcrE*	membrane-bound Yop targeting protein	**2.16**	**1.85**	1.69
pYV0067	*sctN*	Yops secretion ATP synthase	1.01	**-1.97**	-1.32
pYV0073	*yscT*	type III secretion protein	-1.30	**-2.28**	-1.46
pYV0074	*yscU*	type III secretion protein	-1.33	**-2.58**	-1.48
pYV0075	*virG*	Yop targeting lipoprotein	-1.73	**-2.01**	**-1.80**
pYV0076	*lcrF, virF*	thermoregulatory protein	-1.35	**-1.96**	-1.58
pYV0087	*yscK*	type III secretion protein	-1.38	**-1.96**	-1.13
pYV0089	*yscM, lcrQ*	type III secretion regulatory	-1.47	**-2.05**	-1.72
pYV0094	*yopH*	protein-tyrosine phosphatase Yop effector	**3.39**	1.60	1.61
YPK_0051	*fimA-1*	fimbrial protein	**9.57**	-1.43	-1.06
YPK_0053	*fimC-1*	pili assembly chaperone	**2.72**	1.13	-1.17
YPK_0054		fimbrial protein	**2.00**	-1.17	-1.22
YPK_0220	*hofM*	pilus assembly protein	1.11	**2.08**	1.16
YPK_0251	*yhhZ-1*	type VI secretion system effector, Hcp1 family	**-2.16**	**1.84**	-1.47
YPK_0280	*bfd*	bacterioferritin-associated ferredoxin	**-1.98**	**-5.76**	-1.64
YPK_0281	*bfr*	bacterioferritin	**3.07**	-1.18	-1.58
YPK_0385	*hcp1-1*	type VI secretion system effector, Hcp1 family	**1.92**	-1.41	-1.31
YPK_0386	*impB*	type VI secretion protein, VC_A0107 family	**2.55**	-1.11	-1.01
YPK_0387	*impC-1*	type VI secretion protein, EvpB/VC_A0108 family	**3.51**	1.60	1.65
YPK_0388		type VI secretion system lysozyme-related protein	**3.14**	1.46	1.33
YPK_0389	*impG-1, vasA-1*	type VI secretion protein, VC_A0110 family	**2.40**	1.20	1.22
YPK_0390	*impH-1, vasB-1*	type VI secretion protein, VC_A0111 family	**2.39**	1.16	1.46
YPK_0391	*impI, vasC*	type VI secretion cluster, FHA domain containing protein	**1.77**	1.27	-1.17
YPK_0392	*vasD, lip*	type VI secretion cluster, putative lipoprotein	**2.12**	1.18	1.25
YPK_0393	*impJ, vasE*	type VI secretion protein, VC_A0114 family	**2.53**	1.52	1.41
YPK_0394		type VI secretion cluster, conserved protein	**2.00**	1.39	1.28
YPK_0395	*clpB2*	type VI secretion ATPase, ClpV1 family	**1.95**	1.32	1.39
YPK_0398	*vasJ*	type VI secretion-associated protein, VC_A0119 family	**1.78**	1.23	1.18
YPK_0399	*impL, vasK*	type VI secretion protein IcmF	**1.82**	1.27	1.20
YPK_0400	*vasL*	type VI secretion cluster, ImpA domain protein	**1.77**	1.28	1.37
YPK_0694	*smfA-1*	fimbrial protein	**-2.35**	**-1.86**	-1.47
YPK_0696	*papD*	pili assembly chaperone	**1.75**	1.02	1.31
YPK_0791	*yspR*	transcriptional regulator, LuxR family	**-1.87**	1.01	-1.41
YPK_0792	*yspI*	autoinducer synthesis protein	**-3.15**	-1.35	**-1.94**
YPK_0798		type VI secretion protein, VC_A0107 family	1.25	**1.75**	1.26
YPK_0871	*yadF*	YadA domain protein	**2.25**	-1.02	1.05
YPK_1268	*ailA*	virulence-related outer membrane protein	**3.27**	1.56	**1.96**
YPK_1304		type VI secretion system effector, Hcp1 family	**-2.53**	**-2.91**	-1.72
YPK_1475	*fimA-2*	fimbrial protein	**-1.89**	1.71	-1.62
YPK_1479		type VI secretion protein, VC_A0107 family	1.46	**1.76**	1.49
YPK_1481		type VI secretion system effector, Hcp1 family	-1.67	**2.40**	-1.54
YPK_1522	*smfA-2*	fimbrial protein	**-2.35**	**-1.84**	-1.48
YPK_1559	*rovM*	transcriptional regulator, LysR family	1.40	**-7.63**	-1.66
YPK_1606	*ompX/ailD*	virulence-related outer membrane protein	-1.20	**3.16**	**-2.09**
YPK_1655	*ypsR*	transcriptional regulator, LuxR family	-1.58	**-2.20**	-1.64
YPK_1656	*ypsI*	autoinducer synthesis protein	**-5.06**	**-3.82**	**-2.00**
YPK_1705	*ycfJ*	17 kDa surface antigen	**3.74**	**9.70**	1.15
YPK_1761	*yadE*	YadA domain protein	**5.76**	-1.54	1.16
YPK_1775	*fimC-2*	chaperone protein	**1.82**	1.09	1.12
YPK_1786	*fimA-3*	fimbrial protein	**-1.75**	**-3.06**	-1.40
YPK_1876	*rovA*	transcriptional regulator, MarR family	-1.67	**1.84**	**-2.66**
YPK_1953	*srfB*	putative virulence factor SrfB	**-5.02**	**-5.58**	1.16
YPK_2156	*hlyA*	filamentous haemagglutinin domain protein	-1.25	-1.58	**-1.84**
YPK_2429	*invA*	invasin region 3	-1.06	**2.54**	-1.15
YPK_2758	*psaB*	pili assembly chaperone	-1.68	**1.94**	-1.70
YPK_2759	*psaA*	pH 6 antigen precursor (antigen 4) (adhesin)	-1.18	**12.53**	-1.43
YPK_2760	*psaF*	conserved hypothetical protein	**-2.87**	-1.44	**-3.05**
YPK_2761	*psaE*	transcriptional regulator, CadC	**-3.48**	-1.28	**-3.18**
YPK_2900	*ybhG, yhiI*	secretion protein HlyD family protein	1.68	**1.93**	1.37
YPK_3060	*yhhZ-2*	type VI secretion system effector, Hcp1 family	-1.43	**2.67**	-1.43
YPK_3214	*ymoA*	haemolysin expression modulating family protein	-1.34	-1.21	**-1.76**
YPK_3289	*crl*	transcriptional regulator Crl	**-2.41**	-1.20	**-1.78**
YPK_3550	*icmF*	type VI secretion protein IcmF	**5.40**	**2.01**	1.23
YPK_3551		type IV / VI secretion system protein, DotU family	**7.82**	**2.48**	1.48
YPK_3552		type VI secretion protein, VC_A0114 family	**9.03**	**3.31**	**2.14**
YPK_3553		type VI secretion cluster, putative lipoprotein	**11.73**	**3.65**	**2.17**
YPK_3556		pentapeptide repeat protein	**9.28**	**3.54**	1.74
YPK_3557		pentapeptide repeat protein	**6.26**	**2.86**	1.74
YPK_3558	*vgrG*	type VI secretion system Vgr family protein	**8.29**	**2.52**	1.52
YPK_3559	*clpB*	type VI secretion ATPase, ClpV1 family	**4.25**	**1.77**	1.20
YPK_3560	*impH-2, vasB-2*	type VI secretion protein, VC_A0111 family	**7.04**	**2.63**	1.20
YPK_3561	*impG-2, vasA-2*	type VI secretion protein, VC_A0110 family	**5.48**	**2.81**	1.56
YPK_3562	*impH-3*	type VI secretion system lysozyme-related protein	**11.86**	**3.88**	1.70
YPK_3563	*impC-2*	type VI secretion cluster, unknown protein DUF796	**15.52**	**8.71**	1.73
YPK_3564	*impC-3*	type VI secretion protein, EvpB/VC_A0108 family	**11.93**	**2.94**	**2.14**
YPK_3565		type VI secretion protein, VC_A0107 family	**9.65**	**2.79**	**2.16**
YPK_3566		ImpA domain protein	**5.90**	**1.92**	1.06
YPK_4042	*fimA-5*	fimbrial protein	**-2.24**	**-1.95**	-1.29

YPK_4085	*HasA*	heme-binding A family protein	**-3.46**	**-3.00**	**-1.99**
YPK_4109	*raxA*	secretion protein HlyD family protein	-1.01	**-1.77**	-1.09
CELL MOTILITY AND CHEMOTAXIS					
YPK_1745	*flhD*	flagellar transcriptional activator	**-17.65**	**-14.68**	-1.56
YPK_1746	*flhC*	flagellar transcriptional activator FlhC	**-9.69**	**-10.49**	-1.14
YPK_1747	*motA*	chemotaxis protein MotA	**-4.78**	**-5.14**	-1.21
YPK_1748	*motB*	OmpA/MotB domain protein	**-2.42**	**-2.65**	-1.11
YPK_1749	*cheA*	CheA signal transduction histidine kinase	**-2.59**	**-3.10**	1.29
YPK_1750	*cheW*	CheW protein	**-3.85**	**-4.97**	-1.11
YPK_1753	*cheD*	methyl-accepting chemotaxis sensory transducer	**-2.14**	**-2.41**	-1.01
YPK_1759	*cheZ*	chemotaxis phosphatase, CheZ	-1.66	**-2.05**	-1.16
YPK_2378	*fliZ*	flagella biosynthesis protein FliZ	**-15.14**	**-19.04**	-1.41
YPK_2380	*fliA*	RNA polymerase, sigma 28 subunit, FliA/WhiG	**-20.62**	**-22.06**	1.07
YPK_2381	*fliC*	flagellin domain protein	**-27.81**	**-39.53**	-1.69
YPK_2382	*fliD*	flagellar hook-associated 2 domain protein	**-6.01**	**-6.23**	1.03
YPK_2383	*fliS*	flagellar protein FliS	**-3.32**	**-3.69**	-1.22
YPK_2384	*fliT*	flagellar export chaperone	**-4.58**	**-5.57**	-1.50
YPK_2390	*fliE*	flagellar hook-basal body complex subunit FliE	**-6.28**	**-8.33**	1.24
YPK_2391	*fliF*	flagellar M-ring protein FliF	**-4.72**	**-4.84**	1.18
YPK_2392	*fliG*	flagellar motor switch protein FliG	**-6.57**	**-7.65**	1.29
YPK_2393	*fliH*	flagellar assembly protein FliH	**-4.29**	**-3.95**	1.21
YPK_2394	*fliI*	ATPase, FliI/YscN family	**-4.81**	**-5.49**	-1.24
YPK_2395	*fliJ*	flagellar export protein FliJ	**-4.71**	**-5.16**	1.08
YPK_2396	*fliK-1*	flagellar hook-length control protein	**-2.98**	**-3.61**	1.22
YPK_2398	*fliL*	flagellar basal body-associated protein FliL	**-8.36**	**-8.56**	-1.28
YPK_2399	*fliM*	flagellar motor switch protein FliM	**-3.12**	**-2.83**	-1.05
YPK_2400	*fliN*	flagellar motor switch protein FliN	**-3.83**	**-3.97**	1.19
YPK_2401	*fliO*	flagellar biosynthesis protein FliO	**-3.30**	**-3.77**	1.15
YPK_2402	*fliP*	flagellar biosynthetic protein FliP	**-3.45**	**-4.22**	-1.11
YPK_2403	*fliQ*	flagellar biosynthetic protein FliQ	**-2.40**	**-2.48**	1.12
YPK_2415	*flgL*	flagellar hook-associated protein 3	**-2.08**	**-2.04**	1.23
YPK_2416	*flgK*	flagellar hook-associated protein FlgK	**-2.39**	**-2.63**	1.54
YPK_2417	*flgJ*	flagellar rod assembly protein/muramidase FlgJ	**-3.64**	**-3.63**	-1.06
YPK_2418	*flgI*	flagellar P-ring protein	**-2.70**	**-3.06**	1.28
YPK_2419	*flgH*	flagellar L-ring protein	**-2.67**	**-3.07**	1.43
YPK_2420	*flgG*	flagellar basal-body rod protein FlgG	**-5.49**	**-5.15**	1.22
YPK_2421	*flgF*	flagellar basal-body rod protein FlgF	**-3.28**	**-4.07**	1.66
YPK_2422	*flgE*	flagellar basal body FlaE domain protein	**-4.10**	**-4.42**	1.58
YPK_2423	*flgD*	flagellar hook capping protein	**-7.69**	**-7.87**	1.54
YPK_2424	*flgC*	flagellar basal-body rod protein FlgC	**-11.36**	**-10.73**	1.43
YPK_2425	*flgB*	flagellar basal-body rod protein FlgB	**-16.49**	**-18.73**	1.04
YPK_2426	*flgA*	flagella basal body P-ring formation protein FlgA	**-3.25**	**-4.74**	-1.10
YPK_2427	*flgM*	anti-sigma-28 factor, FlgM	**-2.11**	**-2.47**	1.07
YPK_2428	*flgN*	FlgN family protein	**-3.31**	**-4.17**	-1.33
YPK_2430	*flhE*	flagellar FlhE family protein	-1.73	**-1.78**	1.18
YPK_2431	*flhA*	flagellar biosynthesis protein FlhA	**-5.32**	**-6.59**	-1.33
YPK_2432	*flhB*	flagellar biosynthetic protein FlhB	**-2.69**	**-3.48**	1.14
STRESS ADAPTATION					
YPK_0011	*ibpA*	heat shock protein Hsp20	**-2.58**	-1.26	**-2.04**
YPK_0012	*ibpB*	heat shock protein Hsp20	**-2.15**	1.23	-1.72
YPK_0035	*sodA*	superoxide dismutase	**-2.23**	**-3.45**	**-1.93**
YPK_0120	*uspA*	UspA domain protein	**-2.38**	-1.40	**-2.02**
YPK_0121	*uspB*	universal stress protein B	**2.65**	1.03	-1.24
YPK_0442	*cspA-1*	cold-shock DNA-binding domain protein	**-4.30**	-1.56	-1.60
YPK_0443	*cspA-2*	cold-shock DNA-binding domain protein	**-4.06**	-1.53	**-1.76**
YPK_0444	*cspA-3*	cold-shock DNA-binding domain protein	**-2.57**	-1.05	**-1.77**
YPK_1124	*cspB-1*	cold-shock DNA-binding domain protein	**-6.04**	**-4.23**	**-2.10**
YPK_1740	*cspC-1*	cold-shock DNA-binding domain protein	**-8.23**	**-4.13**	**-2.03**
YPK_1894	*pspA*	phage shock protein A, PspA	**1.81**	1.46	1.25
YPK_1896	*pspC*	phage shock protein C, PspC	**1.78**	1.22	1.05
YPK_1943	*uspE*	UspA domain protein	**2.93**	**2.52**	1.12
YPK_2017	*cstA-1*	carbon starvation protein CstA	-1.43	**1.75**	1.03
YPK_2355	*uvrC*	exonuclease ABC, C subunit	**2.25**	1.66	1.27
YPK_2474	*cspC-2*	cold-shock DNA-binding domain protein	**-2.81**	**-3.53**	**-2.02**
YPK_2662	*cspB-2*	cold-shock DNA-binding domain protein	**-4.26**	1.56	-1.56
YPK_2694	*cspD-2*	cold-shock DNA-binding domain protein	-1.09	**2.40**	**-2.10**
YPK_2855	*katA*	catalase	**2.66**	**2.20**	1.58
YPK_3031	*cspE*	cold-shock DNA-binding domain protein	1.23	-1.46	**-1.84**
YPK_3032	*cspC-3*	cold-shock DNA-binding domain protein	**-2.02**	**-1.90**	**-1.89**
YPK_3161	*ybbN*	thioredoxin domain	1.13	**1.83**	1.14
YPK_3269	*ggt*	gamma-glutamyltransferase	**2.45**	1.49	1.25
YPK_3388	*katY*	catalase/peroxidase HPI	**2.69**	-1.68	1.20
YPK_3445	*sodC*	superoxide dismutase	-1.35	**4.74**	-1.37
YPK_3876	*terA*	stress protein	1.18	**1.82**	1.73
YPK_3877	*terZ*	stress protein	-1.05	**1.83**	1.60
YPK_3948	*cstA-2*	carbon starvation protein CstA	**-3.83**	-1.74	-1.02
YPK_4035	*trxA*	thioredoxin	**-1.97**	**-3.84**	**-1.83**
YPK_4131	*cpxP*	protein of unknown function Spy-related	**-1.98**	**6.21**	-1.58
INFORMATION STORAGE AND PROCESSING REPLICATION, CELL DEVISION					
YPK_0004	*gyrB*	DNA gyrase, B subunit	1.67	1.70	**1.80**
YPK_0228	*dam*	DNA adenine methylase	**-2.11**	**-2.37**	-1.53
YPK_0317	*smf, dprA*	DNA protecting protein DprA	1.25	**2.07**	1.02
YPK_0888	*dam*	DNA adenine methylase	-1.31	**2.41**	1.04
YPK_1032	*mutH*	DNA mismatch repair endonuclease mutH	-1.10	**2.04**	-1.04
YPK_1043	*RecB*	exodeoxyribonuclease V, beta subunit	**1.87**	1.68	1.35
YPK_1142	*ccrB-1*	camphor resistance CrcB protein	**1.85**	**2.47**	-1.13
YPK_1143	*ccrB-2*	CrcB protein	**2.12**	**2.75**	-1.13
YPK_1301	*xseA*	exodeoxyribonuclease VII, large subunit	**-2.03**	-1.12	-1.38
YPK_1431	*zipA*	cell division protein ZipA	**-1.82**	**-2.27**	**-1.96**
YPK_1680	*maf*	Maf protein	**-2.28**	**-2.30**	**-1.79**
YPK_1854	*lpp*	LPP repeat-containing protein	**-2.64**	**-4.93**	**-2.93**
YPK_2121	*minC*	septum site-determining protein MinC	1.32	**1.84**	1.51
YPK_2122	*minD*	septum site-determining protein MinD	1.51	**2.14**	1.61
YPK_2625	*helD*	UvrD/REP helicase	1.44	**1.92**	1.25
YPK_2641	*rlmL*	RNA methylase	1.29	**2.30**	1.54
YPK_2655	*mukB*	chromosome segregation and condensation protein MukB	1.11	**3.18**	1.37
YPK_2656	*mukE*	chromosome segregation and condensation protein MukE	-1.07	**2.69**	1.31
YPK_2657	*mukF*	chromosome segregation and condensation protein MukF	1.02	**2.58**	1.09
YPK_2685	*ftsK*	cell division FtsK/SpoIIIE	1.52	**3.32**	1.36
YPK_2756	*nfo*	apurinic endonuclease Apn1	1.60	**2.94**	1.58
YPK_2765		NUDIX hydrolase	**2.01**	1.42	1.06
YPK_2815		DNA circulation family protein	1.04	**2.88**	1.16
YPK_2846	*gyrA*	DNA gyrase, A subunit	1.05	**1.92**	1.19
YPK_3144	*ybjD*	SMC (structural maintenance of chromosomes) family protein	1.55	**1.98**	1.54
YPK_3229	*comEA*	competence protein ComEA helix-hairpin-helix repeat protein	1.03	**4.03**	-1.04
YPK_3508	*mutT*	mutator MutT protein	-1.69	**-1.77**	-1.33
YPK_3513	*ftsZ*	cell division protein FtsZ	**2.69**	**2.31**	1.74
YPK_3629	*yjjV*	TatD-related deoxyribonuclease	1.46	**1.75**	1.08
YPK_3783	*priB*	primosomal replication protein N	-1.16	1.61	**1.76**
YPK_3850	*ssb*	single-strand binding protein	-1.44	**-1.90**	-1.15
YPK_4111	*zapB*	septal ring assembly protein ZapB	-1.12	-1.47	**-1.86**
GENERAL TRANSCRIPTION, TRANSCRIPTION FACTORS, SIGNAL TRANSDUCTION					
pYV0007	*repB, copB*	repB, repA2, copB; putative replication transcriptional regulator	**-2.77**	**-2.44**	-1.64
YPK_0160	*malT*	ATP-dependent transcriptional regulator, MalT-like, LuxR family	**-2.44**	-1.15	1.03
YPK_0172	*ompR*	two component transcriptional regulator, winged helix family	1.38	**1.83**	1.20
YPK_0173	*envZ*	integral membrane sensor signal transduction histidine kinase	1.30	**1.80**	1.37
YPK_0248	*crp*	transcriptional regulator, Crp/Fnr family	**-24.13**	-1.43	-1.29
YPK_0308	*rpoA*	DNA-directed RNA	**1.85**	**2.41**	**2.19**

		polymerase, alpha subunit			
YPK_0341	*rpoC*	DNA-directed RNA polymerase, beta' subunit	**1.81**	**1.93**	1.59
YPK_0348	*rsd*	regulator of RpoD, Rsd/AlgQ	-1.11	**-1.83**	-1.48
YPK_0452	*fis*	transcriptional regulator, Fis family	**-2.75**	**-3.07**	-1.40
YPK_0493	*rnk*	GreA/GreB family elongation factor	**-6.24**	**-3.16**	-1.67
YPK_0516	*mlaB*	putative anti-sigma B factor antagonist	**2.13**	1.11	-1.09
YPK_0565		putative kinase protein	**1.79**	1.24	1.40
YPK_0642	*ygiM*	SH3 domain protein	1.62	**3.17**	1.05
YPK_0725		putative transcriptional regulator, CadC	**1.76**	-1.06	-1.01
YPK_0995	*agaR*	transcriptional regulator, DeoR family	**-1.78**	**-1.84**	-1.47
YPK_1156	*kdpD*	osmosensitive K+ channel signal transduction histidine kinase	**1.98**	1.53	1.23
YPK_1183	*rseA*	anti sigma-E protein, RseA	**1.81**	1.07	-1.30
YPK_1184	*rseB*	sigma E regulatory protein, MucB/RseB	**1.91**	1.32	1.18
YPK_1185	*rseC*	positive regulator of sigma E, RseC/MucC	**2.35**	1.62	1.22
YPK_1262	*glnB*	nitrogen regulatory protein P-II	**2.00**	1.50	1.55
YPK_1349	*speG*	GCN5-related N-acetyltransferase	**-2.04**	**-1.87**	-1.41
YPK_1671	*csgD*	transcriptional regulator, LuxR family	**-1.89**	**2.72**	-1.53
YPK_1724	*cscR*	transcriptional regulator, LacI family	**1.78**	1.11	1.21
YPK_1793	*kdgR*	transcriptional regulator, IclR family	**-1.85**	**-1.78**	-1.69
YPK_1927		transcriptional regulator, XRE family	1.40	**2.50**	1.11
YPK_1982	*ynfL*	transcriptional regulator, LysR family	1.73	**2.08**	-1.25
YPK_2009		transcriptional regulator, AraC family	-1.25	**-1.85**	-1.39
YPK_2078	*rssB*	response regulator receiver protein	**2.65**	1.26	1.17
YPK_2083	*rssB*	transcriptional regulator, LysR family	-1.04	-1.01	1.02
YPK_2100	*prkA*	putative serine protein kinase, PrkA	**3.37**	**2.48**	1.53
YPK_2109	*fadR*	fatty acid metabolism transcriptional regulator FadR	-1.32	**-2.56**	-1.71
YPK_2235	*phoH*	PhoH family protein	**3.57**	**1.82**	1.16
YPK_2269	*fimZ*	two component transcriptional regulator, LuxR family	1.08	**-4.23**	-1.49
YPK_2356	*uvrY*	two component transcriptional regulator, LuxR family	**1.78**	1.50	1.05
YPK_2385		transcriptional regulator, AraC family	**-2.29**	**-2.43**	-1.74
YPK_2470	*atoS1*	diguanylate cyclase with PAS/PAC sensor	**3.43**	1.30	1.13
YPK_2484		transcriptional regulator, AraC family	-1.54	**-2.59**	-1.72
YPK_2491	*thuR*	transcriptional regulator, LacI family	1.38	**1.88**	1.28
YPK_2499	*uhpA*	two component transcriptional regulator, LuxR family	**-2.45**	**-2.50**	**-1.76**
YPK_2628	*tfoX*	regulator of competence-specific genes	-1.24	**6.15**	-1.68
YPK_2667	*ihfB*	integration host factor, beta subunit	**1.90**	**1.82**	-1.05
YPK_2686	*lrp*	transcriptional regulator, AsnC family	1.37	**2.44**	1.54
YPK_2780	*uxuR*	GntR domain protein	-1.23	**5.89**	1.01
YPK_2843	*rcsB*	two component transcriptional regulator, LuxR family	-1.55	-1.24	**-1.95**
YPK_3206	*acrR*	transcriptional regulator, TetR family	**-1.83**	-1.48	-1.68
YPK_3231	*hupB*	histone family protein DNA-binding protein	**-1.78**	**-2.48**	-1.71
YPK_3337	*emrR*	transcriptional regulator, MarR family	**2.05**	**4.59**	1.41
YPK_3368	*luxS*	quorum-sensing autoinducer 2 (AI-2), LuxS	**2.23**	-1.50	-1.45
YPK_3372	*csrA*	carbon storage regulator, CsrA	-1.41	**-132.92**	-1.68
YPK_3425	*rpoS*	RNA polymerase, sigma 70 subunit, RpoD family	**3.64**	1.34	-1.01
YPK_3468	*dksA*	transcriptional regulator, TraR/DksA family	**-4.31**	-1.55	-1.55
YPK_3492	*pdhR*	GntR domain protein	**-2.45**	-1.38	-1.03
YPK_3606	*arcA*	two component transcriptional regulator, winged helix family	-1.30	**-2.36**	-1.45
YPK_3612	*trpR*	Trp operon repressor	-1.51	**-2.12**	-1.65
YPK_3638	*hmsT*	diguanylate cyclase	1.24	**-2.69**	-1.61
YPK_3649	*ydeW*	transcriptional regulator, DeoR family	**5.62**	**1.82**	1.28
YPK_3682	*yjgM*	GCN5-related N-acetyltransferase	-1.21	**-1.95**	-1.46
YPK_3731	*nusA*	NusA antitermination	1.07	**1.78**	1.57

		factor			
YPK_3739	*greA*	transcription elongation factor GreA	**-2.66**	-1.70	-1.62
YPK_3762	*argR*	arginine repressor, ArgR	**-2.69**	**-2.63**	-1.28
YPK_3792	*nsrR*	transcriptional regulator, BadM/Rrf2 family	-1.51	**-1.79**	-1.38
YPK_3832		transcriptional regulator, TetR family	**1.75**	1.06	1.00
YPK_3841	*rhaR*	transcriptional regulator, AraC family	**-2.12**	-1.07	-1.07
YPK_3975		GCN5-related N-acetyltransferase	**-1.80**	-1.58	-1.52
YPK_3976	*rpoH*	RNA polymerase, sigma 32 subunit, RpoH	**2.43**	1.16	1.24
YPK_4064	*hdfR*	transcriptional regulator, LysR family	-1.37	**-1.88**	-1.53
YPK_4101	*cytR*	transcriptional regulator, LacI family	**-1.75**	-1.14	1.72
TRANSLATION					
YPK_0023	*glyS*	glycyl-tRNA, B subunit	1.12	1.20	**1.82**
YPK_0277	*fusA*	translation elongation factor G	1.41	**1.82**	1.64
YPK_0282	*rpsJ*	ribosomal protein S10	1.13	**1.81**	1.57
YPK_0283	*rplC*	ribosomal protein L3	1.63	**3.01**	**2.68**
YPK_0284	*rplD*	ribosomal protein L4/L1e	1.59	**3.14**	**2.76**
YPK_0285	*rplW*	ribosomal protein L25/L23	1.59	**3.05**	**2.50**
YPK_0286	*rplB*	ribosomal protein L2	1.56	**2.72**	**2.29**
YPK_0287	*rpsS*	ribosomal protein S19	1.44	**2.34**	**2.04**
YPK_0288	*rplV*	ribosomal protein L22	1.26	**2.13**	**1.92**
YPK_0289	*rpsC*	ribosomal protein S3	1.11	**1.78**	1.73
YPK_0296	*rpsN*	ribosomal protein S14	1.49	**2.05**	1.72
YPK_0297	*rpsH*	ribosomal protein S8	**1.96**	**2.56**	**2.44**
YPK_0298	*rplF*	ribosomal protein L6	1.49	**2.20**	**2.01**
YPK_0299	*rplR*	ribosomal protein L18	**1.86**	**2.44**	**2.27**
YPK_0300	*rpsE*	ribosomal protein S5	1.60	**2.25**	**1.99**
YPK_0301	*rpmD*	ribosomal protein L30	**2.21**	**2.63**	**2.28**
YPK_0302	*rplO*	ribosomal protein L15	**2.20**	**2.27**	**2.08**
YPK_0305	*rpsM*	ribosomal protein S13	**1.84**	**2.28**	**1.92**
YPK_0306	*rpsK*	ribosomal protein S11	1.73	**2.38**	**1.92**
YPK_0307	*rpsD*	ribosomal protein S4	**2.25**	**2.75**	**2.48**
YPK_0316	*def*	peptide deformylase	-1.72	**-2.76**	**-1.77**
YPK_0335	*rplK*	ribosomal protein L11	**-2.40**	-1.57	-1.11
YPK_0336	*rplA*	ribosomal protein L1	**-2.54**	-1.68	-1.24
YPK_0337	*rplJ*	ribosomal protein L10	**-2.22**	**-1.80**	-1.02
YPK_0338	*rplL*	ribosomal protein L7/L12	**-2.29**	**-1.80**	-1.00
YPK_0453	*dusB*	TIM-barrel protein, nifR3 family	**-2.42**	**-2.19**	-1.21
YPK_0504	*yhbH*	sigma 54 modulation protein/ribosomal protein S30EA	**2.30**	-1.04	-1.52
YPK_0524	*rplM*	ribosomal protein L13	**-2.37**	**-1.78**	-1.31
YPK_0525	*rpsI*	ribosomal protein S9	**-2.54**	-1.69	-1.13
YPK_0636	*rpsU*	ribosomal protein S21	**-3.69**	**-3.30**	-1.74
YPK_0641	*cca*	multifunctional tRNA nucleotidyl transferase/2'3'-cyclic phosphodiesterase/2'nucleotidase/phosphatase	**1.78**	**3.41**	1.09
YPK_0924	*lysS*	lysyl-tRNA synthetase	1.52	1.73	**2.05**
YPK_1067	*tsf*	translation elongation factor Ts	1.03	**1.79**	1.71
YPK_1076	*lpxD*	UDP-3-O-(3-hydroxymyristoyl) glucosamine N-acyltransferase	**2.08**	**1.91**	1.49
YPK_1274	*trmJ*	RNA methyltransferase, TrmH family, group 1	**-2.10**	**-1.96**	-1.42
YPK_1678	*rluC*	pseudouridine synthase, RluA family	**-2.09**	**-2.30**	-1.40
YPK_1682	*rpmF*	ribosomal protein L32	**-2.32**	**-3.23**	**-1.79**
YPK_1824	*pheS*	phenylalanyl-tRNA synthetase, alpha subunit	1.14	1.71	**1.76**
YPK_2129		endoribonuclease L-PSP	**-1.98**	**-2.38**	**-1.81**
YPK_2161	*rimJ*	GCN5-related N-acetyltransferase	**2.25**	-1.40	1.09
YPK_2179	*prfA*	peptide chain release factor 1	-1.56	**-1.84**	-1.22
YPK_2554	*metG*	methionyl-tRNA synthetase	**2.01**	**2.66**	**1.96**
YPK_2648	*asnC*	asparaginyl-tRNA synthetase	1.02	**1.79**	1.49
YPK_2668	*rpsA*	ribosomal protein S1	**2.14**	1.66	1.43
YPK_2681	*serS*	seryl-tRNA synthetase	1.29	**2.62**	1.32
YPK_2691	*infA*	translation initiation factor IF-1	**-1.84**	1.31	-1.07
YPK_2795	*rplY*	ribosomal protein L25	**-1.80**	-1.34	-1.50
YPK_2887	*dusC*	dihydrouridine synthase DuS	-1.22	**1.88**	1.36
YPK_3015	*leuS*	leucyl-tRNA synthetase	**1.77**	**2.14**	**1.79**
YPK_3069	*rluF*	pseudouridine synthase	**-2.28**	-1.44	-1.38
YPK_3590	*rpsT*	ribosomal protein S20	**-3.70**	**-5.04**	**-2.10**
YPK_3724	*deaD*	DEAD/DEAH box helicase domain protein	**3.71**	1.48	**2.09**
YPK_3727	*rpsO*	ribosomal protein S15	-1.65	**-2.45**	**-1.96**
YPK_3730	*infB*	translation initiation factor IF-2	1.48	**1.90**	1.74
YPK_3738	*yhbY*	protein of unknown function UPF0044	**-2.87**	**-3.97**	**-2.00**
YPK_3756	*rpmA*	ribosomal protein L27	**-2.38**	**-2.27**	-1.48
YPK_3757	*rplU*	ribosomal protein L21	**-2.52**	**-2.33**	-1.52
YPK_3818	*efp-2*	translation elongation factor P	**-2.40**	**-2.65**	-1.61
YPK_4074	*trmA*	tRNA (uracil-5-)-	**-2.41**	**-2.73**	-1.54

		methyltransferase			
YPK_4098	*rpmE*	ribosomal protein L31	**-4.90**	**-5.37**	**-1.95**
YPK_4135	*trmL, cspR*	RNA methyltransferase, TrmH family, group 2	**-2.13**	**-1.87**	-1.08
YPK_4153	*rpmG*	ribosomal protein L33	**-2.83**	**-2.97**	**-1.84**
YPK_4154	*rpmB*	ribosomal protein L28	**-2.74**	**-2.47**	-1.67
YPK_4160	*rph*	ribonuclease PH	-1.67	**-1.90**	-1.01
YPK_4249	*rpmH*	ribosomal protein L34	-1.35	**-2.09**	-1.70
POSTTRANSLATIONAL MODIFICATION, PROTEIN TURNOVER					
YPK_0242	*ppiA*	peptidyl-prolyl cis-trans isomerase cyclophilin type	**-2.64**	1.46	-1.45
YPK_0268	*slyD*	peptidylprolyl isomerase FKBP-type	**-2.12**	**-2.50**	-1.25
YPK_0437	*yghU*	glutathione S-transferase domain	**1.83**	1.20	1.15
YPK_0520	*degQ*	protease Do	1.25	**2.15**	1.36
YPK_0849	*ycaL, loiP*	peptidase M48 Ste24p	-1.68	**-1.88**	-1.34
YPK_1019		putative protein-disulfide isomerase	**2.49**	1.68	1.36
YPK_1042	*ptrA*	peptidase M16 domain protein	**2.08**	**2.07**	1.06
YPK_1119	*nrdH*	glutaredoxin-like protein NrdH	**2.03**	1.57	1.21
YPK_1134	*ureE*	urease accessory protein UreE	**1.92**	**5.21**	1.64
YPK_1135	*ureF*	urease accessory protein UreF	1.10	**2.50**	1.23
YPK_1137	*ureD*	urease accessory protein UreD	1.25	**2.02**	1.23
YPK_1325	*ydcP-1, yegQ-1, yhbU-1*	peptidase U32	**1.81**	1.34	1.65
YPK_1340	*yegD*	putative chaperone protein	**-2.05**	-1.38	-1.00
YPK_1360	*bcp*	peroxiredoxin	1.09	**-1.81**	-1.06
YPK_1848	*sufB*	FeS assembly protein SufB	**1.77**	1.20	1.68
YPK_1866	*grxD*	glutaredoxin-like protein	-1.22	**-2.63**	-1.74
YPK_1878	*anmK*	anhydro-N-acetylmuramic acid kinase	1.69	**3.88**	1.12
YPK_1883	*gst*	glutathione S-transferase domain	**2.96**	1.51	1.29
YPK_1903	*tpx*	redoxin domain protein	**2.37**	1.34	1.04
YPK_1917	*hslJ*	heat-inducible protein	**2.75**	1.02	-1.04
YPK_2683	*ycaJ*	AAA ATPase central domain protein	1.07	**1.88**	-1.00
YPK_2690	*aat*	leucyltransferase	1.11	**1.79**	1.19
YPK_2692	*clpA*	ATP-dependent Clp protease, ATP-binding subunit clpA	**1.97**	**4.10**	1.66
YPK_2733	*grxA*	glutaredoxin, GrxA family	**-1.86**	-1.54	**-1.94**
YPK_2747	*yliJ, gst*	glutathione S-transferase domain	**2.71**	**2.17**	1.19
YPK_2974	*GrpE*	GrpE protein	**-2.21**	-1.43	-1.51
YPK_3153	*ppiB*	peptidyl-prolyl cis-trans isomerase cyclophilin type	**-2.10**	**-1.96**	-1.68
YPK_3232	*lon*	ATP-dependent protease La	1.62	**2.22**	**2.28**
YPK_3234	*clpP*	ATP-dependent Clp protease, proteolytic subunit ClpP	1.64	**1.83**	1.68
YPK_3235	*tig*	trigger factor	**-1.97**	-1.22	1.07
YPK_3267	*ahpC*	alkyl hydroperoxide reductase/thiol specific antioxidant/ Mal allergen	-1.10	**-1.79**	-1.47
YPK_3366	*ypjD*	cytochrome c assembly protein	-1.46	**-2.52**	**-1.91**
YPK_3444	*ygcF*	radical SAM domain protein	1.11	**2.16**	1.05
YPK_3452	*htrA*	protease Do	**2.65**	**6.41**	**1.75**
YPK_3593	*dnaJ*	chaperone protein DnaJ	1.06	**1.75**	**1.78**
YPK_3778	*fklB*	peptidylprolyl isomerase FKBP-type	**-4.06**	**-2.50**	-1.42
YPK_3796	*hflK*	HflK protein	**2.01**	**2.14**	**1.77**
YPK_3822	*groEL*	chaperonin GroEL	**2.14**	**2.74**	**2.32**
YPK_3823	*groES*	chaperonin Cpn10	1.59	**1.85**	1.65
YPK_3986	*tusA, sirA*	SirA family protein	**-1.94**	**-1.80**	-1.49
YPK_4040	*ppiC*	PpiC-type peptidyl-prolyl cis-trans isomerase	**-2.48**	**-2.58**	-1.42
YPK_4196	*dsbA*	DSBA oxidoreductase	**1.79**	**1.91**	1.23
METABOLISM					
ENERGY PRODUCTION AND CONVERSION					
YPK_0152	*glpD*	FAD dependent oxidoreductase	**-4.09**	1.35	1.01
YPK_0174	*pckA*	phosphoenolpyruvate carboxykinase (ATP)	**3.47**	**2.36**	1.35
YPK_0235	*nirB*	nitrite reductase (NAD(P)H), large subunit	-1.36	**-2.63**	-1.17
YPK_0364	*aceB*	malate synthase A	**1.82**	**2.96**	1.47
YPK_0365	*aceA*	isocitrate lyase	1.73	**1.83**	1.36
YPK_0486	*gabD-1*	succinic semialdehyde dehydrogenase	**2.97**	1.54	1.09
YPK_0492	*cybC-1*	cytochrome b562	-1.08	**-1.84**	-1.52
YPK_0819	*yggX*	probable Fe(2+)-trafficking protein	1.62	**2.10**	1.16
YPK_1031	*tas*	aldo/keto reductase	**1.75**	1.66	1.43
YPK_1174	*grcA*	formate C-acetyltransferase glycine radical	**-2.91**	**-3.61**	**-2.12**
YPK_1194	*fdx*	iron-sulfur cluster-binding protein	**-1.84**	**-1.94**	**-1.78**
YPK_1385	*napF*	ferredoxin-type protein NapF	1.08	**-2.90**	-1.21
YPK_1389	*napC*	periplasmic nitrate (or nitrite) reductase c-type cytochrome, NapC/NirT family	1.11	**-1.95**	-1.16
YPK_1391	*maeB*	malate dehydrogenase (oxaloacetate-decarboxylating) (NADP(+)), Phosphate acetyltransferase	1.20	**1.82**	1.68
YPK_1550	*pta*	phosphate acetyltransferase	1.03	**1.88**	1.64
YPK_1562	*nuoD*	NADH dehydrogenase I, D subunit	1.57	1.73	**1.80**
YPK_1563	*nuoE*	NADH-quinone oxidoreductase, E subunit	**2.09**	1.68	**1.75**
YPK_1564	*nuoF*	NADH-quinone oxidoreductase, F subunit	**1.85**	1.62	**1.76**
YPK_1723	*icdA*	isocitrate dehydrogenase, NADP-dependent	**2.67**	**2.57**	**1.90**
YPK_1974	*aldA*	aldehyde dehydrogenase	1.10	**2.23**	1.21
YPK_2030	*acnA*	aconitate hydratase 1	**3.05**	**3.75**	**1.82**
YPK_2072	*adhE*	iron-containing alcohol dehydrogenase	**-11.06**	**-3.31**	-1.18
YPK_2090	*ydjA*	putative nitroreductase	**-2.32**	**-1.85**	-1.17
YPK_2227	*astD*	succinylglutamic semialdehyde dehydrogenase	**1.90**	**1.93**	1.10
YPK_2363	*wrbA*	flavoprotein WrbA	**2.73**	-1.35	1.07
YPK_2506	*lldD*	FMN-dependent alpha-hydroxy acid dehydrogenase	**2.39**	**1.81**	1.33
YPK_2562	*sfcA*	malate dehydrogenase (oxaloacetate-decarboxylating)	1.05	**2.53**	1.42
YPK_2614		FAD linked oxidase domain protein	1.69	**1.84**	-1.30
YPK_2677	*pflB*	formate acetyltransferase	1.29	**1.86**	1.10
YPK_2771	*gabD-2*	aldehyde dehydrogenase	1.71	**2.75**	1.12
YPK_2884	*dld*	D-lactate dehydrogenase	1.64	**1.97**	1.40
YPK_2906	*morB*	NADH:flavin oxidoreductase/NADH oxidase	1.45	**1.94**	1.11
YPK_2963	*cydB*	cytochrome d ubiquinol oxidase, subunit II	-1.25	**1.75**	1.42
YPK_2964	*cydA*	cytochrome bd ubiquinol oxidase subunit I	**-2.48**	1.12	1.01
YPK_2965	*sucD*	succinyl-CoA synthetase, alpha subunit	-1.11	**2.90**	**1.86**
YPK_2966	*sucC*	succinyl-CoA synthetase, beta subunit	1.09	**3.67**	**2.13**
YPK_2967	*sucB*	2-oxoglutarate dehydrogenase, E2 subunit, dihydrolipoamide succinyltransferase	-1.04	**3.43**	**1.91**
YPK_2968	*sucA*	2-oxoglutarate dehydrogenase, E1 subunit	-1.46	**2.63**	1.49
YPK_2969	*sdhB*	succinate dehydrogenase and fumarate reductase iron-sulfur protein	-1.21	**3.50**	1.74
YPK_2970	*sdhA*	succinate dehydrogenase, flavoprotein subunit	-1.56	**3.33**	1.62
YPK_2971	*sdhD*	succinate dehydrogenase, hydrophobic membrane anchor protein	-1.70	**2.58**	1.35
YPK_2972	*sdhC*	succinate dehydrogenase, cytochrome b556 subunit	**-2.69**	**2.11**	1.19
YPK_2973	*gltA*	citrate synthase I	1.43	**3.01**	**1.91**
YPK_2990	*fldA*	flavodoxin	**-3.59**	**-3.28**	**-1.88**
YPK_3005	*miaB*	tRNA-i(6)A37 thiotransferase enzyme MiaB	**2.87**	**2.41**	1.31
YPK_3253	*dxs*	deoxyxylulose-5-phosphate synthase	**1.88**	1.32	1.49
YPK_3297		glycerophosphoryl diester phosphodiesterase	-1.23	**3.36**	-1.15
YPK_3302	*nqrD*	NADH:ubiquinone oxidoreductase, subunit D	1.03	**1.98**	1.04
YPK_3389	*cybC-2*	cytochrome B562	1.47	**-2.53**	-1.37
YPK_3390	*cybB*	cytochrome B561	1.57	**-1.94**	-1.03
YPK_3404	*fumA*	hydrolyase, Fe-S type, tartrate/fumarate subfamily, beta subunit	1.20	**1.77**	1.67
YPK_3487	*acnB*	aconitate hydratase 2	**2.68**	**1.80**	**2.01**
YPK_3490	*aceF*	pyruvate dehydrogenase complex dihydrolipoamide acetyltransferase	1.43	1.57	**2.19**
YPK_3536	*leuB*	3-isopropylmalate dehydrogenase	1.11	1.53	**1.82**
YPK_3648	*ydeV*	carbohydrate kinase FGGY	**3.86**	1.55	1.06
YPK_3767	*ppa*	inorganic diphosphatase	**-2.83**	**-4.26**	**-1.90**
YPK_3992	*glpQ*	glycerophosphoryl diester phosphodiesterase	1.10	**1.82**	1.11
YPK_4113	*glpK*	glycerol kinase	**-2.47**	**4.10**	**1.78**
YPK_4115	*fpr*	oxidoreductase FAD/NAD(P)-binding domain protein	**1.88**	1.35	1.46
YPK_4216	*mioC*	flavodoxin/nitric oxide synthase	-1.30	**-2.33**	-1.62
YPK_4219	*atpI*	ATP synthase I chain	**-7.82**	-1.49	-1.30
YPK_4220	*atpB*	ATP synthase F0, A subunit	**-6.33**	-1.23	-1.11
YPK_4221	*atpE*	ATP synthase F0, C	**-4.22**	1.17	1.03

		subunit			
YPK_4222	*atpF*	ATP synthase F0, B subunit	**-3.89**	1.28	1.23
YPK_4223	*atpH*	ATP synthase F1, delta subunit	**-3.90**	1.37	1.33
YPK_4224	*atpA*	ATP synthase F1, alpha subunit	**-3.13**	1.57	1.55
YPK_4225	*atpG*	ATP synthase F1, gamma subunit	**-2.43**	**1.88**	**1.90**
YPK_4226	*atpD*	ATP synthase F1, beta subunit	**-2.45**	1.68	1.55
YPK_4227	*atpC*	ATP synthase F1, epsilon subunit	**-3.47**	1.12	1.23
CARBOHYDRATE METABOLISM					
YPK_0016	*malS*	alpha amylase catalytic region	**1.96**	**1.78**	1.20
YPK_0147	*glgB*	1,4-alpha-glucan branching enzyme	1.13	**1.85**	1.11
YPK_0148	*glgX*	glycogen debranching enzyme GlgX	1.46	**2.13**	1.37
YPK_0150	*glgA*	glycogen/starch synthase, ADP-glucose type	1.48	**2.59**	1.11
YPK_0151	*glgP-1*	glycogen/starch/alpha-glucan phosphorylase	**6.79**	**5.10**	**1.78**
YPK_0161	*glgP-2*	glycogen/starch/alpha-glucan phosphorylase	1.45	**2.28**	**1.88**
YPK_0162	*malQ*	4-alpha-glucanotransferase	1.59	**2.54**	1.49
YPK_0379		glycosidase	**-2.12**	1.39	-1.06
YPK_0435		FGGY-family pentulose kinase	-1.07	1.23	**1.83**
YPK_0494	*treC*	alpha,alpha-phosphotrehalase	**3.65**	1.64	1.44
YPK_0850	*tktA*	transketolase	**1.84**	1.55	**1.98**
YPK_0973	*bgaB*	beta-galactosidase	**-1.83**	-1.39	1.13
YPK_1111	*hpxB*	urate catabolism protein	**2.65**	**4.13**	1.34
YPK_1273	*suhB*	inositol-phosphate phosphatase	**-1.78**	-1.37	1.10
YPK_1427	*ptsI*	phosphoenolpyruvate-protein phosphotransferase	**-1.82**	1.33	**1.83**
YPK_1444	*glk*	glucokinase	**-2.98**	-1.25	-1.11
YPK_1727		NmrA family protein	**1.89**	**2.02**	1.13
YPK_1811	*yniA*	fructosamine kinase	**2.18**	-1.68	-1.31
YPK_1834	*pmrJ*	polysaccharide deacetylase	**1.76**	1.30	-1.06
YPK_1843	*ppsA*	phosphoenolpyruvate synthase	**2.10**	**2.19**	1.30
YPK_2014		NAD-dependent epimerase/dehydratase	**2.06**	1.35	1.41
YPK_2019	*mipB*	transaldolase	1.24	**-1.83**	-1.07
YPK_2204	*rpiB-2*	ribose/galactose isomerase	**-3.31**	**-2.68**	**-1.81**
YPK_2502		polysaccharide deacetylase	1.29	**2.14**	1.14
YPK_2536	*galF*	UTP-glucose-1-phosphate uridylyltransferase	**2.56**	**6.72**	1.31
YPK_2537	*galU*	UTP-glucose-1-phosphate uridylyltransferase	**2.35**	**7.26**	1.35
YPK_2624	*mgsA*	methylglyoxal synthase	**-2.00**	-1.13	-1.38
YPK_2706		NAD-dependent epimerase/dehydratase	1.29	**1.93**	1.38
YPK_2763	*fruK*	1-phosphofructokinase	**-2.13**	1.40	1.41
YPK_2769	*rpiA*	ribose 5-phosphate isomerase	1.51	**2.14**	1.03
YPK_2805	*bglA*	glycoside hydrolase family 1	1.49	**2.71**	1.24
YPK_2879		transglycosylase-associated protein	**3.35**	**4.64**	-1.32
YPK_3072	*bglB*	glycoside hydrolase family 3 domain protein	1.68	**2.86**	1.40
YPK_3176	*gsk*	Inosine kinase	-1.24	**-1.92**	-1.51
YPK_3191	*ddhA*	glucose-1-phosphate cytidylyltransferase	1.27	**1.84**	1.27
YPK_3308	*gmhA*	phosphoheptose isomerase	-1.42	**-2.03**	-1.20
YPK_3395	*araD-2*	L-ribulose-5-phosphate 4-epimerase	1.12	**2.37**	-1.06
YPK_3491	*aceE*	2-oxo-acid dehydrogenase E1 subunit, homodimeric type	1.37	1.48	**2.35**
YPK_3625	*deoB*	phosphopentomutase	**1.95**	1.22	**2.20**
YPK_3775	*cysQ*	3'(2'),5'-bisphosphate nucleotidase	-1.25	**-2.32**	-1.51
YPK_3804		carbohydrate kinase, YjeF related protein	-1.15	**-1.77**	-1.36
YPK_3882		putative ATP/GTP-binding protein	**1.75**	1.31	1.51
YPK_4228	*glmU*	UDP-N-acetylglucosamine pyrophosphorylase	**1.89**	-1.24	1.28
AMINO ACID METABOLISM					
YPK_0008	*ilvA, tdcB*	threonine dehydratase	1.20	**1.96**	1.50
YPK_0077	*hutH*	histidine ammonia-lyase	**1.88**	1.57	1.16
YPK_0088	*dppA*	4-phytase	1.34	**1.77**	1.48
YPK_0141	*asd*	aspartate-semialdehyde dehydrogenase	-1.16	**-2.33**	1.03
YPK_0225	*aroK*	shikimate kinase	**-2.08**	**-1.81**	-1.31
YPK_0245	*argD*	succinylornithine transaminase family	**-1.98**	**-1.95**	-1.28
YPK_0363	*metA*	homoserine O-succinyltransferase	**-1.80**	1.17	1.06
YPK_0372	*lysC*	aspartate kinase	**-3.63**	**-4.54**	-1.04
YPK_0518	*murA*	UDP-N-acetylglucosamine 1-carboxyvinyltransferase	1.37	**1.80**	1.16
YPK_0529	*gltD*	glutamate synthase, small subunit	**1.78**	**-1.75**	1.15
YPK_0530	*gltB*	glutamate synthase (ferredoxin)	**1.85**	-1.18	1.57
YPK_0671	*metC*	cystathionine beta-lyase	-1.29	**-2.38**	-1.23
YPK_0749	*pepT-1*	peptidase T	-1.55	**-4.54**	1.15
YPK_0845	*speA*	arginine decarboxylase	1.67	**2.08**	1.57
YPK_0859	*serA-1*	D-isomer specific 2-hydroxyacid dehydrogenase NAD-binding	1.47	**-2.08**	1.22
YPK_0868	*gcsH*	glycine cleavage system H protein	**-2.17**	**-2.70**	-1.44
YPK_0891		phosphoadenosine phosphosulfate reductase	-1.02	**2.18**	-1.02
YPK_1063	*dapD*	2,3,4,5-tetrahydropyridine-2,6-dicarboxylate N-succinyltransferase	**-2.98**	**-2.49**	-1.70
YPK_1096	*metN-1*	D-methionine ABC transporter, ATPase subunit	**-2.16**	1.08	-1.00
YPK_1097	*gmhB*	D,D-heptose 1,7-bisphosphate phosphatase	-1.02	**-1.77**	-1.39
YPK_1131	*ureA*	urease, gamma subunit	1.07	**3.66**	1.13
YPK_1132	*ureB*	urease, beta subunit	1.10	**3.76**	1.18
YPK_1133	*ureC*	urease, alpha subunit	1.55	**5.22**	1.66
YPK_1136	*ureG*	urease accessory protein UreG	1.30	**2.30**	1.21
YPK_1167		allophanate hydrolase subunit 1	**-1.84**	-1.21	1.49
YPK_1252		lytic transglycosylase catalytic	**-1.75**	-1.45	-1.44
YPK_1265	*glyA*	glycine hydroxymethyltransferase	**2.27**	1.50	**2.20**
YPK_1302	*guaB*	inosine-5'-monophosphate dehydrogenase	**3.45**	1.34	**1.75**
YPK_1429	*cysK*	cysteine synthase A	**1.84**	1.32	1.40
YPK_1558	*alaA*	aminotransferase class I and II	**1.80**	1.08	**1.84**
YPK_1737		NAD(P)H quinone oxidoreductase, PIG3 family	**2.47**	**1.96**	1.72
YPK_1849	*sufC*	FeS assembly ATPase SufC	**1.76**	1.35	**1.98**
YPK_1869	*gloA*	lactoylglutathione lyase	**-2.91**	**-2.41**	**-1.76**
YPK_1950	*ilvB*	acetolactate synthase, large subunit, biosynthetic type	-1.41	**2.89**	1.21
YPK_2069	*oppB*	alkaline phosphatase	1.49	**1.87**	1.63
YPK_2184	*prsA*	ribose-phosphate pyrophosphokinase	**1.84**	1.27	1.59
YPK_2225	*astE*	succinylglutamate desuccinylase	**1.87**	**1.79**	1.34
YPK_2226	*astB*	succinylarginine dihydrolase	**1.80**	1.70	-1.23
YPK_2228	*astA*	arginine N-succinyltransferase	**1.83**	**1.83**	-1.01
YPK_2229	*astC*	succinylornithine transaminase family	**1.86**	**2.20**	1.06
YPK_2254	*glsA*	glutaminase	**1.86**	**-2.56**	1.29
YPK_2257	*aspAT*	putative aminostransferase	1.06	**-2.09**	-1.15
YPK_2442	*ptrB*	oligopeptidase B	1.74	**1.83**	1.59
YPK_2451	*sdaA*	L-serine dehydratase 1	1.15	**1.84**	1.26
YPK_2525	*hisG*	ATP phosphoribosyltransferase	1.10	**3.57**	1.36
YPK_2526	*hisD*	histidinol dehydrogenase	1.43	**4.77**	1.55
YPK_2527	*hisC*	histidinol-phosphate aminotransferase	**1.77**	**4.89**	**1.85**
YPK_2528	*hisB*	histidinol-phosphatase	1.59	**4.11**	**1.79**
YPK_2529	*hisH*	imidazole glycerol phosphate synthase, glutamine amidotransferase subunit	1.46	**3.83**	1.69
YPK_2530	*hisA*	phosphoribosylformimino-5-aminoimidazole carboxamide ribotide isomerase	1.36	**3.84**	1.25
YPK_2531	*hisF*	imidazoleglycerol phosphate synthase, cyclase subunit	1.55	**4.45**	1.65
YPK_2532	*hisI*	phosphoribosyl-ATP diphosphatase	1.13	**2.95**	1.26
YPK_2571	*frmA, adhC*	S-(hydroxymethyl)glutathione dehydrogenase/class III alcohol dehydrogenase	1.25	1.72	**1.90**
YPK_2670	*aroA*	3-phosphoshikimate 1-carboxyvinyltransferase	1.60	**2.16**	1.68
YPK_2703	*poxB*	thiamine pyrophosphate protein TPP binding domain protein	**2.18**	**7.42**	1.55
YPK_2705	*ltaA*	threonine aldolase	1.16	**2.07**	-1.09
YPK_2709	*pheA-1*	chorismate mutase	**2.06**	**4.36**	1.02
YPK_2746		HAD-superfamily subfamily IB hydrolase, TIGR01490	**2.13**	**2.16**	1.22
YPK_2773	*serA-2*	D-isomer specific 2-hydroxyacid dehydrogenase NAD-binding	1.35	**1.76**	-1.07
YPK_2867	*ddc*	aromatic-L-amino-acid decarboxylase	**3.43**	1.31	1.23

YPK_2932	*bioA*	adenosylmethionine-8-amino-7-oxononanoate aminotransferase	**-1.95**	**-1.88**	-1.34
YPK_2949	*aroG*	phospho-2-dehydro-3-deoxyheptonate aldolase	1.52	**2.40**	1.33
YPK_3001	*asnB*	asparagine synthase (glutamine-hydrolyzing)	**1.97**	**2.08**	1.54
YPK_3273	*brnQ*	branched-chain amino acid transport system II carrier protein	**-2.71**	-1.15	-1.08
YPK_3282	*aroL*	shikimate kinase	**-2.13**	**-2.13**	-1.36
YPK_3357	*aroF*	phospho-2-dehydro-3-deoxyheptonate aldolase	-1.60	**-1.96**	1.18
YPK_3436	*cysD*	sulfate adenylyltransferase, small subunit	-1.08	1.35	**1.85**
YPK_3537	*leuC*	3-isopropylmalate dehydratase, large subunit	1.19	1.59	**1.85**
YPK_3584	*dapB*	dihydrodipicolinate reductase	-1.58	**-1.80**	1.03
YPK_3595	*yaaH*	GPR1/FUN34/yaaH family protein	**-5.37**	**-4.08**	**-1.81**
YPK_3604	*thrA*	aspartate kinase	**-2.03**	**-2.32**	1.23
YPK_3819		lysine 2,3-aminomutase YodO family protein	**2.14**	1.44	1.44
YPK_3825	*aspA*	aspartate ammonia-lyase	1.61	**2.67**	1.43
YPK_3853	*tyrB*	aromatic-amino-acid transaminase	1.45	1.06	**1.82**
YPK_3884	*metF-1*	methylenetetrahydrofolate reductase	**2.50**	-1.41	-1.56
YPK_3952	*metE*	5-methyltetrahydropteroyltriglutamate--homocysteine S-methyltransferase	1.41	**2.26**	**3.13**
YPK_3994	*ybhA, ybjI, yidA, yigL*	putative sugar phosphatase	**-1.94**	**-3.11**	-1.74
YPK_4057	*ilvD*	dihydroxy-acid dehydratase	1.05	1.33	**1.91**
YPK_4089	*argC*	N-acetyl-gamma-glutamyl-phosphate reductase	-1.52	**-1.80**	-1.11
YPK_4094	*metL*	aspartate kinase	**-2.04**	1.27	1.27
YPK_4095	*metB*	O-succinylhomoserine (thiol)-lyase	**-1.90**	-1.09	-1.18
YPK_4096	*metJ*	methionine repressor, MetJ	**-2.27**	**-1.89**	-1.58
YPK_4144	*tdh*	L-threonine 3-dehydrogenase	1.20	**2.67**	1.16
YPK_4214	*asnA*	aspartate-ammonia ligase	**-2.81**	**-2.79**	-1.13
NUCLEOTIDE METABOLISM					
YPK_0356	*purD*	phosphoribosylamine-glycine ligase	-1.02	-1.14	**1.83**
YPK_1118	*nrdI*	NrdI protein	**2.16**	**1.91**	1.36
YPK_1289	*ndk*	nucleoside-diphosphate kinase	**-8.02**	**-2.40**	-1.53
YPK_1303	*guaA*	GMP synthase, large subunit	**2.35**	-1.06	1.56
YPK_1350	*purN*	phosphoribosylglycinamide formyltransferase	-1.37	**-1.95**	-1.18
YPK_1351	*purI*	phosphoribosylformylglycinamidine cyclo-ligase	-1.20	**-1.83**	1.10
YPK_1364	*purC*	phosphoribosylaminoimidazole-succinocarboxamide synthase	-1.10	**-2.92**	-1.22
YPK_1675	*pyrC*	dihydroorotase, homodimeric type	**1.77**	1.31	1.64
YPK_1718	*purB*	adenylosuccinate lyase	1.14	1.19	**1.75**
YPK_2043	*trpG*	glutamine amidotransferase of anthranilate synthase	**-2.30**	-1.48	-1.23
YPK_2080	*purU*	formyltetrahydrofolate deformylase	-1.43	**-1.95**	-1.28
YPK_2447	*purT*	phosphoribosylglycinamide formyltransferase 2	**-1.85**	**-2.46**	1.03
YPK_2561	*cdd*	cytidine deaminase	-1.26	-1.04	**5.56**
YPK_2644	*pyrD*	dihydroorotate oxidase	**1.83**	**2.79**	1.36
YPK_2669	*cmk*	cytidylate kinase	**2.54**	**2.12**	1.42
YPK_3155	*purE*	phosphoribosylaminoimidazole carboxylase, catalytic subunit	**-2.19**	**-2.06**	-1.10
YPK_3156	*purK*	phosphoribosylaminoimidazole carboxylase, ATPase subunit	**-1.98**	**-1.94**	1.03
YPK_3194	*adk*	nucleoside-triphosphate-adenylate kinase	**-2.14**	-1.57	-1.07
YPK_3291	*gpt*	xanthine phosphoribosyltransferase	**-4.27**	**-4.28**	**-1.92**
YPK_3453	*dgt*	deoxyguanosinetriphosphate triphosphohydrolase	1.66	**2.30**	1.20
YPK_3501	*guaC*	guanosine monophosphate reductase	**-2.11**	**-3.41**	-1.58
YPK_3624	*deoD*	purine nucleoside phosphorylase	1.18	**-1.94**	1.52
YPK_3626	*deoA*	thymidine phosphorylase	**2.22**	1.20	**2.52**
YPK_3627	*deoC-2*	deoxyribose-phosphate aldolase	**2.81**	1.16	**3.83**
YPK_3950	*udp*	uridine phosphorylase	1.10	-1.12	**8.07**
YPK_4015	*cyaA*	putative adenylate cyclase	**1.96**	-1.37	-1.08
YPK_4157	*dut*	deoxyuridine 5'-triphosphate nucleotidohydrolase Dut	-1.64	**-1.84**	-1.08
YPK_4159	*pyrE*	orotate phosphoribosyltransferase	**-1.75**	**-2.35**	-1.22
YPK_4182	*xanP*	uracil-xanthine permease	**-2.07**	**-4.39**	-1.07
COENZYME METABOLISM					
YPK_0328	*coaA*	pantothenate kinase	**-3.31**	**-2.81**	**-1.93**
YPK_0342	*thiH*	thiazole biosynthesis protein ThiH	1.25	1.37	**2.02**
YPK_0343	*thiG*	thiazole biosynthesis family protein	1.26	1.51	**2.03**
YPK_0344	*thiS*	thiamine biosynthesis protein ThiS	1.07	1.44	**1.94**
YPK_0345	*thiF*	UBA/THIF-type NAD/FAD binding protein	1.13	1.49	**1.95**
YPK_0346	*thiE*	thiamine-phosphate pyrophosphorylase	1.13	1.63	**1.94**
YPK_0347	*thiC*	thiamine biosynthesis protein ThiC	1.06	**1.76**	**2.04**
YPK_0649	*ribB*	3,4-dihydroxy-2-butanone 4-phosphate synthase	**1.75**	1.49	1.32
YPK_1261	*nadE*	NAD+ synthetase	**2.08**	1.44	**1.78**
YPK_1393	*hemF*	coproporphyrinogen oxidase	-1.71	**-1.92**	-1.47
YPK_1532	*folC*	FolC bifunctional protein	**2.04**	**3.27**	1.52
YPK_1880	*pdxH*	pyridoxamine 5'-phosphate oxidase	1.43	**2.36**	1.05
YPK_2029	*ribA*	GTP cyclohydrolase II	**-2.04**	**-2.55**	-1.24
YPK_2038	*btuR*	cob(I)alamin adenosyltransferase	**1.82**	1.58	1.51
YPK_2089	*selD*	selenide, water dikinase	-1.44	**-1.90**	-1.20
YPK_2180	*hemA*	glutamyl-tRNA reductase	-1.35	**-2.03**	-1.41
YPK_2930	*bioF*	8-amino-7-oxononanoate synthase	**-1.92**	-1.67	-1.06
YPK_2931	*bioB*	biotin synthase	**-1.98**	-1.66	-1.03
YPK_2952	*pnuC*	nicotinamide mononucleotide transporter PnuC	-1.05	**1.85**	-1.09
YPK_2953	*nadA*	quinolinate synthetase complex, A subunit	1.11	**2.19**	1.44
YPK_3252	*ispA*	polyprenyl synthetase	**1.78**	1.34	1.63
YPK_3369	*gshA*	glutamate--cysteine ligase	**1.85**	1.41	1.54
YPK_3437	*cysG*	uroporphyrin-III C-methyltransferase	**-2.39**	**-2.09**	-1.02
YPK_3443	*ygcM*	queuosine biosynthesis protein QueD	**-4.33**	**-4.91**	**-1.81**
YPK_3474	*panD*	aspartate 1-decarboxylase	**1.88**	**-3.71**	1.02
YPK_3497	*nadC*	nicotinate-nucleotide pyrophosphorylase	-1.51	**-2.08**	-1.17
YPK_3578	*folA*	dihydrofolate reductase	**-2.95**	-1.35	**-1.85**
YPK_3758	*ispB*	polyprenyl synthetase	-1.28	**-1.81**	-1.15
YPK_4145	*kbl*	2-amino-3-ketobutyrate coenzyme A ligase	1.01	**2.70**	1.22
LIPID METABOLISM					
YPK_0447		3-hydroxyisobutyrate dehydrogenase	**1.79**	1.52	-1.18
YPK_1070	*dxr*	1-deoxy-D-xylulose 5-phosphate reductoisomerase	**1.94**	**2.82**	1.26
YPK_1082	*accA*	acetyl-CoA carboxylase, carboxyl transferase, alpha subunit	**-2.54**	**-3.04**	-1.48
YPK_1193	*acpS*	holo-acyl-carrier-protein synthase	**2.00**	1.08	1.40
YPK_1324	*yegS*	diacylglycerol kinase catalytic region	1.38	**2.36**	1.05
YPK_1506	*fadL*	membrane protein involved in aromatic hydrocarbon degradation	**-2.44**	**2.48**	1.64
YPK_1508	*fadI*	acetyl-CoA C-acyltransferase FadI	-1.35	**2.02**	-1.07
YPK_1509	*fadJ*	fatty acid oxidation complex, alpha subunit FadJ	1.27	**3.03**	1.12
YPK_1924	*acpD*	NAD(P)H dehydrogenase (quinone)	1.14	**-1.94**	-1.33
YPK_2510		short-chain dehydrogenase/reductase SDR	**2.55**	**2.36**	1.17
YPK_2636	*fabF2*	3-oxoacyl-(acyl-carrier-protein) synthase 2	**1.88**	**1.88**	1.53
YPK_2735		membrane protein	1.46	**1.90**	1.21
YPK_2736		undecaprenyl-diphosphatase	**2.11**	**5.44**	1.01
YPK_3283		putative methyltransferase	-1.16	**2.49**	**-1.75**
YPK_3582	*carB*	carbamoyl-phosphate synthase, large subunit	-1.03	1.42	**1.86**
YPK_3933	*fadB*	fatty oxidation complex, alpha subunit FadB	**-2.91**	**2.69**	-1.06
YPK_3934	*fadA*	acetyl-CoA C-acyltransferase FadA	-1.13	**3.23**	1.27
SECONDARY METABOLITES BIOSYNTHESIS AND CATABOLISM					
YPK_0118		serralysin	-1.09	**3.11**	1.22
YPK_0261	*tauD*	taurine dioxygenase	**-2.92**	-1.40	-1.09
YPK_0514	*yrbD*	mammalian cell entry related domain protein	**1.96**	1.27	-1.02
YPK_0515	*yrbC*	toluene tolerance family protein	**3.62**	**2.14**	1.46
YPK_0789		intradiol ring-cleavage dioxygenase	**5.30**	1.29	-1.02
YPK_1687	*acpP*	acyl carrier protein	**-2.00**	**-4.07**	-1.49
YPK_1858	*cfa*	cyclopropane-fatty-acyl-phospholipid synthase	**3.61**	1.50	1.18
YPK_2472	*rrmA*	rRNA (guanine-N(1)-)-methyltransferase	**-2.46**	**-2.69**	-1.65
YPK_2509		5-oxopent-3-ene-1,2,5-tricarboxylate	1.62	**1.97**	-1.06

		decarboxylase			
YPK_2658	*smtA*	methyltransferase type 11	**-1.81**	1.21	-1.58
YPK_2707		NAD-dependent epimerase/dehydratase	1.23	**1.89**	1.30
YPK_2929	*bioC*	biotin biosynthesis protein BioC	**-1.77**	-1.47	1.03
YPK_3921	*rcs*	acetate-CoA ligase	1.15	**3.33**	1.47
YPK_3951	*ysgA*	carboxymethylenebutenolidase	1.59	**3.37**	**1.79**
YPK_4218	*gidB*	methyltransferase GidB	**-2.84**	**-3.76**	-1.63
INORGANIC ION METABOLISM					
YPK_0136	*gntK, idnK*	carbohydrate kinase, thermoresistant glucokinase family	1.10	**-1.86**	-1.47
YPK_0159	*glpE*	rhodanese domain protein	**-2.29**	**-2.50**	-1.45
YPK_1001	*cynT, can*	carbonic anhydrase	-1.62	**2.33**	-1.36
YPK_1355	*yfgD*	arsenate reductase	**2.26**	**1.81**	1.74
YPK_1386	*napD*	NapD family protein	1.38	**-2.01**	1.15
YPK_1492	*phnA*	alkylphosphonate utilization operon protein PhnA	**-2.37**	-1.60	**-1.77**
YPK_1602	*dps*	ferritin Dps family protein	1.73	1.30	**-1.84**
YPK_1661	*mdoG*	periplasmic glucan biosynthesis protein MdoG	**2.31**	**2.91**	1.45
YPK_1914	*qacE*	small multidrug resistance protein	**-1.77**	**-2.72**	-1.62
YPK_2364	*efeB*	Dyp-type peroxidase family	-1.09	**-1.80**	1.62
YPK_2438	*ftnA*	Ferroxidase	**1.81**	1.59	**-2.23**
YPK_2743	*metQ-2*	NLPA lipoprotein	-1.17	**2.08**	1.13
YPK_2866	*ynjE, sseA*	rhodanese domain protein	1.09	**1.90**	-1.06
YPK_3205	*ychN*	DsrE family protein	-1.73	-1.58	**-1.87**
YPK_3875	*terB*	tellurite resistance TerB	1.42	**2.81**	**1.76**
YPK_3888	*hemP*	hemin uptake protein	**-2.97**	**-3.71**	-1.15
YPK_3890	*hmuS*	haemin-degrading family protein	1.12	**7.75**	**1.86**
YPK_4013	*cyaY*	iron donor protein CyaY	-1.54	**-2.58**	-1.46
YPK_4140		rhodanese domain protein	**-1.83**	**-2.05**	-1.36
YPK_4245	*trmE*	tRNA modification GTPase TrmE	-1.13	**-1.88**	-1.27
TRANSPORT					
YPK_0048	*mdfA*	major facilitator superfamily MFS_1	**-1.75**	-1.34	-1.15
YPK_0068	*fhuC-1, fepC-1, fecE-1*	ABC transporter related	-1.44	**-1.75**	1.06
YPK_0070	*fhuB-2, fepG-2, fecD-2*	transport system permease protein	-1.41	**-1.78**	-1.11
YPK_0083	*uhpC*	phosphoglycerate transporter	-1.63	**13.74**	-1.51
YPK_0098	*dctA*	sodium:dicarboxylate symporter	-1.01	**2.33**	-1.18
YPK_0122	*pitA*	phosphate transporter	**-2.03**	**-2.26**	-1.28
YPK_0238	*tsgA*	major facilitator superfamily MFS_1	1.45	-1.28	**3.98**
YPK_0247		integral membrane protein, YccS/YhfK family	**1.82**	-1.14	1.02
YPK_0258	*tauA-1*	taurine ABC transporter, periplasmic binding protein	**-1.81**	-1.08	1.20
YPK_0259	*tauB*	ABC transporter related	**-2.20**	-1.35	-1.01
YPK_0260	*tauC*	binding-protein-dependent transport systems inner membrane component	**-3.04**	**-2.00**	-1.30
YPK_0378	*malE*	extracellular solute-binding protein family 1	-1.02	**2.57**	1.31
YPK_0380	*malK*	ABC transporter related	**-1.89**	**1.87**	1.38
YPK_0381	*lamB-1*	porin LamB type	-1.72	**1.82**	1.30
YPK_0431	*yphF-1, ytfQ-1*	carbohydrate uptake (CUT2 family) ABC transporter, periplasmic carbohydrate-binding protein	**-2.47**	1.07	1.42
YPK_0495	*treB*	PTS system, trehalose-specific IIBC subunit	**2.72**	1.51	1.18
YPK_0507	*lptA*	lipopolysaccharide transport periplasmic protein LptA	1.53	**1.80**	1.20
YPK_0512	*mlaF*	ABC transporter related	**2.16**	1.34	1.03
YPK_0513	*mlaE*	putative ABC transporter system permease protein	**1.81**	1.20	1.04
YPK_0698	*fepB*	periplasmic binding protein	**4.07**	-1.13	1.14
YPK_0748	*abgT*	AbgT putative transporter	1.27	**-4.70**	1.56
YPK_0968	*cycB, ganO*	extracellular solute-binding protein family 1	**-1.94**	-1.42	1.22
YPK_0975	*lamB-2*	porin LamB type	**-2.04**	-1.47	1.01
YPK_1094	*metQ-1*	lipoprotein, YaeC family	**-1.83**	-1.10	-1.17
YPK_1114	*proW*	binding-protein-dependent transport systems inner membrane component	1.20	**1.82**	1.13
YPK_1125	*ddpA-1*	extracellular solute-binding protein family 5	**2.26**	**1.86**	1.23
YPK_1128	*ddpD-1*	ABC transporter related	**2.50**	1.52	1.13
YPK_1129	*ddpF-1*	ABC transporter related	**1.84**	1.25	1.08
YPK_1157	*kdpC*	potassium-transporting ATPase, C subunit	**1.96**	1.31	-1.05
YPK_1158	*kdpB*	K+-transporting ATPase, B subunit	**1.96**	1.52	1.06
YPK_1159	*kdpA*	potassium-transporting ATPase, A subunit	**2.05**	1.60	1.12
YPK_1333	*ydcT*	spermidine/putrescine ABC transporter ATPase subunit	**2.66**	**2.18**	1.34
YPK_1375	*afuA, fbpA*	extracellular solute-binding protein family 1	-1.28	**6.37**	**2.68**
YPK_1376	*afuB, fbpB*	binding-protein-dependent transport systems inner membrane component	-1.23	**3.85**	1.70
YPK_1377	*afuC*	ABC transporter related	-1.41	**2.80**	1.51
YPK_1408	*cysP*	sulfate ABC transporter, periplasmic sulfate-binding protein	**-1.79**	**-1.75**	1.03
YPK_1409	*cysT*	sulfate ABC transporter, inner membrane subunit	**-1.77**	**-1.92**	-1.18
YPK_1410	*cysW*	sulfate ABC transporter, inner membrane subunit CysW	**-1.89**	**-1.94**	-1.19
YPK_1428	*ptsH*	phosphotransferase system, phosphocarrier protein HPr	**-2.53**	1.04	1.47
YPK_1430	*cysZ*	putative sulfate transport protein CysZ	-1.33	**-1.81**	**-1.82**
YPK_1438	*nupC1*	nucleoside transporter	**3.91**	**-2.61**	**3.43**
YPK_1538	*hisJ*	cationic amino acid ABC transporter, periplasmic binding protein	-1.22	**2.01**	1.44
YPK_1546	*ulaA*	putative sugar-specific permease SgaT/UlaA	**-5.09**	**-2.41**	1.45
YPK_1547	*ulaB*	phosphotransferase system lactose/cellobiose-specific IIB subunit	**-6.35**	**-2.91**	1.26
YPK_1548	*ulaC*	putative PTS IIA-like nitrogen-regulatory protein PtsN	**-7.05**	**-3.83**	-1.06
YPK_1555		citrate transporter	-1.19	**-1.85**	-1.64
YPK_1598	*glnQ*	ABC transporter related	**2.17**	**2.71**	1.54
YPK_1599	*glnP*	polar amino acid ABC transporter, inner membrane subunit	**2.19**	**2.92**	1.18
YPK_1600	*glnH*	cationic amino acid ABC transporter, periplasmic binding protein	1.22	**1.78**	-1.19
YPK_1694	*ptsG*	PTS system, glucose-specific IIBC subunit	**-23.68**	**-1.86**	1.03
YPK_1744	*mgtB*	magnesium-translocating P-type ATPase	-1.25	-1.51	**-2.02**
YPK_1791	*yebQ*	major facilitator superfamily MFS_1	1.02	**-3.08**	-1.10
YPK_1795	*gltP*	sodium:dicarboxylate symporter	**-2.99**	**-2.58**	1.10
YPK_1886	*tppB*	amino acid/peptide transporter	**-2.85**	1.13	-1.24
YPK_1906	*mppA*	extracellular solute-binding protein family 5	**2.03**	**1.94**	1.14
YPK_1939	*arcD, lys1, lysP*	arginine/ornithine antiporter	**-1.78**	-1.11	-1.39
YPK_1949	*ilvN*	amino acid-binding ACT domain protein	-1.24	**3.50**	1.19
YPK_1958	*tauA-2*	ABC transporter, periplasmic substrate-binding protein	**1.78**	1.09	1.27
YPK_1979	*clcB*	chloride channel core	1.25	**2.56**	-1.03
YPK_1983	*ynfM*	major facilitator superfamily MFS_1	-1.07	**1.76**	-1.03
YPK_2070	*oppA*	extracellular solute-binding protein family 5	1.23	**2.34**	**2.05**
YPK_2174	*ychM*	sulfate transporter	-1.02	**5.43**	-1.16
YPK_2233	*chaA*	calcium/proton exchanger	**-2.71**	**-1.81**	-1.61
YPK_2246	*ybbA-2*	ABC transporter related	**1.92**	1.31	1.44
YPK_2252	*efeU-1*	iron permease FTR1	-1.62	**-2.35**	-1.30
YPK_2253		major facilitator superfamily MFS_1	**2.18**	**-1.76**	1.49
YPK_2256	*ansP*	amino acid permease-associated region	-1.47	**3.33**	1.10
YPK_2367	*putP*	sodium/proline symporter	**-3.32**	1.65	1.32
YPK_2376	*fliY*	extracellular solute-binding protein family 3	**-1.89**	-1.49	1.03
YPK_2463	*yoaE*	Integral membrane protein TerC	**-1.86**	-1.20	1.15
YPK_2464	*manX*	PTS system, mannose/fructose/sorbose family, IIB subunit	**-1.92**	1.17	1.72
YPK_2466	*manZ*	PTS system, mannose/fructose/sorbose family, IID subunit	**-1.87**	1.09	1.49
YPK_2477	*aroP*	amino acid permease-associated region	**-1.81**	-1.35	1.12
YPK_2487	*mdlA-2*	ABC transporter related	-1.54	**-1.77**	1.10
YPK_2512		major facilitator superfamily MFS_1	1.56	**1.88**	1.20
YPK_2517	*yeeF*	amino acid permease-associated region	**-1.87**	**-1.93**	1.33
YPK_2556	*yphF-3, ytfQ-3*	putative sugar ABC transporter	-1.39	**1.97**	**1.77**
YPK_2564	*mglC*	monosaccharide-transporting ATPase	**-2.36**	1.09	1.09
YPK_2565	*mglA*	ABC transporter related	**-2.86**	1.30	1.17
YPK_2566	*mglB*	periplasmic binding protein/LacI transcriptional regulator	**-5.00**	1.68	1.10
YPK_2618	*tusE*	sulfur relay protein, TusE/DsrC/DsvC family	**-1.84**	-1.38	-1.45
YPK_2676	*focA*	formate/nitrite transporter	**-2.00**	-1.69	**-1.99**
YPK_2688	*cydD*	ABC transporter, CydDC cysteine exporter (CydDC-	1.11	**1.97**	1.24

		E) family, permease/ATP-binding protein CydD			
YPK_2689	*cydC*	ABC transporter, CydDC cysteine exporter (CydDC-E) family, permease/ATP-binding protein CydC	1.22	**2.68**	-1.02
YPK_2695	*macB-2*	ABC transporter related	1.17	**2.32**	1.00
YPK_2710	*artP*	ABC transporter related	**-3.72**	1.57	-1.32
YPK_2711	*artI*	cationic amino acid ABC transporter, periplasmic binding protein	**-3.94**	1.74	-1.18
YPK_2712	*artQ*	polar amino acid ABC transporter, inner membrane subunit	**-2.92**	**1.93**	-1.00
YPK_2713	*artM*	polar amino acid ABC transporter, inner membrane subunit	**-2.53**	**1.76**	1.01
YPK_2724	*artJ*	cationic amino acid ABC transporter, periplasmic binding protein	**-2.54**	**2.01**	1.10
YPK_2739	*sdaC*	serine transporter	**-3.64**	-1.12	-1.51
YPK_2742	*metN-2*	ABC transporter related	1.09	**2.24**	1.41
YPK_2749	*fhuC-2, fepC-2, fecE-2*	ABC transporter related	**-2.18**	-1.70	-1.06
YPK_2750	*fhuB-3, fepG-3, fecD-3*	transport system permease protein	**-1.85**	-1.01	1.20
YPK_2751	*fhuD-3, fepB-3, fecB-3*	periplasmic binding protein	**-2.30**	-1.40	1.07
YPK_2752	*lysP*	amino acid permease-associated region	**-3.19**	**-2.66**	-1.07
YPK_2764	*fruB*	phosphocarrier, HPr family	**-2.61**	1.19	1.22
YPK_2767	*yphE-4, ytfR-4*	ABC transporter related	1.35	**1.76**	-1.01
YPK_2768	*yphF-4, ytfQ-4*	ABC transporter, periplasmic sugar-binding protein	1.44	**1.80**	1.15
YPK_2789	*yejF*	ABC transporter related	1.34	**2.64**	1.26
YPK_2853	*tyrP*	aromatic amino acid transporter	-1.41	**1.93**	-1.24
YPK_2862	*opuBD-1*	binding-protein-dependent transport systems inner membrane component	1.13	**2.30**	1.10
YPK_2863	*opuA*	ABC transporter related	1.32	**2.74**	1.05
YPK_2864	*opuBD-2*	binding-protein-dependent transport systems inner membrane component	1.23	**2.30**	-1.05
YPK_2865	*opuC*	substrate-binding region of ABC-type glycine betaine transport system	1.66	**3.98**	1.27
YPK_2940	*modF*	ABC transporter related	**-1.96**	1.21	-1.39
YPK_3010	*ybeJ/gltI*	extracellular solute-binding protein family 3	**-1.76**	1.33	-1.29
YPK_3158	*ybbA-1*	ABC transporter related	-1.14	**1.84**	1.18
YPK_3189	*ddhC*	DegT/DnrJ/EryC1/StrS aminotransferase	1.19	**1.75**	1.28
YPK_3190	*ddhB*	CDP-glucose 4,6-dehydratase	1.70	**2.64**	**1.90**
YPK_3272	*proY*	amino acid permease-associated region	**-2.21**	1.01	-1.06
YPK_3309	*fadE*	acyl-CoA dehydrogenase	1.32	**2.07**	1.09
YPK_3339	*emrB*	drug resistance transporter, EmrB/QacA subfamily	1.07	**2.17**	1.26
YPK_3442	*cysJ*	sulfite reductase (NADPH) flavoprotein, alpha chain	**-2.40**	**-2.08**	-1.12
YPK_3460	*fhuB*	transport system permease protein	**-1.76**	**-2.46**	-1.07
YPK_3461	*fhuD*	periplasmic binding protein	-1.44	**-2.26**	-1.05
YPK_3462	*fhuC*	ABC transporter related	**-1.79**	**-2.74**	-1.31
YPK_3597		major facilitator superfamily MFS_1	-1.35	**-2.18**	-1.13
YPK_3618	*yjjK*	ABC transporter related	**1.81**	1.48	**1.77**
YPK_3686	*ddpA-2*	extracellular solute-binding protein family 5	**1.82**	1.11	1.26
YPK_3688	*ddpC-2*	binding-protein-dependent transport systems inner membrane component	-1.74	**-1.89**	-1.30
YPK_3874	*terC*	integral membrane protein TerC	1.26	**1.78**	1.65
YPK_3891	*hmuT*	periplasmic binding protein	1.22	**5.54**	1.55
YPK_3892	*hmuU*	transport system permease protein	-1.11	**4.65**	1.22
YPK_3893	*hmuV*	ABC transporter related	-1.32	**2.41**	1.00
YPK_3920	*gltP*	sodium:dicarboxylate symporter	**-2.62**	**-1.82**	-1.12
YPK_3923	*actP*	cation/acetate symporter ActP	1.15	**2.85**	1.10
YPK_3954	*madN*	carboxylate/amino acid/amine transporter	**-2.08**	**-2.97**	-1.37
YPK_3970	*livF*	ABC transporter related	**2.46**	-1.06	1.25
YPK_3971	*livG*	ABC transporter related	**2.61**	-1.23	1.33
YPK_3972	*livM*	inner-membrane translocator	**2.09**	-1.23	1.23
YPK_3973	*livH*	inner-membrane translocator	**3.08**	1.00	1.57
YPK_3974	*livK*	extracellular ligand-binding receptor	**3.15**	-1.57	1.30
YPK_4001	*rarD*	RarD protein, DMT superfamily transporter	-1.36	**-1.92**	-1.20
YPK_4018	*hemX*	putative uroporphyrinogen III C-methyltransferase	1.38	**1.80**	1.39
YPK_4112	*glpF*	MIP family channel protein	**-7.60**	1.62	-1.47
YPK_4125	*sbp1*	sulfate ABC transporter, periplasmic sulfate-binding protein	**-2.91**	-1.48	1.16
YPK_4127	*fieF*	cation diffusion facilitator family transporter	-1.44	**-2.19**	**-1.85**
YPK_4181	*gltS*	sodium/glutamate symporter	**-3.37**	1.55	1.00
YPK_4231	*pstS*	phosphate ABC transporter, periplasmic phosphate-binding protein	**2.61**	1.44	1.07
YPK_4237		extracellular solute-binding protein family 3	**-2.15**	-1.04	1.27
YPK_4238		polar amino acid ABC transporter, inner membrane subunit	**-1.76**	1.24	1.07
YPK_4239		polar amino acid ABC transporter, inner membrane subunit	**-2.77**	-1.38	-1.62
GENERAL MEMBRANE TRANSPORT, SECRETION AND STRUCTURAL PROTEINS					
YPK_0262	*rafQ*	glycosyl transferase family 9	**-2.20**	-1.50	-1.42
YPK_0312	*mscL*	large conductance mechanosensitive channel protein	-1.44	**-3.26**	-1.65
YPK_0410		YD repeat protein	**2.13**	-1.04	1.15
YPK_0654	*tolC*	type I secretion outer membrane protein, TolC family	**1.75**	**1.93**	1.62
YPK_0673	*exbD*	TonB system transport protein ExbD	-1.12	**-2.62**	1.14
YPK_0729	*fliK-2*	putative flagellar hook-length control protein	1.68	**1.88**	1.45
YPK_0740		putative integral membrane efflux protein	-1.23	**-1.87**	-1.43
YPK_1073	*rscP*	membrane-associated zinc metalloprotease	1.24	**1.85**	1.00
YPK_1074	*yaeT*	outer membrane protein assembly complex, YaeT protein	**2.12**	**2.43**	1.64
YPK_1075	*ompH*	outer membrane chaperone Skp (OmpH)	**1.79**	1.14	-1.17
YPK_1090	*cutF*	copper resistance lipoprotein NlpE	1.01	**1.96**	-1.49
YPK_1533	*dedD*	phosphogluconate dehydratase	1.70	**2.61**	1.30
YPK_1641	*mscM*	mechanosensitive ion channel MscS	1.60	**1.88**	1.42
YPK_1662	*mdoH*	glycosyl transferase family 2	**1.87**	**2.73**	1.09
YPK_1665	*htrB*	lipid A biosynthesis lauroyl (or palmitoleoyl) acyltransferase	**2.32**	1.04	1.12
YPK_1783	*prc*	carboxyl-terminal protease	**1.92**	1.66	1.71
YPK_2022	*osmB*	osmotically inducible lipoprotein B precursor	1.11	**2.50**	-1.20
YPK_2055	*tonB*	TonB family protein	**-2.02**	**-2.66**	-1.17
YPK_2508		mandelate racemase/muconate lactonizing protein	**2.42**	1.74	1.15
YPK_2630	*ompA*	OmpA domain protein transmembrane region-containing protein	**1.85**	**2.76**	1.68
YPK_2649	*ompF*	porin Gram-negative type	**-2.34**	**-2.00**	-1.29
YPK_2678		glycosyl transferase family 25	-1.28	**1.93**	-1.27
YPK_2684	*lolA*	outer membrane lipoprotein carrier protein LolA	1.06	**2.07**	-1.03
YPK_2696	*macA-2*	efflux transporter, RND family, MFP subunit	1.31	**3.56**	1.37
YPK_2740	*dacC*	serine-type D-Ala-D-Ala carboxypeptidase	**2.16**	**4.21**	1.63
YPK_2784	*spr*	NLP/P60 protein	**-3.53**	**3.40**	-1.09
YPK_2839	*ompC-2*	porin Gram-negative type	-1.12	**3.72**	-1.28
YPK_2885	*pbpG*	peptidase S11 D-alanyl-D-alanine carboxypeptidase 1	-1.01	**1.76**	1.17
YPK_2954		tol-pal system protein YbgF	**2.46**	**3.84**	1.39
YPK_2955	*pal*	peptidoglycan-associated lipoprotein	**1.99**	**3.05**	-1.06
YPK_2956	*tolB*	Tol-Pal system beta propeller repeat protein TolB	**2.51**	**5.13**	1.15
YPK_3009	*lnt*	apolipoprotein N-acyltransferase	1.16	**2.00**	1.32
YPK_3028	*tatE*	twin-arginine translocation protein, TatA/E family subunit	**1.84**	**2.48**	-1.09
YPK_3182	*fcl*	NAD-dependent epimerase/dehydratase	1.72	**1.77**	1.64
YPK_3185	*wzy*	O-antigen biosynthesis protein	**-2.24**	**-3.07**	**-1.91**
YPK_3187		glycosyl transferase family 2	-1.51	**-2.22**	**-1.78**
YPK_3238	*yajG*	uncharacterized lipoprotein	**-2.21**	**-2.31**	**-1.95**
YPK_3263	*yajC*	preprotein translocase, YajC subunit	**-1.82**	-1.68	-1.36
YPK_3338	*emrA*	efflux pump membrane	1.09	**2.73**	1.32

		protein			
YPK_3463	*mrcB*	penicillin-binding protein 1B	1.46	**2.62**	1.57
YPK_3512	*lpxC*	UDP-3-0-acyl N-acetylglucosamine deacetylase	**1.93**	1.66	1.14
YPK_3521	*mraY*	phospho-N-acetylmuramoyl-pentapeptide-transferase	-1.23	**-1.76**	-1.24
YPK_3613	*slt*	lytic transglycosylase catalytic	1.04	**2.06**	1.36
YPK_3632	*osmY*	hyperosmotically inducible periplasmic protein	**3.55**	**28.04**	1.17
YPK_3733	*secG*	preprotein translocase, SecG subunit	**-2.42**	**-2.20**	-1.26
YPK_3779	*ytfB*	opacity-associated protein A	1.36	-1.21	-1.13
YPK_4028	*rffH*	glucose-1-phosphate thymidylyltransferase	1.70	**2.13**	1.29
YPK_4030	*wecC*	nucleotide sugar dehydrogenase	1.53	**2.26**	1.31
YPK_4031	*rffE*	UDP-N-acetylglucosamine 2-epimerase	1.41	**1.92**	1.22
YPK_4032	*wzzE*	lipopolysaccharide biosynthesis protein	**1.90**	**3.07**	1.29
YPK_4149	*kdtA*	three-deoxy-D-manno-octulosonic-acid transferase domain protein	-1.47	**-1.81**	-1.40
YPK_4229	*glmS*	glucosamine-fructose-6-phosphate aminotransferase, isomerizing	**2.34**	-1.19	1.33
DEFENSE MECHANISMS					
YPK_1644	*cas-1*	CRISPR-associated protein Cas1	1.00	**2.98**	-1.07
YPK_1645	*cas-3*	CRISPR-associated helicase Cas3 family	1.06	**1.92**	-1.01
YPK_1646	*csy-1*	CRISPR-associated protein, Csy1 family	1.34	**2.50**	1.51
YPK_1647	*csy-2*	CRISPR-associated protein, Csy2 family	1.26	**1.96**	1.09
YPK_1648	*csy-3*	CRISPR-associated protein, Csy3 family	1.43	**2.59**	1.09
YPK_1649	*csy-4*	CRISPR-associated protein, Csy4 family	**1.89**	**3.22**	1.30
YPK_1760	*cwlA, xlyA, xlyB*	N-acetylmuramyl-L-alanine amidase, negative regulator of AmpC, AmpD	**2.97**	**3.21**	-1.09
YPK_2050	*yciC*	protein of unknown function UPF0259	-1.47	**-2.10**	-1.38
YPK_2836	*ampH*	beta-lactamase	**1.91**	**1.76**	1.44
YPK_3642	*mexB*	acriflavin resistance protein	1.34	**-2.44**	1.08
YPK_3665		type I restriction-modification system, M subunit	**-2.01**	**-2.42**	-1.34
YPK_3671	*mcrC*	5-methylcytosine restriction system component	-1.67	**-2.00**	-1.35
YPK_3672	*hsdM-2*	type I restriction-modification system, M subunit	**-2.35**	**-2.83**	1.21
YPK_3674	*hsdR*	type I site-specific deoxyribonuclease, HsdR family	**-1.80**	**-1.82**	1.09
OTHERS					
pYV0019		putative transposase	**1.92**	1.46	1.43
pYV0039		putative transposase	**-1.96**	**-1.85**	-1.43
pYV0046		putative transposase remnant	**-1.76**	-1.21	-1.21
pYV0095		putative transposase	**2.08**	1.09	1.08
YPK_0025	*yiaF*	putative lipoprotein	**3.89**	-1.20	1.19
YPK_0066		transposase IS3/IS911 family protein	**1.75**	1.17	1.16
YPK_0067		integrase catalytic region	**1.94**	1.02	-1.07
YPK_0080	*eptB*	sulfatase	-1.72	**-1.84**	-1.32
YPK_0100		peptidase M16 domain protein	1.67	**2.19**	1.36
YPK_0106	*yhjD*	ribonuclease	1.18	**1.81**	1.04
YPK_0154		protein of unknown function DUF943	**-2.34**	**-1.75**	**-1.84**
YPK_0158	*glpG*	rhomboid family protein	-1.69	**-2.11**	-1.41
YPK_0166		protein of unknown function DUF1471	**2.45**	-1.15	**-1.76**
YPK_0189		DNA circulation family protein	-1.27	**-1.81**	-1.51
YPK_0311	*arfA*	protein of unknown function DUF331	-1.08	**-1.75**	-1.41
YPK_0353	*yjaG*	protein of unknown function DUF416	**-1.99**	-1.17	-1.62
YPK_0355	*yjaH*	protein of unknown function DUF1481	1.38	**1.86**	1.37
YPK_0375	*yjbA*	phosphate-starvation-inducible E	1.12	**-1.94**	-1.27
YPK_0406		putative cytoplasmic protein	**2.23**	1.24	1.25
YPK_0427		transposase mutator type	1.47	**2.91**	1.44
YPK_0445	*pcp*	17 kDa surface antigen	-1.17	**-9.78**	-1.57
YPK_0456	*yhdT*	protein of unknown function DUF997	**-1.97**	-1.29	-1.33
YPK_0462	*yedY*	oxidoreductase molybdopterin binding	**2.10**	-1.09	1.13
YPK_0487		guanine-specific ribonuclease N1 and T1	**2.17**	1.23	1.06
YPK_0502	*yhbJ*	conserved hypothetical protein	1.57	**1.77**	1.26
YPK_0508	*yrbK*	protein of unknown function DUF1239	1.61	**2.04**	1.19
YPK_0509	*kdsC*	3-deoxy-D-manno-octulosonate 8-phosphate phosphatase, YrbI family	1.67	**2.36**	1.29
YPK_0521	*yhcB*	protein of unknown function DUF1043	**-2.31**	**-1.93**	**-2.05**
YPK_0534	*elbB*	ThiJ/PfpI domain protein	**1.95**	**1.90**	1.48
YPK_0551		putative lipoprotein	-1.44	**-1.85**	-1.34
YPK_0602		YheO domain protein	**-1.84**	**-1.83**	-1.45
YPK_0613	*xtmA*	putative phage terminase, small subunit	**1.86**	1.45	1.46
YPK_0638		protein of unknown function DUF205	**-2.03**	**-2.59**	**-2.02**
YPK_0647		protein of unknown function DUF526	-1.50	**-2.42**	-1.58
YPK_0661	*mdaB*	NAD(P)H dehydrogenase (quinone)	**-2.13**	**-4.10**	-1.09
YPK_0822	*yggL*	protein of unknown function DUF469	-1.39	**-1.82**	-1.30
YPK_0856	*yggE*	protein of unknown function DUF541	**3.29**	**18.46**	1.58
YPK_0861	*zapA*	protein of unknown function DUF710	-1.60	**-3.34**	-1.74
YPK_0885		regulatory CII family protein	-1.13	**2.35**	1.07
YPK_0887		gpB bacteriophage P2-like protein	**-1.80**	**2.38**	-1.56
YPK_0890		putative replication initiation protein	-1.63	**3.48**	-1.08
YPK_0895		transcriptional activator Ogr/delta	-1.10	-1.73	**-1.79**
YPK_0951		filamentation induced by cAMP protein Fic	1.14	**1.87**	-1.23
YPK_1020		beta-lactamase domain protein	**2.36**	**1.84**	1.42
YPK_1049	*sufE*	cysteine desulfurase, sulfur acceptor subunit CsdE	-1.16	**-1.81**	-1.56
YPK_1058	*syd*	Syd family protein	-1.31	**-2.01**	-1.49
YPK_1086		transcriptional antiterminator, Rof	-1.63	**-2.46**	**-1.84**
YPK_1087		protein of unknown function UPF0253	**-1.75**	**-2.92**	**-1.95**
YPK_1088		YaeQ family protein	1.07	-1.16	1.01
YPK_1177	*yplB*	ankyrin	**1.87**	1.19	-1.14
YPK_1200		Arc domain protein DNA binding domain protein	**-1.95**	-1.67	-1.33
YPK_1296	*yfgL*	outer membrane assembly lipoprotein YfgL	**1.76**	1.55	1.41
YPK_1323		inhibitor of vertebrate lysozyme	**2.03**	**1.95**	1.09
YPK_1326	*yegP*	protein of unknown function DUF1508	**2.39**	-1.03	-1.15
YPK_1398	*yfeY*	protein of unknown function DUF1131	1.51	**2.24**	1.19
YPK_1451		protein of unknown function DUF799	-1.35	**-1.94**	-1.01
YPK_1512		Smr protein/MutS2	-1.58	**-1.77**	-1.59
YPK_1530	*dedA*	SNARE associated Golgi protein	1.40	**1.98**	1.34
YPK_1557	*yfbR*	metal dependent phosphohydrolase	-1.09	**-1.89**	-1.24
YPK_1577		protein of unknown function DUF187	1.15	**1.96**	1.06
YPK_1585	*elaB*	protein of unknown function DUF883 ElaB	**2.99**	-1.58	-1.74
YPK_1601		protein of unknown function DUF218	-1.22	**1.79**	1.06
YPK_1624	*trp14A*	transposase IS3/IS911 family protein	**2.07**	-1.21	-1.04
YPK_1676		antibiotic biosynthesis monooxygenase	-1.70	**-2.52**	-1.72
YPK_1681	*yceD*	protein of unknown function DUF177	**-2.59**	**-2.75**	-1.74
YPK_1697	*ycfL*	protein of unknown function DUF1425	**1.82**	**2.15**	1.65
YPK_1741		DsrB protein	**-2.13**	**-3.34**	-1.70
YPK_1772		protein of unknown function DUF1480	**1.92**	1.12	**-2.05**
YPK_1776		spore coat U domain protein	**2.01**	-1.07	1.01
YPK_1778		spore coat U domain protein	**3.70**	1.05	1.17
YPK_1806		transposase mutator type	1.43	**2.99**	1.56
YPK_1807		transposase	1.35	**2.14**	1.04
YPK_1870	*sepC*	Rhs family protein-like protein	**2.76**	1.55	1.28
YPK_1885		protein of unknown function DUF1282	**4.04**	**1.94**	-1.14
YPK_1926		protein of unknown function DUF891	1.71	**2.54**	1.14
YPK_1951		protein of unknown function DUF1460	**2.06**	**2.31**	-1.40
YPK_1952		putative virulence factor	-1.62	**-2.15**	1.06
YPK_1977		protein of unknown function DUF1283	1.42	**3.17**	1.26
YPK_1978		protein of unknown function DUF1161	**2.39**	**16.59**	-1.64
YPK_1987		protein of unknown	**1.90**	**4.12**	1.46

		function DUF945			
YPK_1995		oxidoreductase domain protein	**1.87**	1.04	1.10
YPK_2048		transport-associated	**4.42**	**2.66**	-1.47
YPK_2079		SEC-C motif domain protein	-1.11	-1.74	-1.26
YPK_2102	*yeaH*	protein of unknown function DUF444	**2.57**	**2.20**	-1.01
YPK_2103		protein of unknown function DUF6 transmembrane	**2.19**	1.13	-1.35
YPK_2105		pirin domain protein	-1.64	**-2.14**	-1.54
YPK_2108	*spoVR*	SpoVR family protein	**2.60**	**1.83**	1.40
YPK_2120		protein of unknown function DUF709	1.55	**1.86**	-1.08
YPK_2146		protein of unknown function DUF28	**1.76**	1.23	1.45
YPK_2205		Sel1 domain protein repeat-containing protein	1.13	**1.82**	1.16
YPK_2260		amidohydrolase 2	**9.21**	-1.29	1.07
YPK_2264		putative lipoprotein	**1.79**	-1.28	-1.28
YPK_2291		transposase	1.22	**1.89**	1.18
YPK_2292		transposase mutator type	1.29	**2.00**	1.12
YPK_2358	*ydgC, glpM*	GlpM family protein	-1.48	**-1.77**	**-1.81**
YPK_2388	*doc*	death-on-curing family protein	-1.04	**-1.84**	-1.74
YPK_2444	*yqfB*	protein of unknown function DUF437	**3.75**	1.53	-1.15
YPK_2448	*yoaH*	protein of unknown function UPF0181	-1.51	**-2.53**	**-1.83**
YPK_2473		protein of unknown function DUF152	**2.19**	1.32	1.15
YPK_2488		protein of unknown function RIO1	**1.80**	1.23	1.36
YPK_2489		YCII-related	1.33	**-1.98**	**-1.77**
YPK_2514		protein of unknown function DUF496	**-3.11**	**-3.67**	**-1.96**
YPK_2548	*fhuF*	ferric iron reductase	**-1.98**	**-2.63**	-1.55
YPK_2559	*yohJ*	LrgA family protein	**-1.93**	-1.31	-1.71
YPK_2572	*frmB, fghA*	S-formylglutathione hydrolase	-1.34	**1.87**	1.17
YPK_2629	*sulA*	cell division inhibitor SulA	**-1.85**	1.21	-1.49
YPK_2638	*pqiB*	mammalian cell entry related domain protein	1.33	**1.94**	1.18
YPK_2639	*pqiA*	integral membrane protein, PqiA family	1.41	**2.13**	1.17
YPK_2643		protein of unknown function DUF1379	-1.40	-1.11	**-1.94**
YPK_2652		beta-lactamase domain protein	1.52	**2.36**	1.15
YPK_2653		protein of unknown function DUF882	1.53	**2.64**	1.25
YPK_2661		protein of unknown function DUF343	**-1.79**	-1.06	**-1.75**
YPK_2666	*comEC*	DNA internalization-related competence protein ComEC/Rec2	1.09	**1.85**	-1.16
YPK_2693	*clpS*	ATP-dependent Clp protease adaptor protein ClpS	1.28	**1.81**	1.03
YPK_2708		putative lipoprotein	**1.75**	**2.43**	1.35
YPK_2744		2OG-Fe(II) oxygenase	**-1.96**	1.59	1.08
YPK_2797	*yejL*	protein of unknown function DUF1414	-1.61	-1.53	**-1.92**
YPK_2802		Colicin D	1.18	**2.44**	-1.14
YPK_2808		tail assembly chaperone gp38	**-2.24**	**2.06**	-1.41
YPK_2809		putative bacteriophage tail fiber protein	**-1.80**	**2.28**	1.04
YPK_2810		putative bacteriophage protein GP48	-1.17	**2.90**	-1.00
YPK_2811		baseplate J family protein	-1.25	**2.10**	-1.00
YPK_2812		GP46 family protein	-1.10	**2.43**	1.03
YPK_2813		phage baseplate assembly protein V	-1.02	**3.47**	1.15
YPK_2814		Mu P family protein	-1.05	**2.85**	1.39
YPK_2817		putative bacteriophage protein	-1.25	**3.80**	1.08
YPK_2819		Mu tail sheath family protein	-1.24	**3.97**	1.39
YPK_2820		putative bacteriophage protein	-1.32	**3.62**	1.11
YPK_2827		antitermination Q family protein	-1.06	**2.21**	1.07
YPK_2830	*msgA*	DinI family protein	**-2.22**	1.17	-1.42
YPK_2854		YfaZ family protein	**1.81**	1.19	1.14
YPK_2874		protein of unknown function DUF1456	**-2.76**	**-1.96**	**-1.99**
YPK_2918	*ybhL, ybhM, yccA*	protein of unknown function UPF0005	**-2.08**	-1.64	**-2.06**
YPK_2947	*psiF*	PsiF repeat protein	**2.58**	**3.58**	-1.14
YPK_2961		*cyd* operon protein YbgE	**-1.90**	-1.39	-1.67
YPK_2962		*cyd* operon protein YbgT	**-1.96**	-1.39	-1.58
YPK_2978		protein of unknown function UPF0125	1.29	**1.83**	1.06
YPK_2989		CopG domain protein DNA-binding domain protein	**-2.67**	**-2.15**	**-1.94**
YPK_3014		protein of unknown function DUF1451	**2.71**	**2.48**	1.25
YPK_3025	*ybeD*	protein of unknown	**-1.89**	-1.69	-1.71

		function DUF493			
YPK_3036		antibiotic biosynthesis monooxygenase	**-2.40**	**-1.84**	**-1.76**
YPK_3075	*dkgA-2*	2,5-didehydrogluconate reductase	**1.92**	**2.29**	1.37
YPK_3076		aldo/keto reductase	**2.25**	**2.20**	1.38
YPK_3118		phage-related membrane protein	-1.35	**-1.83**	-1.69
YPK_3122		Mu tail sheath family protein	**1.80**	1.29	1.13
YPK_3147		tetratricopeptide TPR_2 repeat protein	**-1.78**	**-2.09**	-1.53
YPK_3157	*ybbP-3*	protein of unknown function DUF214	1.09	**2.05**	1.18
YPK_3166		GumN family protein	1.15	**2.04**	1.05
YPK_3186		LPS side chain defect: putative O-antigen transferase	-1.70	**-2.42**	**-1.81**
YPK_3216	*ybaY*	putative lipoprotein	-1.74	**2.86**	-1.70
YPK_3228	*ybaW*	thioesterase superfamily protein	-1.24	**1.94**	-1.10
YPK_3247	*yajQ*	protein of unknown function DUF520	**-2.07**	-1.54	-1.22
YPK_3281	*yaiE*	protein of unknown function DUF1255	**-1.76**	**-2.07**	-1.52
YPK_3317	*mtnK*	5-methylthioribose kinase	**-2.29**	1.26	1.11
YPK_3505	*yacG*	protein of unknown function DUF329	-1.31	**-2.49**	-1.62
YPK_3528	*ygaW*	protein of unknown function DUF1144	**1.84**	1.38	-1.29
YPK_3607	*creA*	CreA family protein	1.22	**-2.01**	-1.65
YPK_3619		filamentation induced by cAMP protein Fic	**-1.89**	-1.20	-1.24
YPK_3623	*smp*	putative membrane protein Smp	-1.13	**-1.76**	-1.58
YPK_3630	*yjjU*	patatin	1.22	**2.70**	-1.13
YPK_3631		protein of unknown function DUF1328	**3.79**	**22.04**	1.19
YPK_3663		protein of unknown function DUF898 transmembrane	**-1.83**	-1.24	-1.04
YPK_3668		integrase family protein	-1.54	**-1.78**	-1.18
YPK_3677	*yjgQ*	permease YjgP/YjgQ family protein	1.17	**2.31**	1.03
YPK_3678	*yjgP*	permease YjgP/YjgQ family protein	1.01	**1.96**	-1.10
YPK_3683		protein of unknown function DUF1260	**2.67**	1.45	1.67
YPK_3746	*xtmA2*	putative phage terminase, small subunit	**1.93**	1.36	1.51
YPK_3763	*yhcN*	protein of unknown function DUF1471	1.19	**-1.79**	**2.71**
YPK_3768		AIG2 family protein	-1.43	**-2.16**	**-1.75**
YPK_3773		protein of unknown function DUF1107	1.30	**2.43**	-1.50
YPK_3838	*insB*	IS1 transposase	-1.40	**-2.10**	-1.64
YPK_3922		protein of unknown function DUF485	1.09	**2.34**	1.24
YPK_3925		integrase catalytic region	**2.05**	-1.13	-1.19
YPK_3983		domain of unknown function DUF1820	**-1.93**	**-2.27**	**-1.92**
YPK_3984	*yhhN*	YhhN family protein	-1.05	**-2.23**	-1.73
YPK_4063	*yifE*	protein of unknown function DUF413	-1.51	**-2.04**	-1.66
YPK_4097		YiaAB two helix domain protein	-1.44	**-2.57**	-1.57
YPK_4116		protein of unknown function DUF805	**-2.40**	**-2.93**	-1.09
YPK_4128		transposase, IS4 family protein	-1.41	**-2.68**	**-1.94**
YPK_4164		phage transcriptional regulator, AlpA	**-1.79**	-1.40	-1.39
YPK_4187	*yrfG-4, yigB-4, yihX-4*	HAD-superfamily hydrolase, subfamily IA, variant 3	**3.48**	1.24	-1.32
YPK_4247	*yidD*	protein of unknown function DUF37	**-1.84**	-1.63	-1.05
HYPOTHETICAL					
pYV0010		hypothetical protein	**-2.04**	**-3.78**	-1.17
pYV0012		hypothetical protein	-1.40	**-3.27**	1.09
pYV0026		hypothetical protein	1.04	**-2.49**	-1.46
pYV0027		hypothetical protein	1.07	**-2.51**	-1.45
pYV0044		hypothetical protein	**-2.21**	**-2.04**	-1.42
pYV0077	*yscA*	hypothetical protein	-1.35	**-2.96**	**-1.76**
pYV0078		hypothetical protein	-1.11	**-2.06**	-1.40
YPK_0006		hypothetical protein YPK_0006	**-1.99**	**-2.25**	-1.37
YPK_0030	*yibL*	conserved hypothetical protein	**-2.75**	**-4.29**	**-2.10**
YPK_0031		conserved hypothetical protein	**1.78**	1.08	1.34
YPK_0044		conserved hypothetical protein	**-3.93**	**-1.98**	**-2.24**
YPK_0046		conserved hypothetical protein	**-2.12**	1.60	-1.74
YPK_0047		conserved hypothetical protein	-1.55	**-1.83**	-1.64
YPK_0049		hypothetical protein YPK_0049	**-1.97**	**-2.19**	-1.39
YPK_0062		conserved hypothetical protein	-1.65	**-1.96**	-1.39
YPK_0063		hypothetical protein YPK_0063	**-2.59**	**-3.74**	**-1.99**

YPK_0132		conserved hypothetical protein	-1.68	**-2.95**	-1.19
YPK_0153		conserved hypothetical protein	-1.74	**-2.12**	-1.32
YPK_0156		hypothetical protein YPK_0156	**-1.95**	**-2.01**	-1.36
YPK_0250		hypothetical protein YPK_0250	**-1.89**	**2.08**	-1.72
YPK_0397		conserved hypothetical protein	**2.00**	1.25	1.15
YPK_0405		hypothetical protein YPK_0405	**1.77**	1.25	1.23
YPK_0411		conserved hypothetical protein	-1.21	**-2.49**	-1.41
YPK_0441		hypothetical protein YPK_0441	-1.51	**-1.99**	-1.55
YPK_0457		hypothetical protein YPK_0457	**-4.11**	**-4.43**	**-2.05**
YPK_0497		conserved hypothetical protein	**8.64**	**1.84**	1.47
YPK_0522		hypothetical protein YPK_0522	-1.46	**-2.00**	-1.49
YPK_0528		conserved hypothetical protein	-1.05	**1.88**	-1.12
YPK_0566		conserved hypothetical protein	**1.79**	1.27	1.09
YPK_0574		hypothetical protein YPK_0574	-1.11	**-1.79**	-1.45
YPK_0579		conserved hypothetical protein	**1.86**	1.70	1.24
YPK_0580		hypothetical protein YPK_0580	1.22	**1.83**	-1.28
YPK_0609		conserved hypothetical protein	-1.39	**-2.10**	**-1.79**
YPK_0615		hypothetical protein YPK_0615	-1.70	**-2.10**	-1.54
YPK_0631		hypothetical protein YPK_0631	-1.66	**-3.26**	-1.59
YPK_0633		hypothetical protein YPK_0633	**-2.36**	**-5.11**	-1.68
YPK_0653		conserved hypothetical protein	-1.42	**-2.19**	-1.58
YPK_0732		conserved hypothetical protein	**-1.99**	-1.13	**-1.90**
YPK_0742		conserved hypothetical protein	**-2.69**	**-3.57**	-1.60
YPK_0759		conserved hypothetical protein	-1.20	**-1.81**	-1.22
YPK_0769		hypothetical protein YPK_0769	**-2.25**	-1.31	**-2.04**
YPK_0777		conserved hypothetical protein	-1.53	**2.07**	-1.40
YPK_0840		hypothetical protein YPK_0840	**-2.10**	**-2.06**	-1.41
YPK_0870		conserved hypothetical protein	**2.00**	1.61	-1.15
YPK_0884		conserved hypothetical protein	-1.27	**2.37**	-1.04
YPK_0886		hypothetical protein YPK_0886	1.19	**2.97**	1.38
YPK_0889		conserved hypothetical protein	-1.36	**3.38**	-1.19
YPK_0894		hypothetical protein YPK_0894	**-2.03**	-1.23	**-1.85**
YPK_0946		conserved hypothetical protein	-1.40	**2.14**	-1.63
YPK_0947		conserved hypothetical protein	-1.02	**1.79**	1.03
YPK_0954		conserved hypothetical protein	**1.98**	**3.40**	1.36
YPK_0963		conserved hypothetical protein	**-2.31**	-1.48	**-1.93**
YPK_0969		hypothetical protein YPK_0969	**-1.86**	-1.44	1.26
YPK_1030		conserved hypothetical protein	-1.47	**-1.94**	-1.53
YPK_1051		hypothetical protein YPK_1051	-1.46	**-1.98**	-1.37
YPK_1056	*ygdH*	conserved hypothetical protein	1.08	**2.65**	1.14
YPK_1062		conserved hypothetical protein	-1.04	**-2.31**	-1.47
YPK_1121		conserved hypothetical protein	1.05	**3.36**	-1.42
YPK_1150		conserved hypothetical protein	**-2.04**	-1.45	-1.45
YPK_1160		conserved hypothetical protein	-1.19	-1.45	**-2.30**
YPK_1178		conserved hypothetical protein	**1.78**	1.13	-1.30
YPK_1186		conserved hypothetical protein	1.33	**4.39**	-1.32
YPK_1216		hypothetical protein YPK_1216	**-1.75**	**-1.77**	**-1.76**
YPK_1244		hypothetical protein YPK_1244	-1.46	-1.68	**-2.17**
YPK_1256		hypothetical protein YPK_1256	1.17	**-2.22**	**-2.87**
YPK_1295	*yfgM*	conserved hypothetical protein	**1.90**	1.64	1.48
YPK_1369		hypothetical protein YPK_1369	-1.36	**-1.81**	-1.19
YPK_1397	*ygiW*	conserved hypothetical protein	**2.00**	**3.24**	1.07
YPK_1405		conserved hypothetical protein	**-1.97**	**-1.96**	-1.48
YPK_1413		conserved hypothetical protein	**-3.16**	**-3.00**	-1.69
YPK_1434		conserved hypothetical protein	**-1.94**	**-2.62**	-1.65
YPK_1440		conserved hypothetical protein	1.66	**5.73**	-1.23
YPK_1457		conserved hypothetical protein	1.05	**5.19**	-1.55
YPK_1458		hypothetical protein YPK_1458	-1.26	**1.76**	-1.07
YPK_1507		conserved hypothetical protein	-1.49	**-2.32**	-1.68
YPK_1537		hypothetical protein YPK_1537	1.41	-1.22	**-1.77**
YPK_1556		conserved hypothetical protein	1.62	**2.01**	-1.72
YPK_1587		hypothetical protein YPK_1587	-1.18	1.39	**-2.17**
YPK_1617		conserved hypothetical protein	-1.34	**-1.90**	-1.65
YPK_1623		conserved hypothetical protein	**-2.30**	**-2.39**	-1.66
YPK_1626		conserved hypothetical protein	-1.39	-1.09	**-2.20**
YPK_1659		conserved hypothetical protein	**-2.08**	**-2.70**	**-1.97**
YPK_1670		conserved hypothetical protein	**-1.82**	-1.06	-1.60
YPK_1725		conserved hypothetical protein	**-3.81**	**-3.72**	**-1.95**
YPK_1729		conserved hypothetical protein	-1.38	**-2.33**	**-1.76**
YPK_1731		conserved hypothetical protein	-1.30	**-3.69**	-1.65
YPK_1734		hypothetical protein YPK_1734	-1.42	**-2.06**	-1.60
YPK_1735	*ylaC*	conserved hypothetical protein	-1.49	**-2.05**	**-1.76**
YPK_1738		hypothetical protein YPK_1738	1.39	**1.85**	-1.49
YPK_1762		conserved hypothetical protein	**2.83**	1.06	1.13
YPK_1763		hypothetical protein YPK_1763	1.38	**-2.16**	-1.66
YPK_1765		conserved hypothetical protein	**1.89**	-1.17	-1.26
YPK_1767		conserved hypothetical protein	-1.21	**-2.11**	-1.29
YPK_1769		conserved hypothetical protein	**-2.29**	-1.44	**-2.05**
YPK_1818		conserved hypothetical protein	**-13.93**	**-1.85**	-1.55
YPK_1819		conserved hypothetical protein	-1.46	**-2.79**	**-2.06**
YPK_1827		conserved hypothetical protein	1.11	**-2.26**	-1.21
YPK_1865		conserved hypothetical protein	-1.18	**-2.29**	-1.63
YPK_1867		hypothetical protein YPK_1867	-1.54	**-1.88**	**-1.75**
YPK_1879		conserved hypothetical protein	1.30	**3.27**	-1.36
YPK_1887		conserved hypothetical protein	1.06	**2.01**	1.42
YPK_1899	*ycjF*	conserved hypothetical protein	**1.79**	1.44	1.33
YPK_1921	*ydbL*	conserved hypothetical protein	**2.01**	1.43	1.45
YPK_1938		conserved hypothetical protein	-1.24	**-1.94**	**-1.81**
YPK_1954		conserved hypothetical protein	**-6.28**	**-6.23**	-1.10
YPK_1989		hypothetical protein YPK_1989	**-7.00**	1.21	-1.10
YPK_1990		conserved hypothetical protein	**-3.63**	1.68	1.08
YPK_2005		conserved hypothetical protein	-1.51	**-2.22**	**-1.93**
YPK_2020		conserved hypothetical protein	-1.59	**-3.77**	-1.69
YPK_2025		conserved hypothetical protein	-1.50	**-2.84**	**-2.04**
YPK_2034		conserved hypothetical protein	-1.72	**-2.65**	-1.51
YPK_2035		conserved hypothetical protein	**-2.09**	**-3.80**	**-2.01**
YPK_2058		conserved hypothetical protein	1.08	**12.84**	-1.64
YPK_2059		conserved hypothetical protein	**-2.99**	-1.05	-1.19
YPK_2062		conserved hypothetical protein	-1.57	**-1.95**	-1.58
YPK_2065		conserved hypothetical protein	**-2.95**	**-1.78**	-1.71
YPK_2082		hypothetical protein YPK_2082	1.11	1.08	1.02
YPK_2084		conserved hypothetical protein	**-1.97**	-1.49	-1.05
YPK_2101		hypothetical protein YPK_2101	**2.55**	**1.92**	1.07

YPK_2183		hypothetical protein YPK_2183	**1.92**	1.18	1.37
YPK_2185		conserved hypothetical protein	-1.13	**2.08**	-1.18
YPK_2197		conserved hypothetical protein	**2.20**	**3.71**	-1.05
YPK_2198		conserved hypothetical protein	**2.19**	**3.26**	1.04
YPK_2199		conserved hypothetical protein	**2.91**	**3.91**	-1.13
YPK_2200		hypothetical protein YPK_2200	**21.47**	**7.16**	**-1.93**
YPK_2236		conserved hypothetical protein	**3.17**	**1.79**	-1.04
YPK_2251		conserved hypothetical protein	1.26	**-2.13**	-1.16
YPK_2263		conserved hypothetical protein	**1.77**	-1.45	-1.12
YPK_2298		conserved hypothetical protein	-1.73	**2.76**	-1.53
YPK_2299		conserved hypothetical protein	-1.45	**3.10**	-1.56
YPK_2308		hypothetical protein YPK_2308	1.23	**1.97**	1.09
YPK_2309		conserved hypothetical protein	**1.96**	**1.85**	1.22
YPK_2339		conserved hypothetical protein	1.06	**2.97**	-1.32
YPK_2357		conserved hypothetical protein	**-2.38**	**-2.66**	**-2.05**
YPK_2359		conserved hypothetical protein	-1.53	**-1.82**	**-1.95**
YPK_2368		conserved hypothetical protein	**-3.47**	1.31	1.19
YPK_2379		conserved hypothetical protein	**-4.41**	**-6.14**	1.08
YPK_2389		conserved hypothetical protein	-1.01	**-2.22**	-1.73
YPK_2397		conserved hypothetical protein	**-2.63**	**-2.80**	1.13
YPK_2405		hypothetical protein YPK_2405	-1.59	-1.48	**-2.16**
YPK_2433		conserved hypothetical protein	-1.03	**2.28**	1.09
YPK_2441		conserved hypothetical protein	**2.12**	**-2.08**	**-1.88**
YPK_2443		conserved hypothetical protein	**3.64**	1.70	-1.09
YPK_2471		conserved hypothetical protein	**-5.82**	**-5.33**	**-1.93**
YPK_2475		conserved hypothetical protein	**-3.03**	**-3.43**	**-2.08**
YPK_2480		conserved hypothetical protein	-1.72	**-2.65**	**-1.87**
YPK_2481		conserved hypothetical protein	1.22	1.51	**-1.89**
YPK_2482		conserved hypothetical protein	**-2.07**	**-4.04**	**-1.84**
YPK_2483		hypothetical protein YPK_2483	1.12	**-1.92**	**-2.05**
YPK_2485		conserved hypothetical protein	-1.13	**-3.51**	**-1.80**
YPK_2486		conserved hypothetical protein	-1.14	**-4.74**	**-1.89**
YPK_2500	*yaiL*	conserved hypothetical protein	-1.46	**-2.07**	-1.63
YPK_2501		conserved hypothetical protein	-1.37	**-2.15**	-1.40
YPK_2507		conserved hypothetical protein	**2.21**	**1.84**	1.09
YPK_2522		hypothetical protein YPK_2522	-1.46	**-2.57**	-1.40
YPK_2523		conserved hypothetical protein	-1.29	**-1.86**	-1.28
YPK_2623		conserved hypothetical protein	1.22	**2.02**	1.12
YPK_2726		conserved hypothetical protein	**-2.61**	-1.58	-1.61
YPK_2731		conserved hypothetical protein	**-3.04**	**-1.91**	-1.69
YPK_2745		conserved hypothetical protein	**-3.44**	1.08	-1.21
YPK_2772		conserved hypothetical protein	1.58	**2.05**	-1.12
YPK_2781		conserved hypothetical protein	**-8.43**	**5.22**	**-2.11**
YPK_2790		conserved hypothetical protein	-1.23	-1.19	**-1.80**
YPK_2801		conserved hypothetical protein	1.46	**2.61**	1.29
YPK_2804		conserved hypothetical protein	**-2.04**	**6.61**	-1.55
YPK_2806		hypothetical protein YPK_2806	1.33	**1.96**	1.12
YPK_2816		conserved hypothetical protein	1.08	**2.17**	1.03
YPK_2818		conserved hypothetical protein	-1.24	**4.87**	1.32
YPK_2821		conserved hypothetical protein	1.03	**4.13**	1.36
YPK_2822		conserved hypothetical protein	-1.11	**3.00**	1.29
YPK_2868		conserved hypothetical protein	**2.45**	1.08	-1.00
YPK_2880		conserved hypothetical protein	1.17	**6.05**	-1.02
YPK_2892		conserved hypothetical protein	1.51	**1.87**	1.35
YPK_2984		conserved hypothetical protein	**-1.94**	**-2.09**	-1.73
YPK_2988		hypothetical protein YPK_2988	**-2.26**	**-2.01**	**-1.84**
YPK_3035		conserved hypothetical protein	**-11.46**	**-5.14**	**-2.17**
YPK_3038		conserved hypothetical protein	-1.57	**-2.38**	**-1.86**
YPK_3061		conserved hypothetical protein	-1.23	**2.04**	-1.26
YPK_3062		conserved hypothetical protein	**-1.80**	**2.06**	-1.53
YPK_3070		conserved hypothetical protein	-1.26	**2.00**	-1.40
YPK_3089		conserved hypothetical protein	**1.76**	**1.82**	1.04
YPK_3101		hypothetical protein YPK_3101	-1.19	**1.83**	-1.16
YPK_3121		conserved hypothetical protein	**1.86**	1.56	1.25
YPK_3123		conserved hypothetical protein	**1.80**	-1.00	-1.20
YPK_3138		hypothetical protein YPK_3138	1.12	**1.99**	1.17
YPK_3203		conserved hypothetical protein	**-2.02**	-1.21	-1.74
YPK_3212		conserved hypothetical protein	-1.33	**-2.15**	**-1.78**
YPK_3218		hypothetical protein YPK_3218	**-1.99**	**-1.94**	-1.56
YPK_3236		conserved hypothetical protein	**-1.83**	-1.27	-1.14
YPK_3240		conserved hypothetical protein	**-3.16**	**-1.86**	-1.41
YPK_3285		conserved hypothetical protein	**-1.95**	**-2.70**	**-2.05**
YPK_3396		conserved hypothetical protein	**-1.83**	-1.38	-1.45
YPK_3481	*yacC*	conserved hypothetical protein	**-2.00**	**-2.25**	-1.56
YPK_3486	*yacL*	conserved hypothetical protein	**2.28**	1.47	1.59
YPK_3549		conserved hypothetical protein	**6.01**	1.42	-1.11
YPK_3554		conserved hypothetical protein	**7.92**	**3.05**	**1.79**
YPK_3555		conserved hypothetical protein	**6.25**	**2.62**	**1.80**
YPK_3567		conserved hypothetical protein	**4.33**	**-2.03**	-1.20
YPK_3576		conserved hypothetical protein	**-2.01**	-1.65	-1.57
YPK_3608		hypothetical protein YPK_3608	1.49	**-2.06**	-1.71
YPK_3615		conserved hypothetical protein	-1.29	**-1.88**	-1.66
YPK_3644		conserved hypothetical protein	1.15	**-2.64**	-1.09
YPK_3645		hypothetical protein YPK_3645	-1.59	**-2.16**	**-1.76**
YPK_3656		conserved hypothetical protein	**4.10**	**17.85**	1.70
YPK_3721		hypothetical protein YPK_3721	-1.32	**-1.92**	-1.62
YPK_3749		hypothetical protein YPK_3749	-1.66	-1.31	**-1.78**
YPK_3753		hypothetical protein YPK_3753	-1.58	**-2.27**	-1.30
YPK_3764		hypothetical protein YPK_3764	-1.31	**-1.88**	-1.60
YPK_3774	*ytfJ*	conserved hypothetical protein	**1.79**	**1.84**	1.13
YPK_3821		conserved hypothetical protein	-1.36	**-1.83**	-1.52
YPK_3836		hypothetical protein YPK_3836	-1.58	**-4.87**	-1.40
YPK_3837		conserved hypothetical protein	**-2.30**	**-2.99**	**-2.04**
YPK_3867		conserved hypothetical protein	1.28	**6.38**	1.23
YPK_3956		conserved hypothetical protein	**-2.05**	**-2.05**	-1.47
YPK_3963		conserved hypothetical protein	-1.47	**3.60**	-1.66
YPK_4014		hypothetical protein YPK_4014	-1.29	**-1.79**	**-1.76**
YPK_4039		conserved hypothetical protein	**-1.94**	-1.65	-1.58
YPK_4053		conserved hypothetical protein	**-4.88**	**-3.66**	**-2.21**
YPK_4092		hypothetical protein YPK_4092	**-1.95**	**-2.16**	-1.30
YPK_4107		conserved hypothetical protein	**6.05**	-1.05	-1.05
YPK_4108		conserved hypothetical protein	**2.16**	**2.30**	-1.36
YPK_4124		hypothetical protein YPK_4124	**-2.06**	-1.45	1.12

YPK_4130	hypothetical protein YPK_4130	-1.35	**-1.80**	**-2.05**
YPK_4172	hypothetical protein YPK_4172	-1.26	**-1.91**	-1.47
YPK_4242	conserved hypothetical protein	**-1.80**	**-1.75**	-1.44

8 REFERENCES

Abernathy J, Corkill C, Hinojosa C, Li X, Zhou H (2013) Deletions in the pyruvate pathway of *Salmonella* Typhimurium alter SPI1-mediated gene expression and infectivity. *J Anim Sci Biotechnol* **4:** 5

Achtman M, Zurth K, Morelli G, Torrea G, Guiyoule A, Carniel E (1999) *Yersinia pestis*, the cause of plague, is a recently emerged clone of *Yersinia pseudotuberculosis*. *Proc Natl Acad Sci U S A* **96:** 14043–14048

Al Zaid Siddiquee K, Arauzo-Bravo MJ, Shimizu K (2004) Metabolic flux analysis of *pykF* gene knockout *Escherichia coli* based on ^{13}C-labeling experiments together with measurements of enzyme activities and intracellular metabolite concentrations. *Appl Microbiol Biotechnol* **63:** 407–417

Allison KR, Brynildsen MP, Collins JJ (2011) Metabolite-enabled eradication of bacterial persisters by aminoglycosides. *Nature* **473:** 216–220

Ansong C, Schrimpe-Rutledge AC, Mitchell HD, Chauhan S, Jones MB, Kim YM, McAteer K, Deatherage Kaiser BL, Dubois JL, Brewer HM, Frank BC, McDermott JE, Metz TO, Peterson SN, Smith RD, Motin VL, Adkins JN (2013) A multi-omic systems approach to elucidating *Yersinia* virulence mechanisms. *Mol Biosyst* **9:** 44–54

Atkinson S, Chang CY, Patrick HL, Buckley CM, Wang Y, Sockett RE, Cámara M, Williams P (2008) Functional interplay between the *Yersinia pseudotuberculosis* YpsRI and YtbRI quorum sensing systems modulates swimming motility by controlling expression of *flhDC* and *fliA*. *Mol Microbiol* **69:** 137–151

Atkinson S, Goldstone RJ, Joshua GW, Chang CY, Patrick HL, Cámara M, Wren BW, Williams P (2011) Biofilm development on *Caenorhabditis elegans* by *Yersinia* is facilitated by quorum sensing-dependent repression of type III secretion. *PLoS Pathog* **7:** e1001250

Becker J, Klopprogge C, Herold A, Zelder O, Bolten CJ, Wittmann C (2007) Metabolic flux engineering of l-lysine production in *Corynebacterium glutamicum*—over expression and modification of G6P dehydrogenase. *J Biotechnol* **132:** 99–109

Becker J, Reinefeld J, Stellmacher R, Schäfer R, Lange A, Meyer H, Lalk M, Zelder O, von Abendroth G, Schröder H, Haefner S, Wittmann C (2013) Systems-wide analysis and engineering of metabolic pathway fluxes in bio-succinate producing *Basfia succiniciproducens*. *Biotechnol Bioeng* **110:** 3013–3023

Berger A, Dohnt K, Tielen P, Jahn D, Becker J, Wittmann C (2014) Robustness and plasticity of metabolic pathway flux among uropathogenic isolates of *Pseudomonas aeruginosa*. *PLoS One* **9:** e88368

Beste DJ, Bonde B, Hawkins N, Ward JL, Beale MH, Noack S, Nöh K, Kruger NJ, Ratcliffe RG, McFadden J (2011) ^{13}C Metabolic flux analysis identifies an

unusual route for pyruvate dissimilation in mycobacteria which requires isocitrate lyase and carbon dioxide fixation. *PLoS Pathog* **7:** e1002091

Birkenstock T, Liebeke M, Winstel V, Krismer B, Gekeler C, Niemiec MJ, Bisswanger H, Lalk M, Peschel A (2012) Exometabolome analysis identifies pyruvate dehydrogenase as a target for the antibiotic triphenylbismuthdichloride in multiresistant bacterial pathogens. *J Biol Chem* **287:** 2887–2895

Bölin I, Norlander L, Wolf-Watz H (1982) Temperature-inducible outer membrane protein of *Yersinia pseudotuberculosis* and *Yersinia enterocolitica* is associated with the virulence plasmid. *Infect Immun* **37:** 506–512

Bolstad BM, Irizarry RA, Astrand M, Speed TP (2003) A comparison of normalization methods for high density oligonucleotide array data based on variance and bias. *Bioinformatics* **19:** 185–193

Bosio CF, Jarrett CO, Gardner D, Hinnebusch BJ (2012) Kinetics of innate immune response to *Yersinia pestis* after intradermal infection in a mouse model. *Infect Immun* **80:** 4034–4045

Bowden SD, Ramachandran VK, Knudsen GM, Hinton JC, Thompson A (2010) An incomplete TCA cycle increases survival of *Salmonella* Typhimurium during infection of resting and activated murine macrophages. *PLoS One* **5:** e13871

Brown SA, Palmer KL, Whiteley M (2008) Revisiting the host as a growth medium. *Nat Rev Microbiol* **6:** 657–666

Brown TA (2002) *Genomes, 2nd edition*. Wiley-Liss, Oxford, UK

Burger A, Wachter H (1998) *Hunnius Pharmazeutisches Wörterbuch*. Walter de Gruyter, Berlin, DE

Buschke N, Becker J, Schäfer R, Kiefer P, Biedendieck R, Wittmann C (2013) Systems metabolic engineering of xylose-utilizing *Corynebacterium glutamicum* for production of 1,5-diaminopentane. *Biotechnol J* **8:** 557–570

Casadesus J, Low DA (2013) Programmed Heterogeneity: Epigenetic Mechanisms in Bacteria. *J Biol Chem* **288:** 13929–13935

Cascales E (2008) The type VI secretion toolkit. *EMBO Rep* **9:** 735–741

Cathelyn JS, Crosby SD, Lathem WW, Goldman WE, Miller VL (2006) RovA, a global regulator of *Yersinia pestis*, specifically required for bubonic plague. *Proc Natl Acad Sci U S A* **103:** 13514–13519

Cathelyn JS, Ellison DW, Hinchliffe SJ, Wren BW, Miller V (2007) The RovA regulons of *Yersinia enterocolitica* and *Yersinia pestis* are distinct: evidence that many RovA-regulated genes were acquired more recently than the core genome. *Mol Microbiol* **66:** 189–205

Chan BC, Ip M, Gong H, Lui SL, See RH, Jolivalt C, Fung KP, Leung PC, Reiner NE, Lau CB (2013) Synergistic effects of diosmetin with erythromycin against ABC transporter over-expressed methicillin-resistant *Staphylococcus aureus* (MRSA)

RN4220/pUL5054 and inhibition of MRSA pyruvate kinase. *Phytomedicine* **20:** 611–614

Chang AC, Cohen SN (1978) Construction and characterization of amplifiable multicopy DNA cloning vehicles derived from the P15A cryptic miniplasmid. *J Bacteriol* **134:** 1141–1156

Chang DE, Smalley DJ, Tucker DL, Leatham MP, Norris WE, Stevenson SJ, Anderson AB, Grissom JE, Laux DC, Cohen PS, Conway T (2004) Carbon nutrition of *Escherichia coli* in the mouse intestine. *Proc Natl Acad Sci U S A* **101:** 7427–7432

Chopra I, Roberts M (2001) Tetracycline antibiotics: mode of action, applications, molecular biology, and epidemiology of bacterial resistance. *Microbiol Mol Biol Rev* **65:** 232–260

Chubukov V, Uhr M, Le Chat L, Kleijn RJ, Jules M, Link H, Aymerich S, Stelling J, Sauer U (2013) Transcriptional regulation is insufficient to explain substrate-induced flux changes in *Bacillus subtilis*. *Mol Syst Biol* **9:** 709

Commichau FM, Forchhammer K, Stülke J (2006) Regulatory links between carbon and nitrogen metabolism. *Curr Opin Microbiol* **9:** 167–172

Conway T (1992) The Entner-Doudoroff pathway: history, physiology and molecular biology. *FEMS Microbiol Rev* **9:** 1–27

Dacheux D, Epaulard O, de Groot A, Guery B, Leberre R, Attree I, Polack B, Toussaint B (2002) Activation of the *Pseudomonas aeruginosa* type III secretion system requires an intact pyruvate dehydrogenase *aceAB* operon. *Infect Immun* **70:** 3973–3977

Datsenko KA, Wanner BL (2000) One-step inactivation of chromosomal genes in *Escherichia coli* K-12 using PCR products. *Proc Natl Acad Sci U S A* **97:** 6640–6645

Dauner M, Sauer U (2001) Stoichiometric growth model for riboflavin-producing *Bacillus subtilis*. *Biotechnol Bioeng* **76:** 132–143

Derbise A, Lesic B, Dacheux D, Ghigo JM, Carniel E (2003) A rapid and simple method for inactivating chromosomal genes in *Yersinia*. *FEMS Immunol Med Microbiol* **38:** 113–116

Dube P (2009) Interaction of *Yersinia* with the gut: mechanisms of pathogenesis and immune evasion. *Curr Top Microbiol Immunol* **337:** 61–91

Dubnau D, Losick R (2006) Bistability in bacteria. *Mol Microbiol* **61:** 564–572

Dunn IJ, Heinzle E, Ingham J, Přenosil JE (2003) *Biological reaction engineering: dynamic modelling fundamentals with simulation examples*. Wiley-VCH Verlag GmbH & Co. KGaA, Weinheim, DE

Emmerling M, Dauner M, Ponti A, Fiaux J, Hochuli M, Szyperski T, Wüthrich K, Bailey JE, Sauer U (2002) Metabolic flux responses to pyruvate kinase knockout in *Escherichia coli*. *J Bacteriol* **184:** 152–164

Escalante A, Salinas CA, Gosset G, Bolívar F (2012) Current knowledge of the *Escherichia coli* phosphoenolpyruvate–carbohydrate phosphotransferase system: peculiarities of regulation and impact on growth and product formation. *Appl Microbiol Biotechnol* **94:** 1483–1494

Evans MR, Fink RC, Vazquez-Torres A, Porwollik S, Jones-Carson J, McClelland M, Hassan HM (2011) Analysis of the ArcA regulon in anaerobically grown *Salmonella enterica* sv. Typhimurium. *BMC Microbiol* **11:** 58

Ferrell JE Jr. (2002) Self-perpetuating states in signal transduction: positive feedback, double-negative feedback and bistability. *Curr Opin Cell Biol* **14:** 140–148

Fuhrer T, Sauer U (2009) Different biochemical mechanisms ensure network-wide balancing of reducing equivalents in microbial metabolism. *J Bacteriol* **191:** 2112–2121

Fürch T, Preusse M, Tomasch J, Zech H, Wagner-Döbler I, Rabus R, Wittmann C (2009) Metabolic fluxes in the central carbon metabolism of *Dinoroseobacter shibae* and *Phaeobacter gallaeciensis*, two members of the marine *Roseobacter* clade. *BMC Microbiol* **9:** 209

Gardner TS, Cantor CR, Collins JJ (2000) Construction of a genetic toggle switch in *Escherichia coli*. *Nature* **403:** 339–342

Gentleman RC, Carey VJ, Bates DM, Bolstad B, Dettling M, Dudoit S, Ellis B, Gautier L, Ge Y, Gentry J, Hornik K, Hothorn T, Huber W, Iacus S, Irizarry R, Leisch F, Li C, Maechler M, Rossini AJ, Sawitzki G, Smith C, Smyth G, Tierney L, Yang JY, Zhang J (2004) Bioconductor: open software development for computational biology and bioinformatics. *Genome Biol* **5:** R80

Girgis HS, Harris K, Tavazoie S (2012) Large mutational target size for rapid emergence of bacterial persistence. *Proc Natl Acad Sci U S A* **109:** 12740–12745

Göhler AK, Kökpinar Ö, Schmidt-Heck W, Geffers R, Guthke R, Rinas U, Schuster S, Jahreis K, Kaleta C (2011) More than just a metabolic regulator - elucidation and validation of new targets of PdhR in *Escherichia coli*. *BMC Syst Biol* **5:** 197

Grützkau A, Hanski C, Hahn H, Riecken EO (1990) Involvement of M cells in the bacterial invasion of Peyer's patches: a common mechanism shared by *Yersinia enterocolitica* and other enteroinvasive bacteria. *Gut* **31:** 1011–1015

Hannu T, Mattila L, Nuorti JP, Mikkola J, Siitonen A, Leirisalo-Repo M (2003) Reactive arthritis after an outbreak of *Yersinia pseudotuberculosis* serotype O:3 infection. *Ann Rheum Dis* **62:** 866–869

Haverkorn van Rijsewijk BR, Nanchen A, Nallet S, Kleijn RJ, Sauer U (2011) Large-scale ^{13}C-flux analysis reveals distinct transcriptional control of respiratory and fermentative metabolism in *Escherichia coli*. *Mol Syst Biol* **7:** 477

Heesemann J, Sing A, Trülzsch K (2006) *Yersinia's* stratagem: targeting innate and adaptive immune defense. *Curr Opin Microbiol* **9:** 55–61

Herbst K (2011) The temperature- and growth phase-dependent regulation of the global virulence regulator RovA from *Yersinia pseudotuberculosis*. *Ph.D. thesis:* TU Braunschweig

Herbst K, Bujara M, Heroven AK, Opitz W, Weichert M, Zimmermann A, Dersch P (2009) Intrinsic thermal sensing controls proteolysis of *Yersinia* virulence regulator RovA. *PLoS Pathogens* **5:** e1000435

Heroven AK, Böhme K, Dersch P (2012a) The Csr/Rsm system of *Yersinia* and related pathogens: A post-transcriptional strategy for managing virulence. *RNA Biol* **9:** 379–391

Heroven AK, Böhme K, Rohde M, Dersch P (2008) A Csr-type regulatory system, including small non-coding RNAs, regulates the global virulence regulator RovA of *Yersinia pseudotuberculosis* through RovM. *Mol Microbiol* **68:** 1179–1195

Heroven AK, Nagel G, Tran HJ, Parr S, Dersch P (2004) RovA is autoregulated and antagonizes H-NS-mediated silencing of invasin and *rovA* expression in *Yersinia pseudotuberculosis*. *Mol Microbiol* **53:** 871–888

Heroven AK, Sest M, Pisano F, Scheb-Wetzel M, Böhme K, Klein J, Münch R, Schomburg D, Dersch P (2012b) Crp induces switching of the CsrB and CsrC RNAs in *Yersinia pseudotuberculosis* and links nutritional status to virulence. *Front Cell Infect Microbiol* **2:** 158

Herrero M, de Lorenzo V, Timmis KN (1990) Transposon vectors containing non-antibiotic resistance selection markers for cloning and stable chromosomal insertion of foreign genes in Gram-negative bacteria. *J Bacteriol* **172:** 6557–6567

Hofreuter D, Novik V, Galán JE (2008) Metabolic diversity in *Campylobacter jejuni* enhances specific tissue colonization. *Cell Host Microbe* **4:** 425–433

Howard BM, Pinney RJ, Smith JT (1993) Function of the SOS process in repair of DNA damage induced by modern 4-quinolones. *J Pharm Pharmacol* **45:** 658–662

Isberg RR, Barnes P (2001) Subversion of integrins by enteropathogenic *Yersinia*. *J Cell Sci* **114:** 21–28

Isberg RR, Leong JM (1990) Multiple beta 1 chain integrins are receptors for invasin, a protein that promotes bacterial penetration into mammalian cells. *Cell* **60:** 861–871

Iuchi S, Lin EC (1988) *arcA (dye)*, a global regulatory gene in *Escherichia coli* mediating repression of enzymes in aerobic pathways. *Proc Natl Acad Sci U S A* **85:** 1888–1892

Jahn S, Haverkorn van Rijsewijk BR, Sauer U, Bettenbrock K (2013) A role for $EIIA^{Ntr}$ in controlling fluxes in the central metabolism of *E. coli* K12. *Biochim Biophys Acta* **1833:** 2879–2889

Jalava K, Hakkinen M, Valkonen M, Nakari UM, Palo T, Hallanvuo S, Ollgren J, Siitonen A, Nuorti JP (2006) An outbreak of gastrointestinal illness and Erythema nodosum from grated carrots contaminated with *Yersinia pseudotuberculosis*. *J Infect Dis* **94:** 1209–1216

Kaasch AJ, Dinter J, Goeser T, Plum G, Seifert H (2012) *Yersinia pseudotuberculosis* bloodstream infection and septic arthritis: case report and review of the literature. *Infection* **40:** 185–190

Kiefer P, Heinzle E, Zelder O, Wittmann C (2004) Comparative metabolic flux analysis of lysine-producing *Corynebacterium glutamicum* cultured on glucose or fructose. *Appl Environ Microbiol* **70:** 229–239

Köhler W, Eggers HJ, Fleischer B, Marre R, Pfister H, Pulverer G (2001) *Medizinische Mikrobiologie*. Urban & Fischer Verlag, München - Jena, DE

Kohlstedt M, Becker J, Wittmann C (2010) Metabolic fluxes and beyond—systems biology understanding and engineering of microbial metabolism. *Appl Microbiol Biotechnol* **88:** 1065–1075

Krömer JO, Fritz M, Heinzle E, Wittmann C (2005) *In vivo* quantification of intracellular amino acids and intermediates of the methionine pathway in *Corynebacterium glutamicum*. *Anal Biochem* **340:** 171–173

Krömer JO, Sorgenfrei O, Klopprogge K, Heinzle E, Wittmann C (2004) In-depth profiling of lysine-producing *Corynebacterium glutamicum* by combined analysis of the transcriptome, metabolome, and fluxome. *J Bacteriol* **186:** 1769–1784

Lawhon SD, Maurer R, Suyemoto M, Altier C (2002) Intestinal shortchain fatty acids alter *Salmonella typhimurium* invasion gene expression and virulence through BarA/SirA. *Mol Microbiol* **45:** 1451–1464

Leung V, Lévesque CM (2012) A stress-inducible quorum-sensing peptide mediates the formation of persister cells with noninherited multidrug tolerance. *J Bacteriol* **194:** 2265–2274

Link H, Kochanowski K, Sauer U (2013) Systematic identification of allosteric protein-metabolite interactions that control enzyme activity *in vivo*. *Nat Biotechnol* **31:** 357–361

Liu X, De Wulf P (2004) Probing the ArcA-P Modulon of *Escherichia coli* by Whole Genome Transcriptional Analysis and Sequence Recognition Profiling. *J Biol Chem* **279:** 12588–12597

Lozano R, Naghavi M, Foreman K, et al (2012) Global and regional mortality from 235 causes of death for 20 age groups in 1990 and 2010: a systematic analysis for the global burden of disease Study 2010. *Lancet* **380:** 2095–2128

Lüttmann D, Heermann R, Zimmer B, Hillmann A, Rampp IS, Jung K, Görke B (2009) Stimulation of the potassium sensor KdpD kinase activity by interaction with the phosphotransferase protein IIA Ntr in *Escherichia coli*. *Mol Microbiol* **72:** 978–994

Ma C, Sim S, Shi W, Du L, Xing D, Zhang Y (2010) Energy production genes *sucB* and ubiF are involved in persister survival and tolerance to multiple antibiotics and stresses in *Escherichia coli*. *FEMS Microbiol Lett* **303:** 33–40

Mandell GL, Bennett JE, Dolin R (2009) *Mandell, Douglas, and Bennett's principles and practice of infectious diseases*. Churchill Livingstone, London, UK

Mercado-Lubo R, Leatham MP, Conway T, Cohen PS (2009) *Salmonella enterica* serovar Typhimurium mutants unable to convert malate to pyruvate and oxaloacetate are avirulent and immunogenic in BALB/c mice. *Infect Immun* **77:** 1397–1405

Meza E, Becker J, Bolivar F, Gosset G, Wittmann C (2012) Consequences of phosphoenolpyruvate:sugar phosphotranferase system and pyruvate kinase isozymes inactivation in central carbon metabolism flux distribution in *Escherichia coli*. *Microb Cell Fact* **11:** 127

Miller JH (1992) *A short course in bacterial genetic: a laboratory manual and handbook for* Escherichia coli *and related bacteria*. Cold Spring Harbor Laboratory Press, Cold Spring Harbor, New York, USA

Monk IR, Casey PG, Cronin M, Gahan CG, Hill C (2008) Development of multiple strain competitive index assays for *Listeria* monocytogenes using pIMC; a new site-specific integrative vector. *BMC Microbiol* **8:** 96

Morens DM, Fauci AS (2013) Emerging infectious diseases: threats to human health and global stability. *PLoS Pathog* **9:** e1003467

Morens DM, Folkers GK, Fauci AS (2008) Emerging infections: a perpetual challenge. *Lancet Infect Dis* **8:** 710–719

Motin VL, Georgescu AM, Fitch JP, Gu PP, Nelson DO, Mabery SL, Garnham JB, Sokhansanj BA, Ott LL, Coleman MA, Elliott JM, Kegelmeyer LM, Wyrobek AJ, Slezak TR, Brubaker RR, Garcia E (2004) Temporal global changes in gene expression during temperature transition in *Yersinia pestis*. *J Bacteriol* **186:** 6298–6305

Mowat AM (2003) Anatomical basis of tolerance and immunity to intestinal antigens. *Nat Rev Immunol* **3:** 331–341

Mutschler E, Geisslinger G, Kroemer HK, Ruth P, Schäfer-Korting M (2005) *Mutschler Arzneimittelwirkungen kompakt*. Wissenschaftliche Verlagsgesellschaft mbH, Stuttgart, DE

Nagel G, Lahrz A, Dersch P (2001) Environmental control of invasin expression in *Yersinia pseudotuberculosis* is mediated by regulation of RovA, a transcriptional activator of the SlyA/Hor family **41:** 1249–1269

Nakano T, Kawaguchi H, Nakao K, Maruyama T, Kamiya H, Sakurai M (1989) Two Outbreaks of *Yersinia pseudotuberculosis* 5a Infection in Japan. *Scand J Infect Dis* **21:** 175–179

Neidhardt FC, Ingraham JL, Schaechter M (1990) *Physiology of the bacterial cell: a molecular approach*. Sinauer Associates Inc., Sunderland, Massachusetts, USA

Nielsen J, Oliver S (2005) The next wave in metabolome analysis. *Trends Biotechnol* **23:** 544–546

Njoroge JW, Nguyen Y, Curtis MM, Moreira CG, Sperandio V (2012) Virulence meets metabolism: Cra and KdpE gene regulation in enterohemorrhagic *Escherichia coli*. *MBio* **3:** e00280-12

O'Hara K, Kanda T, Ohmiya K, Ebisu T, Kono M (1998) Purification and Characterization of macrolide 2'-phosphotransferase from a strain of *Escherichia coli* that is highly resistant to erythromycin. *Antimicrob Agents Chemother* **33:** 1354–1357

Olivares J, Bernardini A, Garcia-Leon G, Corona F, Sanchez MB, Martinez JL (2013) The intrinsic resistome of bacterial pathogens. *Front Microbiol* **4:** 103

Quek LE, Wittmann C, Nielsen LK, Krömer JO (2009) OpenFLUX: efficient modelling software for ^{13}C-based metabolic flux analysis. *Microb Cell Fact* **8:** 25

Revelles O, Millard P, Nougayrède JP, Dobrindt U, Oswald E, Létisse F, Portais JC (2013) The carbon storage regulator (Csr) system exerts a nutrient-specific control over central metabolism in *Escherichia coli* strain Nissle 1917. *PLoS One* **8:** e66386

Rimhanen-Finne R, Niskanen T, Hallanvuo S, Makary P, Haukka K, Pajunen S, Siitonen A, Ristolainen R, Pöyry H, Ollgren J, Kuusi M (2009) *Yersinia pseudotuberculosis* causing a large outbreak associated with carrots in Finland, 2006. *Epidemiol Infect* **137:** 342–347

Roberts MC (2005) Update on acquired tetracycline resistance genes. *FEMS Microbiol Lett* **245:** 195–203

Sambrook J, Green MR (2001) *Molecular Cloning: a Laboratory Manual*. Cold Spring Harbor Laboratory Press, Cold Spring Habor, USA

Sauer U (2006) Metabolic networks in motion: ^{13}C-based flux analysis. *Mol Syst Biol* **2:** 62

Sauer U, Canonaco F, Heri S, Perrenoud A, Fischer E (2004) The soluble and membrane-bound transhydrogenases UdhA and PntAB have divergent functions in NADPH metabolism of *Escherichia coli*. *J Biol Chem* **279:** 6613–6619

Schilling O, Frick O, Herzberg C, Ehrenreich A, Heinzle E, Wittmann C, Stülke J (2007) Transcriptional and metabolic responses of *Bacillus subtilis* to the availability of organic acids: transcription regulation is important but not sufficient to account for metabolic adaptation. *Appl Environ Microbiol* **73:** 499–507

Silver JD, Ritchie ME, Smyth GK (2009) Microarray background correction: maximum likelihood estimation for the normal-exponential convolution. *Biostatistics* **10:** 352–363

Sleisenger MH (1981) Pathophysiology of the gastrointestinal tract. In *Pathophysiology: the biological principles of diseases.* Smith LH, Thier SO (eds) pp 1526–1537. W. B. Saunders Co, Philadelphia, Pennsylvania, USA

Smits WK, Eschevins CC, Susanna KA, Bron S, Kuipers OP, Hamoen LW (2005) Stripping *Bacillus*: ComK auto-stimulation is responsible for the bistable response in competence development. *Mol Microbiol* **56:** 604–614

Smits WK, Kuipers OP, Veening JW (2006) Phenotypic variation in bacteria: the role of feedback regulation. *Nat Rev Microbiol* **4:** 259–271

Smyth GK (2004) Linear models and empirical bayes methods for assessing differential expression in microarray experiments. *Stat Appl Genet Mol Biol* **3:** Article3

Smyth GK (2005) Limma: linear models for microarray data. In *Bioinformatics and computational biology solutions using R and Bioconductor.* Gentleman R, Carey V, Dudoit S, Irizarry R, Huber W (eds) pp 397–420. Springer, New York, USA

Somerville GA, Proctor RA (2009) At the crossroads of bacterial metabolism and virulence factor synthesis in Staphylococci. *Microbiol Mol Biol Rev* **73:** 233–248

Spiro S, Guest JR (1991) Adaptive responses to oxygen limitation in *Escherichia coli*. *Trends Biochem Sci* **16:** 310–314

Spoering AL, Vulic M, Lewis K (2006) GlpD and PlsB participate in persister cell formation in *Escherichia coli*. *J Bacteriol* **188:** 5136–5144

Stock I, Wiedemann B (1999) Natürliche Antibiotika-Empfindlichkeit von *Yersinia pseudotuberculosis* Stämmen. *Chemotherapie Journal* **8:** 219–226

Sugimoto M, Ikeda S, Niigata K, Tomita M, Sato H, Soga T (2012) MMMDB: Mouse Multiple Tissue Metabolome Database. *Nucleic Acids Res* **40:** D809

Tauxe RV (2004) Salad and pseudoappendicitis: *Yersinia pseudotuberculosis* as a foodborne pathogen. *J Infect Dis* **185:** 761–763

Trotter EW, Rolfe MD, Hounslow AM, Craven CJ, Williamson MP, Sanguinetti G, Poole RK, Green J (2011) Reprogramming of *Escherichia coli* K-12 metabolism during the initial phase of transition from an anaerobic to a micro-aerobic environment. *PLoS One* **6:** e25501

Valgepea K, Adamberg K, Nahku R, Lahtvee PJ, Arike L, Vilu R (2010) Systems biology approach reveals that overflow metabolism of acetate in *Escherichia coli* is triggered by carbon catabolite repression of acetyl-CoA synthetase. *BMC Syst Biol* **4:** 166

Vanderpool CK (2007) Physiological consequences of small RNA-mediated regulation of glucose-phosphate stress. *Curr Opin Microbiol* **10:** 146–151

Vanderpool CK, Gottesman S (2007) The novel transcription factor SgrR coordinates the response to glucose-phosphate Stress. *J Bacteriol* **189:** 2238–2248

Walker JM (2002) *The Protein Protocols Handbook*. Humana Press, Totowa, New Jersey, USA

Warnes GR, Bolker B, Bonebakker L, Gentleman R, Liaw WHA, Lumley T, Maechler M, Magnusson A, Moeller S, Schwartz M, Venables B (2012) gplots: Various R programming tools for plotting data. *http://CRAN.R-project.org/package=gplots*

Wittmann C (2002) Metabolic flux analysis using mass spectrometry. *Adv Biochem Eng Biotechnol* **74:** 39–64

Wittmann C (2007) Fluxome analysis using GC-MS. *Microb Cell Fact* **6:** 6

Wittmann C, Hans M, Heinzle E (2002) *In vivo* analysis of intracellular amino acid labelings by GC/MS. *Anal Biochem* **307:** 379–382

Wittmann C, Heinzle E. (2002) Genealogy profiling through strain improvement by using metabolic network analysis: metabolic flux genealogy of several generations of lysine-producing corynebacteria. *Appl Environ Microbiol* **68:** 5843–5859

Wittmann C, Kiefer P, Zelder O. (2004) Metabolic fluxes in *Corynebacterium glutamicum* during lysine production with sucrose as carbon source. *Appl Environ Microbiol* **70:** 7277–7287

Wittmann C, Kim HM, John G, Heinzle E (2003) Characterization and application of an optical sensor for quantification of dissolved O_2 in shake-flasks. *Biotechnol Lett* **25:** 377–380

Wren BW (2003) The Yersiniae - a model genus to study the rapid evolution of bacterial pathogens. *Nat Rev Microbiol* **1:** 55–64

Yamaguchi A, Ono N, Akasaka T, Noumi T, Sawai T (1990) Metal-tetracycline/H+ antiporter of *Escherichia coli* encoded by a transposon, Tn10. The role of the conserved dipeptide, Ser65-Asp66, in tetracycline transport. *J Biol Chem* **265:** 15525–15530

Yang YH, Dudoit S, Luu P, Lin DM, Peng V, Ngai J, Speed TP (2002) Normalization for cDNA microarray data: a robust composite method addressing single and multiple slide systematic variation. *Nucleic Acids Res* **30:** e15

Yang YH, Thorne NP (2003) Normalization for two-color cDNA microarray data. In *Science and Statistics: A Festschrift for Terry Speed, IMS Lecture Notes -*

Monograph Series, Volume 40. Goldstein DR (ed) pp 403–418. IMS, Beachwood

Young GM, Badger JL, Miller VL (2000) Motility is required to initiate host cell invasion by *Yersinia enterocolitica*. *Infect Immun* **68:** 4323–4326

Yu J, Madsen ML, Carruthers MD, Phillips GJ, Kavanaugh JS, Boyd JM, Horswill AR, Minion FC (2013) Analysis of autoinducer-2 quorum sensing in *Yersinia pestis*. *Infect Immun* **81:** 4053–4062

Zhan L, Han Y, Yang L, Geng J, Li Y, Gao H, Guo Z, Fan W, Li G, Zhang L, Qin C, Zhou D, Yang R (2008) The cyclic AMP receptor protein, Crp, is required for both virulence and expression of the minimal Crp regulon in *Yersinia pestis* Biovar microtus. *Infect Immun* **76:** 5028–5037